UNIVERSIDAD DE LAS PALMAS DE GRAN CANARIA
Facultad de Ciencias del Mar

ON THE RESPIRATORY METABOLISM OF MARINE PLANKTON: ITS APPLICATION IN ASSESSING CARBON FLUXES AND THE ROLE OF SUBSTRATES ON ITS BIOCHEMICAL CONTROL

EL METABOLISMO RESPIRATORIO EN EL PLANCTON MARINO: SU APLICACIÓN EN EL CÁLCULO DE LOS FLUJOS DE CARBONO Y EL PAPEL DE LOS SUSTRATOS EN SU CONTROL BIOQUÍMICO

Tesis doctoral presentada por Natalia Osma Prado
dentro del Programa de Doctorado en Oceanografía

Dirigida por Dra. María M. Gómez Cabrera
y Dr. Theodore T. Packard

UNIVERSIDAD DE LAS PALMAS DE GRAN CANARIA
Facultad de Ciencias del Mar

ON THE RESPIRATORY METABOLISM OF MARINE PLANKTON: ITS APPLICATION IN ASSESSING CARBON FLUXES AND THE ROLE OF SUBSTRATES ON ITS BIOCHEMICAL CONTROL

EL METABOLISMO RESPIRATORIO EN EL PLANCTON MARINO: SU APLICACIÓN EN EL CÁLCULO DE LOS FLUJOS DE CARBONO Y EL PAPEL DE LOS SUSTRATOS EN SU CONTROL BIOQUÍMICO

Tesis doctoral presentada por Natalia Osma Prado
dentro del Programa de Doctorado en Oceanografía

Dirigida por Dra. María M. Gómez Cabrera
y Dr. Theodore T. Packard

La doctoranda | El/La director/a | El/La director/a

Las Palmas de Gran Canaria, noviembre de 2015

On the respiratory metabolism of marine plankton: its application in assessing carbon fluxes and the role of substrates on its biochemical control

Author: Natalia Osma Prado

Advisor: María M. Gómez Cabrera

Advisor: Theodore T. Packard

Marine Ecophysiology Group (EOMAR),
Institute of Sustainable Aquaculture and Aquatic Ecosystems (ECOAQUA),
Marine Sciences Faculty, University of Las Palmas de Gran Canaria (ULPGC),
35017, Las Palmas, Spain.

The following web-page address contains up to date information about this dissertation and related topics:
http://hdl.handle.net/10553/14613
Text printed in Las Palmas de Gran Canaria
First edition, November 2015

A mi abuela, una de las personas que más quiero y
que perdí en el camino de esta tesis.

Acknowledgements / Agradecimientos

En primer lugar, quiero agradecer al Programa de Formación y Perfeccionamiento de Personal Investigador (PFPI) del Gobierno vasco la financiación recibida para el desarrollo de esta tesis, así como la ayuda de movilidad que me fue otorgada para la realización de la estancia. Por otro lado, quiero dar las gracias al programa PFPI de la Universidad de Las Palmas de Gran Canaria por las diversas ayudas que me concedieron para la asistencia a congresos internacionales.

Creo que el sentimiento que tenemos la gran mayoría de doctorandos cuando llegamos al momento de escribir el apartado de los agradecimientos al finalizar la tesis se asemeja a la perfección con lo que siente un atleta cuando está a punto de cruzar la línea de meta. Por un lado, el cansancio se hace evidente como consecuencia de los altibajos sufridos durante todo el recorrido además de por el último esfuerzo realizado en el sprint final de escritura. Pero, por otro lado, le embarga una inmensa satisfacción por el trabajo conseguido y por haber disfrutado (¡y mucho!) del camino. Sin lugar a duda, en este símil atlético la etapa del doctorado sería un duro maratón. Y como en toda buena carrera de fondo, el apoyo de la gente que te rodea es fundamental para llegar al final.

Para empezar, quiero dar las gracias a mis directores por el apoyo que me han brindado a lo largo de estos años. May, te agradezco sinceramente que me hayas ofrecido todos los medios que estaban a tu alcance para que esta tesis llegara a buen puerto. Gracias por confiar en mi criterio y permitirme desarrollar mis ideas porque, sin duda alguna, eso me ha enriquecido como investigadora. Y gracias también porque siempre te has predispuesto a ayudarme cada vez que lo he necesitado, tanto en lo profesional como en lo personal. Aún recuerdo la primera conversación que mantuvimos antes de llegar aquí y que, de una manera u otra, ha sido el origen de este trabajo. Ted, I would like to thank you your unconditional support and encouragement during all these years. You are an outstanding scientist and I feel very fortunate to have worked side by side with you. I have learnt many things from you but, perhaps, one of the most important is to know how I want to face my future in science:

with passion and humbleness. I will miss our interesting conversations about almost everything, with a cup of tea in one hand and a handful of dried fruits in the other.

I will continue with English to thank Lutz Postel for hosting me at the IOW. Thank you for your continuous support during the stay and, of course, I would like to extend my thanks to Anneli for making me feel at home. I am truly grateful to Falk Pollehne, for his sound advice and help with the manuscript. Thanks also to Benni, Claudia and their lovely family, for the good moments we spent together in the cold Rostock and in the sunny islands.

De nuevo en Las Palmas, he tenido la suerte de haber conocido a personas que comenzaron siendo compañeros de estudio y de trabajo, y han terminado siendo amigos que me quedarán para toda la vida. Gracias:

A mis amigos del máster Almudena, JuanMa, Laia, Mireya y Sabrina por todos los buenos momentos que hemos pasado juntos desde aquel primer año. Aunque la vida nos haya dispersado, siempre seréis mi "clan del pececito".

A Federico, porque empezó siendo un compañero de laboratorio y se ha convertido en mi hermanito colombiano. Me vienen a la cabeza tantos momentos (graciosos, buenos, no tan buenos,...) que hemos vivido juntos que sería imposible escribirlos todos. Gracias por cada uno de ellos, Fede.

A las "gitanillas de Jinamar", Yeray, Alejandro y Juan Carlos, y a los que, sin duda alguna, lo hubieran sido de haber estado en Cádiz, Jose, Nauzet e Iván. Gracias chicos, por vuestro apoyo, por las risas, por las charlas, por las fiestas pero, principalmente, por demostrar que por encima de todo siempre está la amistad.

A todo el equipo, Ali, Ico, Mayte y Vanesa, por la suerte que he tenido de caer en un grupo como el nuestro. Gracias también a Manuela, por su apoyo durante mis primeros experimentos en el laboratorio.

A todos los demás compañeros del laboratorio B–201. La ventaja de haber trabajado en uno de los laboratorio más poblados de la facultad es que me ha permitido conocer mucha gente que realmente vale la pena. En especial, quiero agradecer a Mine, Lidia y Cory que siempre hayan estado ahí cuando las he necesitado. Pero también a Marta, Fede, Claire, Mar, Valeria, Inma, Isa, Maite, entre muchos otros que han pasado por el Lab B–201, porque cada uno de vosotros, de una u otra forma, habéis dejado huella en esta tesis.

A Tachi, Oscar, Alex y Raül por todos esos momentos de desahogos y risas que hemos compartido acompañados de un café cuando ya no quedaba nadie en la universidad.

Llegados a este punto, me vais a permitir que vuelva a mis raíces, al Pais Vasco, y que agradezca a mi familia todo el apoyo y cariño que me han trasmitido durante estos años:

A mis padres, Modes y Luismi, por inculcarme desde pequeña el amor por la naturaleza. Con esos largos paseos por los acantilados de Azkorri hicisteis que me picara el gusanillo de la biología y, más tarde, de la oceanografía.

A mis hermanos, Luis y Leyre, por vuestros incansables esfuerzos por entender qué hacía vuestra hermana con sus "bichos". Y por supuesto, a Ekaitz y Susana, porque también formais parte de todo esto.

A mi familia "bis", Iñaki, Charo, Gorka, Ghislaine, Nahi y mis maravillosos sobrinos, Samia y Adam, porque con vuestro cariño siempre me habéis hecho sentir una más.

Quien me conozca y este leyendo estas líneas sabrá que he dejado para el final a la persona que más me ha apoyado en este camino y a la que más cosas tengo que agradecerle. Desde que comencé la carrera de Biología hasta que he redactado las últimas frases de esta tesis, él ha tirado de mí cuando yo no lo hacía. Además, muchos de los experimentos que aquí se muestran no hubieran podido hacerse sin su ayuda. Por todo esto y por mucho más, gracias, Igor. Me siento muy afortunada de haber compartido este maratón contigo y ojalá pueda seguir haciéndolo en el futuro.

Mila esker guztioi,

Nat.

noviembre 2015

Abstract

Respiration is the principal process by which organic matter is remineralized in the water column. During this process, the organic carbon is degraded to CO_2, O_2 is consumed in oxic waters and the energy needed for the metabolic maintenance of the cells is produced. At the intracellular level, respiration is the direct result of the enzymatic activity of the electron transport system (ETS). In this thesis, the study of the marine plankton respiration has been tackled from different perspectives. On the one hand, ETS activity profiles in the water column have been used to construct models of vertical carbon flux (F_C) associated with planktonic metabolism in both the Peruvian and the Benguela upwelling systems. In the Peruvian system, the F_C approach proved to be a useful tool to study the temporal and spatial variability of carbon fluxes as well as the capacity of the system in retaining nutrients through remineralization. In the Benguela system, in turn, the F_C values were compared with the values of sinking particulate organic carbon (POC) collected with the sediment traps. This latter study showed a mismatch between the two approaches, mainly attributed to the primary productivity levels and the nature of the sinking particles. On the other hand, the variability of zooplankton respiratory metabolism was investigated, both in organisms from the field and in cultured organisms, and the effect that factors such as temperature, food quality and starvation exert on respiration was further addressed. In each of these works, the respiratory oxygen consumption (R_{O_2}), the potential respiration (Φ) and the intracellular concentration of the major substrates of the ETS, i.e. the pyridine nucleotides (PN), were determined. In zooplankton from different oceanic regions, the relationship between these parameters was influenced by different environmental factors. The seawater temperature determined the variability of R_{O_2} and Φ, but food availability largely influenced the intracellular concentration of PN. However, when only the effect of starvation was considered in cultured organisms, a strong correlation was recorded between the R_{O_2} and the PN concentration in three species of zooplankton with different structural complexity. In light of these results, a bisubstrate kinetic model was explored to predict the *in vivo* R_{O_2}. The model was based on the measured activity of the ETS, the

kinetic constants, and the substrate concentration. It demonstrated a high efficiency to predict the actual respiration rates under changing trophic conditions, albeit the results also suggested an additional contribution of other metabolites (i.e., ADP) to the overall regulatory mechanisms and, consequently, ADP and related metabolites should be considered for future applications of this model.

In summary, the study of respiration at different levels, i.e., biogeochemical, physiological and biochemical levels, conducted in this thesis has strengthened our knowledge about the importance of respiration in the ocean, inasmuch as the factors that control the oxygen consumption in the cells will ultimately control the role of marine plankton in the remineralization of the organic matter.

Resumen

La respiración es el principal proceso por el que se remineraliza la materia orgánica en la columna de agua. Durante este proceso, el carbono orgánico se degrada hasta dióxido de carbono, se consume oxígeno en las aguas óxicas y se produce la energía necesaria para el mantenimiento metabólico de las células. En las células, la respiración es la causa directa de la actividad de los complejos enzimáticos que conforman el sistema de transporte de electrones (ETS). A lo largo de esta tesis, se ha abordado el estudio de la respiración en el pláncton marino desde diferentes puntos de vista. Por un lado, se utilizaron perfiles de la actividad del ETS en la columna de agua para calcular modelos de flujo vertical de carbono (F_C) asociados al metabolismo de los organismos en los sistemas de afloramiento de Perú y de Benguela. En Perú se estudió la variabilidad espacial y temporal de los flujos de carbono, así como la capacidad del sistema de retener nutrientes a través de la remineralización. En Benguela, en cambio, se compararon los valores de F_C con las medidas de carbono orgánico particulado (POC) obtenidas mediante las trampas de sedimento. Este último estudio mostró un desacople entre ambos métodos, que dependiá principalmente de los niveles de productividad primaria y de la naturaleza de las partículas que se hundían. Por otro lado, se investigó la variabilidad del metabolismo respiratorio del zooplancton, tanto en el medio marino como en organismos en cultivo, y se determinó el efecto que factores como la temperatura, la calidad del alimento y la inanición ejercen sobre la respiración. En cada uno de estos trabajos se midió el consumo respiratorio de oxígeno (R_{O_2}), la respiración potencial (Φ) y la concentración de los principales sustratos del ETS, los piridín nucleótidos (PN). La relación entre estos parámetros en el zooplancton de distintas zonas oceánicas estuvo influenciada por un efecto desigual de los factores estudiados. Mientras que la temperatura del agua de mar determinó la variabilidad del R_{O_2} y la Φ, la concentración intracelular de PN dependiá mayoritariamente de la disponibilidad de alimento. Sin embargo, cuando se considero exclusivamente el efecto de la inanición en cultivos de organismos, se encontró una correlación muy fuerte entre el R_{O_2} y la concentración de PN en tres especies de zooplancton con diferente complejidad estructural. A raíz de estos resul-

tados, se exploró finalmente la capacidad de predecir el R_{O_2} *in vivo* de un modelo cinético bisustrato basado en la actividad del ETS, las constantes cinéticas y las concentraciones intracelulares de sustratos. Este modelo demostró una alta eficacia para predecir los valores reales de respiración durante diferentes condiciones tróficas, aunque los resultados sugirieron asimismo una contribución adicional de otros metabolitos en los mecanismos de regulación, que debería ser considerada en futuras aplicaciones de este modelo.

En resumen, este estudio de la respiración desde diferentes perspectivas ha permitido ahondar en el conocimiento de la importancia de este proceso en los océanos, ya que los factores que controlan las tasas de consumo de oxígeno en las células afectarán en última instancia al papel del plancton marino en la remineralización de la materia orgánica.

Thesis preview

The present thesis entitled *On the respiratory metabolism of marine plankton: its application in assessing carbon fluxes and the role of substrates on its biochemical control* has been conducted within the Doctoral Program of Oceanography (Quality Mention, MCD 2005-00179) from the Universidad de Las Palmas de Gran Canaria and has been supervised by Dr. May Gómez and Dr. Ted Packard. It is comprised of five original research articles developed in the frame of the projects EXZOME (CTM 2008-01616/MAR), CAMVALEX (CTM 2010-09515E) and BIOMBA (CTM 2012-32729), granted to Dr. May Gómez. Moreover, this thesis includes samples collected during several oceanographic cruises from the research projects MALASPINA 2010 (CSD 2008-00077), SUCCESION (MSM18/5, DFG) and JASON-76 (OCE 75-23718A01, NSF) that were granted to Dr. Carlos M. Duarte, Dr. Lutz Postel and Dr. Ted Packard, respectively. A research stay was likewise realized at the Leibniz Institute for Baltic Sea Research (IOW, Germany) during this period.

This thesis is structured in two parts. The former is divided into several chapters that encompasses a general introduction with the major objectives of the work, followed by original contributions in the form of scientific research articles. Then, a synthesis chapter compiles a general discussion of the results, the major conclusions of the thesis and the outline for future research. This first part is completely written in English, fulfilling the demands to obtain the Doctor Europeus Mention (BOULGC, Art. 1, Chap IV, November 5th, 2008). The second part, in turn, is written in Spanish and consists of a brief summary of the English section, with an introduction to the topic, the main results and the conclusions derived from the work. This is a requirement of the PhD Thesis Regulation from the Universidad de Las Palmas de Gran Canaria (BOULPGC, Art. 2, Chap I, November 5th, 2008).

Presentación de la Tesis

La tesis que aquí se presenta bajo el título *El metabolismo respiratorio en el plancton marino: su aplicación en el cálculo de los flujos de carbono y el papel de los sustratos en su control bioquímico* se ha desarrollado dentro del Programa de Doctorado en Oceanografía (Mención de Calidad, MCD 2005-00179) de la Universidad de Las Palmas de Gran Canaria y ha estado dirigida por los doctores May Gómez y Ted Packard. En ella se incluyen cinco contribuciones originales enmarcadas principalmente dentro de los proyectos de investigación EXZOME (CTM 2008-01616/MAR), CAMVALEX (CTM 2010-09515E) y BIOMBA (CTM 2012-32729) otorgados a la Dr. May Gómez. Además, esta tesis incluye muestras tomadas durante las campañas oceanográficas asociadas a los proyectos MALASPINA 2010 (CSD 2008-00077), SUCCESION (MSM18/5, DFG) y JASON-76 (OCE 75-23718A01, NSF), dirigidos por los doctores Carlos M. Duarte, Lutz Postel y Ted Packard, respectivamente. Por último, durante el desarrollo de la misma se realizó una estancia en el Leibniz Institute for Baltic Sea Research (IOW, Alemania).

Esta tesis esta estructurada en dos partes. Una primera que engloba la Introducción con los principales objetivos del trabajo, las Contribuciones Originales en formato de artículo científico, la Discusión General de los resultados, las Conclusiones y las Futuras Líneas de Investigación. Éstos capítulos están escritos íntegramente en inglés, de acuerdo a la normativa para la obtención de la Mención Europea del Títitulo de Doctor (BOULGC, Art. 1, Cap IV, 5 de Noviembre de 2008), donde se expone que, al menos, el resúmen y las conclusiones deben estar en una lengua distinta a la Española (inglés). La segunda parte de la tesis se trata de un resumen en castellano que consta de una breve introducción, los principales resultados y las conclusiones más relevantes del presente trabajo, cumpliéndose así los requisitos expuestos en el Reglamento de Elaboración, Tribunal, Defensa y Evaluación de Tesis Doctorales de la Universidad de Las Palmas de Gran Canaria (BOULPGC, Art. 2, Cap I, 5 de Noviembre de 2008).

Contents

List of Figures

Page

List of Tables

Page

Symbols and Abbreviations

ADH	Alcohol dehydrogenase
ADP	Adenosine-5'-diphosphate
ANOVA	Analysis of variance
ATP	Adenosine-5'-triphosphate
BSA	Bovine serum albumin
BU	Benguela upwelling
CI-LWB	Canary Islands, during the so-called late winter bloom
CI-ST	Canary Islands, during the stratification period
***CI*s**	Confidence intervals
CTD	Conductivity, temperature and depth sensor
CUEA	Coastal Upwelling Ecosystem Analysis
DOC	Dissolved organic carbon
DW	Dry weight
$\mathbf{E_z}$	Euphotic zone
EC	Enzyme commission number
ESD	Espherical diameter
***e*-ratio**	Export ratio
ETS	Electron transport system
$\boldsymbol{F}_{\mathrm{C}}$	Carbon flux
GDH	Glutamate dehydrogenase
GF/F	Glass microfiber filter
HPLC	High performance liquid chromatography
INT	2-p-iodophenyl-3-p-nitrophenyl-5-phenyltetrazolium chloride
IO	Indian Ocean

IOW	Leibniz Institute for Baltic Sea Research
K_{ia}	Dissociation constant
K_m	Michaelis half-saturation constant
***LOQ*s**	Limits of quantification
MTT	Thiazolyl blue
MW	Molecular weight
N	North
NA	North Atlantic
NAD^+	Nicotinamide adenine dinucleotide oxidized
NADH	Nicotinamide adenine dinucleotide reduced
NADt	Total pool of nicotinamide adenine dinucleotide
$NADP^+$	Nicotinamide adenine dinucleotide phosphate oxidized
NADPH	Nicotinamide adenine dinucleotide phosphate reduced
NADPt	Total pool of nicotinamide adenine dinucleotide phosphate
NPP	Net primary production
NRE	Nutrient retention efficiency
NW	North west
ODV	Ocean data view
PCA	Principal component analysis
PES	Phenazine ethosulfate
PN	Pyridine nucleotides
POC	Particulate organic carbon
POM	Particulate organic matter
PON	Particulate organic nitrogen
pP	Particulate phosphate
PSi	Particulate biogenic silica
PSU	Practical salinity units
$R_{NH_4^+}$	Ammonium excretion rate
R_{O_2}	Respiratory oxygen consumption rate
RQ	Respiratory quotient
RSD	Relative standard deviation
RV	Research vessel
S	South
SACW	South Atlantic Central Waters
SD	Standard deviation
SPSS	Statistical package for the social sciences
SST	Sea surface temperature

ST	Sediment trap
SWA	Southwest Atlantic cruise
TCA	Tricarboxilic acid cycle
$T_{\mathbf{eff}}$	Transfer efficiency
U	Enzymatic units
UHPLC	Ultra high performance liquid chromatography
ULPGC	Universidad de Las Palmas de Gran Canaria
UNESCO	United nations educational, scientific and cultural organization
v	Volume
$V_{\mathbf{max}}$	Apparent maximum enzyme reaction rate
$V_{\mathbf{O_2}}$	Modeled rate of O_2 consumption
VPDB	Vienna pee dee belemnite
W	West
$z_{\mathbf{f}}$	Any given depth in the water column
$z_{\mathbf{m}}$	Depth at maximum metabolic rate
$z_{\mathbf{s}}$	Seafloor depth
$z_{\mathbf{t}}$	Top of the water column
Δ	Difference or change in a certain quantity
δ	Difference in isotope ratio to a standard
λ	Wavelength

The beginning is the most important part of the work.

Plato

CHAPTER

1

CAPÍTULO

General Introduction

1.1 Role of respiration in biogeochemical cycles

In the sunlit surface waters of the ocean, phytoplankton convert carbon dioxide into particulate organic carbon (POC) through photosynthesis. Most of this fixed carbon is remineralized in the epipelagic zone or in the upper layers of the mesopelagic zone. Accordingly, only about 5-25 % of the net primary production (NPP) is exported from the euphotic zone and usually less than 3 % reaches bathypelagic depths (De La Rocha and Passow, 2007). From the NPP that is remineralized in the water column, about 15 % is consumed by bacteria (Ducklow, 2000), 30-70 % by microzooplankton (Calbet and Landry, 2004) and 20-35 % by mesozooplankton (Hernández-León and Ikeda, 2005). The transfer of organic matter into the ocean's interior occurs by a combination of gravitational sinking of particles, advection and vertical mixing of dissolved organic matter and active transport by zooplankton (Fig. 1.1), altogether known as the "biological pump" (Volk and Hoffert, 1985). Although mixing and diffusion also transport dissolved and suspended particulate organic matter to the deep ocean (Arístegui et al., 2002; Christensen et al., 1989; Hansell et al., 2012), passively sinking POC is generally regarded as the source of organic carbon for this realm. Hence the study of the downward flux of POC was the focus of international research programs during the last decades (e.g., Joint Global Ocean Flux Study, JGOFS).

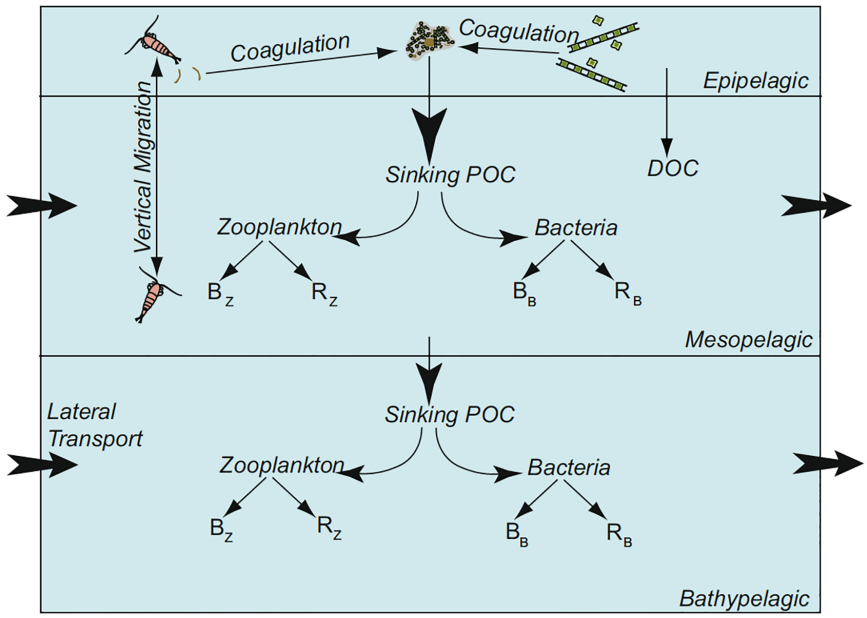

Figure 1.1: Processes affecting the remineralization of the POC exported from the euphotic zone in the mesopelagic and bathypelagic. The sinking POC is consumed by zooplankton and bacteria both for respiration (R_Z and R_B) and for producing biomass (B_Z and B_B). From Burd et al. (2010).

The sinking POC flux can be determined directly by sediment traps (e.g., Honjo et al., 2008) or indirectly by the $^{234}Th/^{238}U$ disequilibrium (Moran et al., 2003) and by inverse modelling (Schlitzer et al., 2003; Usbeck et al., 2003). On steady state, the decrease in the POC flux determined by any of these methods should be balanced by the heterotrophic activity in the water column according to simple mass balance. However, comparisons of the microbial and metazoan carbon demands with the attenuation of the POC flux have evidenced an imbalance between these sinks and sources (Burd et al., 2010; del Giorgio and Duarte, 2002). Although the bulk of the mismatch has been observed to vary spatially, estimates of heterotrophic activities have been found to be genererally 2-3 orders of magnitude higher than the sinking POC both in mesopelagic and bathypelagic waters (Baltar et al., 2009; Reinthaler et al., 2006; Steinberg et al., 2008). The reason for this discrepancy may stem from (*i*) an overestimation of the carbon demands and/or (*ii*) an underestimation of the carbon supply for the deep-sea (Burd et al., 2010). The former can

be explained by the use of inaccurate conversion factors for the dark ocean, which may increase the carbon demand values, whereas the latter may be a consequence of the low efficiency of the sediment traps in collecting slowly settling particles, which could contribute significantly to the total POC flux (Alonso-González et al., 2010). Contrarily, in recent research by Giering et al. (2014) a balance between zooplankton and microplankton respiration and the vertical carbon flux has been reported.

All these findings support the use of plankton respiration as an alternative procedure to assess vertical carbon fluxes in the ocean water column. The conceptual approach developed by Packard and Christensen (2004) used measurements of the activity of the respiratory electron transport system (ETS) in microplankton to construct carbon flux models (F_C). Later, it has also been applied to determine the zooplankton associated F_C in the Canary Islands (Packard and Gómez, 2013). The rationale of this method is the reality that plankton in the ocean water column degrade sinking POC, metabolize this organic matter within their cells and, via respiration, release it as CO_2 gas into the water column. Mathematically, the integration of the depth-profiles of CO_2 production by respiration (R_{CO_2}) from any depth in the water column to the seafloor indicates the amount of POC required to fuel the respiration of the organisms below that depth. It is the reverse of the concept applied by Suess (1980) to calculate respiration rates in the water column from the first derivative of the carbon flux-depth profiles. However, the F_C approach has still to be compared with direct measurements of sinking POC, as has been done with other indirect methods (e.g., Usbeck et al., 2003).

In general, carbon budget studies have evidenced the importance of understanding the processes that govern the remineralization of the organic matter from its production in the sunlit layer to its sedimentation in the oceanic bottom. Given that respiration is the principal process involved in the consumption of these particles, it is mandatory to comprehend the mechanisms that drives the oxygen consumption at the intracellular level as well as the factors that influence this consumption.

1.2 Respiration in the cells: biochemical basis and regulatory mechanisms

The process of respiration is common to all marine organisms. More than 95% of all aerobic and anaerobic respiration in the cells is driven by the activity of the ETS (Nelson et al., 2008). This system is composed of four enzyme complexes which are integral lipo-proteins arranged in a specific orientation in the inner mitochondrial membrane of eukaryotes or in the cytoplasmic membrane of prokaryotes (Fig. 1.2). Complex I, also called NADH dehydrogenase, constitutes an electron entry point of the respiratory system, jointly with Complex II or succinate dehydrogenase. Both complexes reduce ubiquinone into ubiquinol which is, in turn, oxidized by Complex III, also known as bc1 complex, to reduce cytochrome c. Complex IV, or cytochrome c oxidase, is the last complex of the ETS system and it reduces molecular oxygen to water by oxidizing the cytochrome c, in the case of aerobic respiration. Hence, each of these complexes catalyzes a different redox reaction along an increasing scale of standard reduction potentials (E'^{o}) from E'^{o} (NAD^+ | NADH) = -0.32 V to E'^{o} (O_2 | H_2O) = +0.82 V (Nelson et al., 2008). The net reaction is highly exergonic. This redox energy freed from the stepwise transfer of electrons is used to drive protons (H^+) from the inside to the outside of the membrane, which establishes an electrochemical proton gradient termed the "proton-motive force". The ETS complexes that contribute to this proton pumping are Complex I, III and IV. This gradient is harnessed by a fifth complex embedded in the membrane, i.e. the ATP synthase, to produce adenosine-5'-triphosphate (ATP) from adenosine-5'-diphosphate (ADP) and inorganic phosphate (P_i). The coupling between the respiratory ETS and the ATP synthesis in mitochondria was first proposed by Peter Mitchell in the so-called "chemiosmotic theory" (Mitchell, 1966). During respiration, two molecules of NADH are oxidized, the proton-pumping complexes translocate 20 protons from inside to outside the membrane, one molecule of O_2 is reduced to 2 molecules of H_2O by the cytochrome oxidase and 5 to 6 molecules of ATP are produced. Due to the stoichiometric relationship between oxygen consumption and electron flux through the ETS, the ETS is recognized as being the chemical basis of respiratory O_2 consumption (R_{O_2}).

The principal electron donors of the ETS are the pyridine nucleotides, i.e. nicotinamide adenine dinucleotide (NAD) and its phosphorylated form (NADP), and the succinate. Although succinate is known to be a major elec-

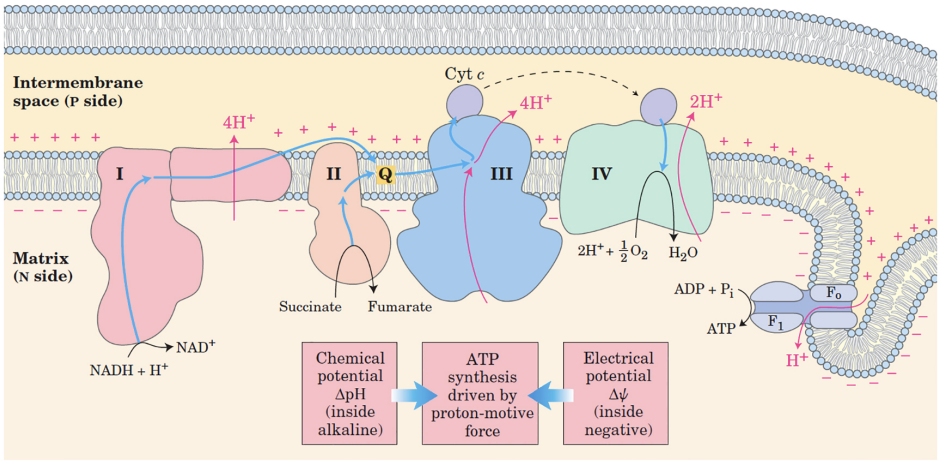

Figure 1.2: Arrangement of the electron transport system in the inner mitochondrial membrane. Blue arrows indicate the electron flow between Complex I and Complex IV, whereas pink arrows stand for the proton pumping across the membrane. The proton-motive force is used by the ATPase (F_oF_1) to synthesize ATP. From Nelson et al. (2008).

tron donor, together with reduced NAD, to mitochondrial electron transfer in non-marine organisms (Nelson et al., 2008), several investigations on bacteria, protozoa, phytoplankton and zooplankton have demonstrated that the succinate dehydrogenase plays a minor role in the overall ETS activity in marine organisms (Kenner and Ahmed, 1975b; Owens and King, 1975a; Savenkoff et al., 1995). Accordingly, this thesis focuses on the role of pyridine nucleotides in respiration.

Both NAD and NADP occur in their oxidized forms (NAD^+, $NADP^+$) and in their reduced forms (NADH, NADPH). NADH and NADPH are universal water-soluble electron carriers that associate reversibly with dehydrogenases (Nelson et al., 2008). NADH transfers electrons from catabolic reactions to the NADH dehydrogenase in the ETS, whereas NADPH generally supplies electrons to anabolic reactions. However, NADPH may also donate electrons to the respiratory ETS in two ways: (*i*) it can reduce NAD^+ to NADH in a reaction catalyzed by the $NAD(P)^+$ transhydrogenase, and (*ii*) it can also be a direct substrate for the ETS (Hatefi, 1973; Moller and Rasmusson, 1998). In addition, NADPH is a major substrate for the microsomal ETS (Strittmatter, 1968). The oxidized nucleotides, NAD^+ and $NADP^+$, are continuously

regenerated in catabolic reactions. While the NAD^+ is mainly reduced during glycolysis and the Krebs cycle, the $NADP^+$ is mostly reduced in the pentose shunt pathway in animal cells as well as during photosynthesis in plant cells. Thus, NAD(P)-linked dehydrogenases remove two hydrogen atoms from their substrates and transfer one to the $NAD(P)^+$ as a hybrid ion and release the other one in the medium.

Because these molecules are involved in almost all the metabolic pathways, it is beyond doubt that they hold a key position in energy metabolism. Hence, since the seminal work of Chance and Williams (1955), where they correlated the mitochondrial metabolic state with the oxidation-reduction levels of nucleotides, there has been a large amount of information on the concentration of these coenzymes in animal tissues. Recent research has unravelled an unexpected large suite of functions of both NAD and NADP in cell signalling, antioxidation and oxidative stress, as well as in cell death (Berger et al., 2004; Moller and Rasmusson, 1998; Pollak et al., 2007; Ying, 2008; Ziegler, 2005), which has prompted their quantification and the study of their redox state both in animal and plant cells. However, the information about their levels and behavior in microorganisms remains limited, with most of the investigations focused on certain bacteria species (Andersen and von Meyenburg, 1977; London and Knight, 1966; Setlow and Setlow, 1977; Wimpenny and Firth, 1972). In marine organisms, there is a practically complete lack of knowledge, except for some information in meroplankton (Schomer and Epel, 1998).

In the ocean, the electron acceptors of the ETS may change according to the environment. In ocean surface and other oxic waters O_2 will be preferably reduced whereas in oxygen minimum zones and anoxic basins either NO_3^-, NO_2^- or SO_4^{2-} can be reduced. Nevertheless, the basic chemistry that catalyzes the oxidation of the pyridine nucleotides and reduction of the electron acceptors is nearly identical in bacteria, protists, phytoplankton and zooplankton (Packard, 1985a; Vosjan, 1982).

On the basis of the strong theoretical link between respiration and the ETS activity as well as of the widespread distribution of this enzymatic system in living organisms, Packard et al. (1971) devised an ETS technique as a proxy for the respiration of all marine organisms in a parcel of seawater. This ETS assay requires, on the one hand, the addition of saturating levels of pyridine nucleotides to ensure the specificity of the reaction and the reproducibility of the measurements (Maldonado et al., 2012). On the other hand, the transferred

electrons are collected by an artificial electron aceptor, the tetrazolium salt INT (2-p-iodophenyl-3-p-nitrophenyl monotetrazolium chloride), which is reduced to a red formazan dye. Hence, the rate of INT reduction in the presence of a surplus of substrate indicates the capacity of living organisms to consume oxygen (or another electron aceptor) or, in other words, their potential respiration (Φ). Stoichiometrycally, the INT-formazan production rate (in μmol) is related by a factor of 2 to ETS activity (in μmol e^-) and by a factor of 0.5 to Φ (in μmol O_2) (Packard and Williams, 1981).

Ever since it was proposed, the ETS assay has proved to be a valuable tool to study respiration rates in the ocean when direct measurements of R_{O_2} are unfeasible, e.g. in the deep-sea waters (Baltar et al., 2009; Ikeda, 2011; Packard et al., 1977, 1988) and deep-sea sediments (Cammen et al., 1990; Christensen and Packard, 1977). The problems of overcrowding, starvation and/or manipulation of organisms that inevitably affect the respiration rates measured by means of incubations (Harris et al., 2000) are likewise overcome with this technique. Moreover, during oceanographic cruises, where a high data acquisition rates is of paramount importance, the ETS measurements provide a fast, simple and least expensive way of assessing mesoscale variation of the respiratory metabolism of planktonic organisms (e.g., Fernández-Urruzola et al., 2014; Herrera et al., 2014b; McKinnon et al., 2015; Minutoli and Guglielmo, 2009; Packard, 1985b) as well as of determining vertical carbon fluxes (Packard and Christensen, 2004), as stated above. Besides the oceanographic research, the ETS activity has also been measured in laboratory experiments to characterize the respiratory metabolism of bacteria (Christensen et al., 1980; Romero-Kutzner et al., 2015), protozoa (Finlay et al., 1983), phytoplankton (Kenner and Ahmed, 1975b; Packard, 1971) and zooplankton (Herrera et al., 2011; Owens and King, 1975a).

The ETS assay requires the addition of a surplus of substrates but organisms in the marine environment are unlikely to be at these conditions. Therefore, the Φ measurements should be converted into the *in vivo* R_{O_2} values. Although the actual R_{O_2} is theoretically close to half the maximum velocity of the ETS (Segel, 1993), this value may vary with physiological state and should be verified for the different environmental conditions. In oceanography, the current way of calculating plankton respiration from ETS activity is to apply an empirically determined R_{O_2}/Φ ratio. Studies such as that of Arístegui and Montero (1995), del Giorgio (1992), and Christensen et al. (1980), have

used to estimate respiration rates in euphotic zone and deep-sea waters. This use is supported by the good relationship between R_{O_2} and ETS activity in all organisms from bacteria to large zooplankton, with a size range over 10 orders of magnitude (Christensen et al., 1980; Finlay et al., 1983; King and Packard, 1975). However, variability has been noticed in the R_{O_2}/Φ in response to changes in species and physiology (Bamstedt, 1979; Hernández-León and Gómez, 1996; Herrera et al., 2011; King and Packard, 1975), which has precluded the use of a single universal value of the ratio. Hernández-León and Gómez (1996) studied the effect of temperature, body size, chlorophyll *a* and primary production on the R_{O_2}/Φ ratios of marine zooplankton and identified the food quality and/or quantity as the most influential factors. These authors further suggested that the variability was associated with changes in the R_{O_2} rather than in the Φ. In this sense, the influence of food composition on the R_{O_2} has been previously documented (e.g., Conover, 1966; Ikeda, 1977; Mayzaud, 1976). Still, how this effect is explained at the intracellular level in marine organisms is unclear. Regardless of the variability in this ratio, del Giorgio (1992) showed that the error associated with this application of the ETS is similar to the errors in other standard ecological methods used in plankton carbon flow studies, such as ^{14}C technique, thymidine uptake, etc.

An alternative approach to estimate the actual R_{O_2} from ETS measurements was proposed by Packard et al. (1996). These authors identified the substrate availability as the most obvious potential mechanism involved in the control of the *in vivo* ETS activity, although they recognized that other allosteric modulators (e.g., ADP and ATP) could contribute to the overall regulation at the intracellular level. Accordingly, they developed a first-principles model based on the assumptions that (*i*) the R_{O_2} is the direct result of the ETS activity and both are stoichiometrically related, (*ii*) the ETS activity is regulated by the availability of substrates at the entrance of the system, and (*iii*) the reaction obeys the rules of the enzyme kinetics. In their study, this bisubstrate kinetic model successfully predicted the R_{O_2} in the marine bacterium *Pseudomonas nautica*. More recently, Aguiar-González et al. (2012) attained a similar good estimation of R_{O_2} by the application of the same approach in other bacteria species grown on a different carbon sources. Packard and Gómez (2008), in turn, demonstrated that this enzyme kinetic model better predicted respiration on short time-scales than a model based on the biomass. However, all these studies constituted heuristic modeling exercises as they included estimated values for the kinetic constants and substrate concentrations rather than measured val-

ues. Thus, they obtained both the Michaelis constant (K_m) and the dissociation constant (K_{ia}) by optimization through successive iterations of measurements made on other organisms, whereas the time course of substrate concentrations were estimated from algorithms based on the carbon sources and organisms biomass. There is little information about the K_m values for the ETS in marine organisms (e.g., Owens and King, 1975a) and, all that exists, is based on monosubstrate reactions. Hence the need of measuring the intracellular concentration of NADH and NADPH as well as the bisubstrate kinetic constants in marine organisms to verify the predictive capacity of the model.

1.3 Thesis objectives and outline

In this thesis, the study of respiration in marine organisms has been covered from different perspectives. At the biogeochemical level, respiration measurements have been applied to calculate vertical carbon fluxes associated with metabolic activity of organisms in the water column. On the other hand, at the physiological level, the variability of respiratory metabolism in zooplankton has been studied, both in the field and in the laboratory, as well as the effect that factors such as temperature, food quality and starvation exert on this process. Finally, the mechanisms that regulate the *in vivo* activity of the enzymes responsible for the oxygen consumption at the intracellular level have been investigated. This integrated study allows to obtain a general picture of the importance of respiration in the ocean, as the factors that control the oxygen consumption in the cells will ultimately affect the role of marine plankton in the remineralization of the organic matter.

The *specific objectives* of this thesis were:

1. To demonstrate the usefulness of the ETS measurements to study the spatio-temporal variability of vertical carbon fluxes as well as to estimate the capacity of the system in retaining nutrients and the heterotrophic energy production of marine plankton. For that, ETS profiles measured on the microplankton of the Peruvian upwelling on consecutive offshore transects were used. This objective is covered in **Chapter 2**.

2. However, to date, it has not been corroborated yet if the values of vertical carbon flux determined from the model (F_C) in objective 1 compare to those obtained by a more traditional methodology such as the sediment

traps. This is, therefore, the objective addressed in **Chapter 3**. The comparison of the two approaches was performed during an oceanographic cruise in the Benguella upwelling system.

3. Due to the importance of respiration in the biogeochemical cycles, the following objective focused on the study of the temporal and spatial variability of the respiratory metabolism in marine zooplankton. The respiratory oxygen consumption (R_{O_2}), the potential rates (Φ) and the concentration of the major substrates of the ETS, i.e. the pyridine nucleotides NAD and NADP were determined in organisms collected during 3 oceanographic cruises in the North Atlantic, Indian Ocean, Benguela upwelling and in the coastal waters off the Canary Islands (Spain). Assuming an important role of intracellular substrates on the respiratory control, we expected to find a relationship between the R_{O_2} and pyridine nucleotides in the ocean. This objective is developed in **Chapter 4**.

4. On the view of the results on the objective 3, a more thorough study of the effect of food availability on the respiratory metabolism was conducted on the laboratory. To accomplish this objective, a culture of the marine dinoflagellate *Oxyrrhis marina* was monitored over a starvation period, during which measurements of the R_{O_2}, Φ and NAD and NADP concentrations were taken. The starting hypothesis of this study, which is covered in **Chapter 5**, was that the pattern described by the R_{O_2} and the concentration of NAD and NADP would show a strong correlation during this period.

5. Finally, the ability of a bisubstrate enzymatic model, based on the ETS activity, kinetics constants and intracellular substrates concentration, to predict the *in vivo* R_{O_2} in different organisms under different trophic conditions was tested. Hence, experiments were conducted to investigate the influence of the food quality and quantity on the respiratory metabolism of two zooplankton species, the rotifer *Brachionus plicatilis* and the mysid, *Leptomysis lingvura*. This objective is addressed in **Chapter 6**.

Science is a way of thinking much more
than it is a body of knowledge

Carl Sagan

CHAPTER

2

CAPÍTULO

Peru upwelling plankton respiration: Calculations of carbon flux, nutrient retention efficiency and heterotrophic energy production

T. T. Packard, N. Osma, I. Fernández-Urruzola, L. A. Codispoti, J. P. Christensen and M. Gómez (2015), Biogeoscience 12, 2641-2654

http://dx.doi.org/10.5194/bg-12-2641-2015

ABSTRACT: Oceanic depth profiles of plankton respiration are described by a power function, $R_{CO_2} = (R_{CO_2})_0\ (z/z_0)^b$, similar to the vertical carbon flux profile. Furthermore, because both ocean processes are closely related, conceptually and mathematically, each can be calculated from the other. The exponent, b, always negative, defines the maximum curvature of the respiration depth-profile and controls the carbon flux. When $|b|$ is large, the carbon-flux (F_C) from the epipelagic ocean is low and the nutrient retention efficiency (NRE) is high, allowing these waters to maintain high productivity. The opposite occurs when $|b|$ is small. This means that the attenuation of respiration in ocean water columns is critical in understanding and predicting both vertical F_C as well as the capacity of epipelagic ecosystems to retain their nutrients. The ratio of

seawater R_{CO_2} to incoming F_C is the NRE, a new metric that represents nutrient regeneration in a seawater layer in reference to the nutrients introduced into that layer via F_C. A depth profile of F_C is the integral of water column respiration. This relationship facilitates calculating ocean sections of F_C from water column respiration. In an F_C section and in a NRE section across the Peruvian upwelling system we found an F_C maximum and a NRE minimum extending down to 400 m, 50 km off the Peruvian coast over the upper part of the continental slope. Finally, considering the coupling between respiratory electron transport system activity and heterotrophic oxidative phosphorylation promoted the calculation of an ocean section of heterotrophic energy production (HEP). It ranged from 250 to 500 J d^{-1} m^{-3} in the euphotic zone to less than 5 J d^{-1} m^{-3} below 200 m on this ocean section.

2.1 Introduction

Respiration is as ubiquitous in the ocean as are the microorganisms that cause it (Lane, 2002; Richards, 1957; Seiwell, 1934). It is controlled by the respiratory electron transport (ETS) activity in eukaryotic mitochondria and prokaryotic cell membranes (Lane, 2005; Nelson and Cox, 2000; Packard, 1969; Packard et al., 1971) and is responsible for the bulk of oceanic O_2 consumption (Packard, 1985b; Redfield et al., 1963; Seiwell, 1937). It is driven by the degradation of dissolved and particulate organic carbon, generates CO_2 (Redfield et al., 1963), acidifies seawater (Harvey, 1955), and produces energy in the form of ATP (heterotrophic energy production) (Madigan et al., 2000; Nelson and Cox, 2000; Ochoa, 1943). Even in anoxic seawater respiration degrades organic matter, produces CO_2, and generates ATP while reducing nitrogen oxides to N_2 or SO_4^- to H_2S (Madigan et al., 2000; Richards, 1965). Plankton community respiration in ocean water column is a key variable in calculating net community productivity (Ducklow and Doney, 2013) in developing oceanic carbon models, in resolving the autotrophic-heterotrophic states of ocean ecosystems (Williams et al., 2013), and in understanding vertical ocean F_C rates (Giering et al., 2014). The research team led by Sarah Giering (Giering et al., 2014) demonstrated that, contrary to previous efforts (Burd et al., 2010), but in accord with classical oceanographic understanding (Redfield et al., 1963; Richards, 1957; Riley, 1951; Suess, 1980), zooplankton and microplankton (prokaryote and eukaryote) respiration balance vertical carbon flux (Eppley and Peterson, 1979; Packard et al., 1988; Riley, 1951). All

these findings support the use of plankton respiration in assessing vertical F_C in the ocean water column. Conceptually, the reciprocal relationship between the water column respiration and the F_C, from the ocean's epipelagic zone, is clear (Martin et al., 1987; Suess, 1980). However, describing this reciprocal relationship mathematically, as a function of ocean depth in the forms,

$$R = f(z) \;\; and \;\; F_C = \int_{z_1}^{z_2} R\, dz$$

was delayed until the helium-tritium studies of Jenkins (Jenkins, 1982, 1984), the sediment trap studies of VERTEX program (Martin et al., 1987), and respiratory electron transport system (ETS) measurements in the Gulf of Maine (Packard and Christensen, 2004). In the latter, microplankton ETS measurements were used to build power function models of respiratory CO_2 production (R_{CO_2}) and F_C. Here, we extend this approach to calculate a microplankton respiration section across the Peruvian upwelling system (Barber et al., 1971; Walsh, 1972) and to model F_C on this transect. We focused our measurements on microplankton because its biomass and metabolism dominate ocean water columns (Arístegui et al., 2009; King et al., 1978; Laufkötter et al., 2013). The section was made at a time of regime-change when the Peruvian upwelling system and the El Niño-Southern Oscillation (ENSO) underwent a shift (Santoso et al., 2013). Here we document some of the biological phenomenon that occurred at that time. With the F_C and the R_{CO_2} models we calculate the nutrient retention efficiency (Packard and Gómez, 2013; Osma et al., 2014), a new metric that quantifies the ability of an ocean layer to retain its nutrients. Conceptually, the nutrient retention efficiency (NRE) is the nutrient remineralization rate within an ocean layer normalized by nutrients entering that layer via carbon flux. Below the euphotic zone, it can be calculated as the inverse of the F_C transfer efficiency (Buesseler et al., 2007b; Buesseler and Boyd, 2009), but we show here that it can also be calculated from a profile of plankton respiration. In addition, using different limits to the F_C integration we calculate the sum of the benthic respiration and carbon burial that occurs on the sea floor. Finally, we use the respiration models and the coupling between ETS activity and oxidative phosphorylation to calculate light-independent heterotrophic energy flow (Karl, 2014). This energy is generated in the form of ATP by ATP synthase, an enzyme motor coupled to a heterotrophic respiratory process such as O_2 utilization or NO_3^- reduction (Ferguson, 2010; Watt et al., 2010). In all types

of respiration, the ATP synthase senses the pH and electromotive force gradient across the membrane in which the ATP synthase is embedded (Lane et al., 2010), and when the gradient is sufficiently strong (~ 225 mV), the molecular motor that is the ATP synthase starts its rotary production of ATP (Walker, 1998). Heterotrophic ATP generation in any ecosystem is largely based on exploiting the Gibbs free energy (ΔG) released during the oxidation of different organic compounds. The biochemistry of ATP and the ETS was unknown in 1925, but even then the idea of capturing biologically useable energy from respiration was appreciated by Lotka (1925). A generation later, Odum built on this concept to describe energy flow in freshwater streams (Odum, 1956). Reviewing this earlier work, Karl recently argued that biological energy production in the ocean should be assessed to provide insight into the variability of ocean productivity (Karl, 2014). Here, we address his concern by calculating Heterotrophic Energy Production (HEP) in a C-Line section. This HEP is the energy produced while ATP is generated by respiratory O_2 consumption (R_{O_2}) in the microplankton community composed of phytoplankton, bacteria, archea, and protozoans in the epipelagic layer and by the R_{O_2} and NO_3^- reduction in microbial communities of bacteria, archea, and protozoans in the meso- and bathypelagic waters of the Peruvian current upwelling system.

2.2 Material and methods

2.2.1 Research site

The site of this Coastal Upwelling Ecosystem Analysis (CUEA) investigation at 15° S off Pisco, Peru (Fig. 2.1) was chosen because the upwelling is strong, persistent, and well known (Fernández et al., 2009; Wooster, 1961). It was the focus of the R/V *Anton Bruun* cruise 15 (Ryther et al., 1970), the R/V *T.G. Thompson Pisco* expedition in 1969 (Barber et al., 1978), and others (Walsh et al., 1971; Wirtky, 1967) before it was the focus of the CUEA-JOINT II program (Brink et al., 1981; Packard, 1981) of which the JASON Expedition was a part (King, 1981; Richards, 1981). However, in spite of the many previous expeditions to this site most of them took place in the austral fall (March-April-May). The JASON-76 expedition was unique because it took place in the late winter and austral spring (August, September, October, and November) when the southeast trade winds would be at their strongest (Wooster, 1961). In this way it was thought that the results might be more comparable with results from

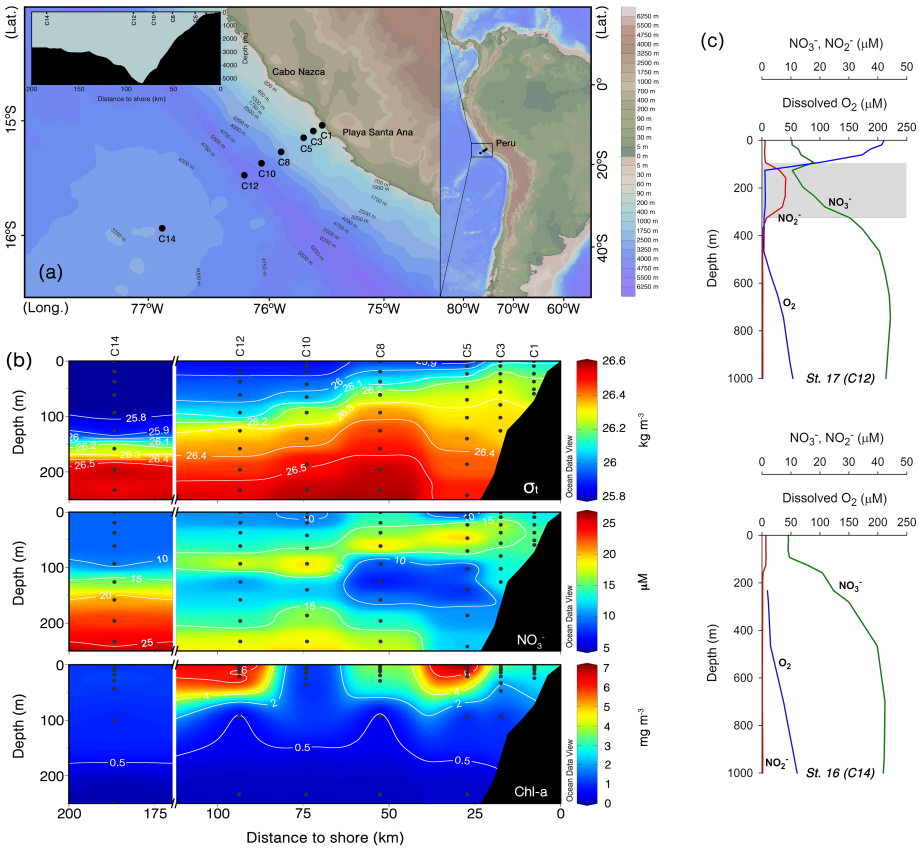

Figure 2.1: (**a**) C-line section orthogonal to the Peruvian coast at 15° S. The innermost C-Line position, C1, was 2.7 km from the coast between Cabo Nazca and Punta Santa Ana. The outermost position, C14, was located west of the Peru-Chile trench 185.2 km from the coast. Depth along this transect ranged from 63 m at C1 to 4755 m at C12. C14 was in 2680 m of water on the gently rising abyssal plain seaward of the trench (inset upper left). (**b**) Density (σ_t), NO_3^- (µM) and phytoplankton chlorophyll (mg m^{-3}) sections along the C-line from C1 to C14 (top, middle and bottom panels, respectively). All sections represent the upwelling from 13 to 20 September 1976. Scale brakes avoid interpolation over a 90 km data gap. The high phytoplankton biomass over the shelf break occurs between C5 and C8, 15 to 35 km from the coast. (**c**) NO_3^-, NO_2^-, and O_2 depth profiles through the mesopelagic waters over the trench at C12 (top) and over the outermost station at C14 (bottom). The vertical plot at C12 documents the first step in denitrification (shaded area), NO_3^- reduction to NO_2^-, at the foot of the oxycline, in the oxygen minimum zone (OMZ) between 150 and 300 m. In contrast, the vertical profiles at C14, 185 km off the coast, show the absence of denitrification in mesopelagic waters.

upwelling studies made in the Northern Hemisphere's spring-time upwelling off NW Africa (Codispoti et al., 1982; Minas et al., 1982). The results presented here are from the September 10 to September 24 leg of JASON-76 on board Duke University's Oceanographic ship, R/V *Eastward*, cruise no. E-5H-67 (Packard and Jones, 1976).

2.2.2 **Sampling**

All sampling was conducted along the C-Line (Fig. 2.1a) that extended seaward from the coast at position C1, just south of Cabo Nazca (Pisco), across the deep trench to position C14, 185 km offshore (Packard, 1981). Hydrographic sections were made at the beginning of the expedition (10 - 11 September) and again after a lapse of 10 days (20 - 21 September). The endpoint coordinates were from 15°3.2' S, 75°26.0' W to 15°55.8' S, 75°31.4' W (Kogelshatz et al., 1978; Packard and Jones, 1976). In addition, between 10 and 24 September, productivity stations, that focused on the biological, nutrient chemistry, and biochemical properties at depths where the light was 100, 50, 30, 15, 5, 1, and 0.1 % of the surface incident radiation (light depths), were established at C-Line positions (Packard and Jones, 1976). These productivity stations were not made in order along the C-Line section, hence the irregularity of their numerical sequence in Tables 2.3 - 2.7. In addition, some locations along the C-Line were occupied several times. For this reason, as well as to coordinate the results presented here with the results of other CUEA reports (Brink et al., 1981), both the C-Line location and the station number are given through the paper. The productivity casts were made each morning before 10:00 LT with 30 L Niskin PVC bottles to six light depths (1, 5, 15, 30, 50, and 100 %). Each Niskin bottle was flushed at depth in yo-yo fashion both by the action of the ship's roll and by meter oscillations with the winch. On deck it was drained immediately, without prefiltration, into a well-rinsed carboy for subsampling and returned to depth for the next sample. The six samples were taken within 1h. Subsamples were drawn for phytoplankton productivity, inorganic nutrient salts, (ammonium, reactive phosphorus, NO_3^-, NO_2^- and silicate), ETS and NO_3^- reductase activities, and particulate protein (Packard and Jones, 1976). Station coordinates are given in Table 2.1. The inorganic nutrient salts, salinity, temperature, and O_2 can be found in CUEA data reports 38 and 45 (Hafferty et al., 1978; Kogelshatz et al., 1978). Chlorophyll and phytoplankton productivity (^{14}C uptake) are reported in CUEA data report (Barber et al.,

1978). The ^{14}C uptake data were calculated on an hourly basis (Table 2.1) from the 24 h productivity data (Kogelshatz et al., 1978). Light was measured as daily total solar radiation with an Eppley Model 8-48 pyranometer placed above the ship's bridge (Packard and Jones, 1976). Below the mesopelagic zone, the seawater was sampled for ETS activity with 30 L Niskin PVC bottles down to 2000 m, depending on the depth of the water column (Tables 2.2 and 2.3).

2.2.3 **ETS activity, respiratory O_2 consumption, CO_2 production, and denitrification**

Respiratory ETS activity in the euphotic zone (E_z) was measured according to Kenner and Ahmed (1975a) as described in Packard and Williams (1981). In deeper waters it was measured according to (Packard et al., 1971) and multiplied by 3.35 to render the two data sets comparable as explained in Christensen and Packard (1979). Here, ETS activity is used as a direct measure of potential respiration and a proxy for respiration. Both potential respiration and respiration were calculated from the combined ETS data set according to Packard and Christensen (2004) and Packard and Codispoti (2007). Tables 2.2 and 2.3 explain the calculations in detail. Table 2.3 presents the calculations as R_{O_2} in units of μmol O_2 m^{-3} h^{-1} for oxic waters. Using ETS activity as a proxy for R_{O_2} requires selection of a ratio of R_{O_2} to potential respiration (Φ). Since direct measurements of R_{O_2} can not be made below the E_z, a true calibration can not be made. The R_{O_2} to Φ ratio should be around 0.5 if Φ represents V_{max} of the ETS and standard physiological rates, governed by enzyme activities, operate close to one-half of their potential capacity (Cleland, 1967). With our methodology (Packard and Williams, 1981) and by our analysis (Packard and Christensen, 2004) we calculated a R_{O_2} to Φ ratio, 0.26 (Table 2.2), that successfully predicted R_{O_2} in the epipelagic and the mesopelagic waters of the Nansen Basin of the Arctic Ocean (Packard and Codispoti, 2007). In that study, R_{O_2} was a long-term average R_{O_2} calculated by the AOU-He-tritium method of Jenkins (1982, 1984) as used by W. Roether in Zheng et al. (1997). We have chosen to use the same R_{O_2}-to-Φ ratio of 0.26 here (Tables 2.2 and 2.3). R_{CO_2} (Fig. 2.2a) was then calculated from R_{O_2} using a Redfield ratio (C/O_2) of 0.71 from Takahashi et al. (1985). This is the best available way to calculate water respiration from our water column ETS measurements.

Table 2.1: Oceanographic characteristics of Peru upwelling C-Line stations during Duke University's JASON-76 R/V *Eastward* cruise no. E-5H-67. E_z depth is the 1 % light level. Original data are in CUEA data reports (Kogelshatz et al., 1978; Packard and Jones, 1976).

CUEA C-Line Position (JASON Station)	Coordinates	Date in Sept 1976	Distance to coast (km)	Ocean depth (m)	Surface temperature (°C)	Surface salinity (PSU)	Euphotic zone (m)	Surface chlorophyll (mg m^{-3})	Surface respiration (μmol O_2 m^{-3} h^{-1})	Surface net productivity (mg C m^{-3} h^{-1})
C1 (22)	15° 03.2' S 75° 26.0' W	20	2.7	63	14.28	34.902	24	3.06	56.11	6.84
C3 (15)	15° 05.9' S 75° 31.4' W	12	12.9	117	14.26	-	42	2.09	24.11	3.67
C3 (21)	15° 06.5' S 75° 31.0' W	19	12.9	120	14.10	34.869	33	3.67	83.99	8.08
C5 (20)	15° 09.9' S 75° 35.7' W	18	24.7	500	15.59	34.921	21	6.96	119.13	18.24
C5 (37)	15° 10.5' S 75° 36.2' W	24	24.7	607	15.00	34.921	27	3.77	79.97	8.88
C8 (19)	15° 16.9' S 75° 47.8' W	17	49.9	1880	14.97	34.902	29	4.11	80.32	9.65
C8 (36)	15° 16.9' S 75° 14.8' W	23	49.9	2150	16.10	35.069	29	3.90	87.67	12.35
C10 (18)	15° 22.0' S 75° 59.8' W	16	70.9	4300	15.92	35.077	36	1.06	34.35	1.64
C12 (17)	15° 28.0' S 76° 08.0' W	15	92.6	4000	15.75	35.046	40	1.14	47.14	1.93
C12 (35)	15° 29.0' S 76° 07.8' W	22	92.6	4755	15.46	34.950	21	7.47	144.71	16.64
C14 (16)	15° 55.8' S 76° 51.6' W	13	185.2	2680	16.48	35.147	43	0.92	40.90	1.63

In waters where respiration is based on using oxides of nitrogen (NO_3^-, NO_2^-, N_2O, or NO) in place of O_2, calculations are different. Since microbial respiratory NO_3^- reduction to nitrogen gas (denitrification) occurs in the water column between 47 and 400 m between positions C3 to C12 (Garfield et al., 1979; Codispoti and Packard, 1980) (Fig. 2.2a), Table 2.3 presents denitrification rates from these depths (shaded numbers) as R_{N_2} in units of μmol N_2 m^{-3} h^{-1}. In these oxygen-defficient waters we used a Redfield ratio, C/N_2, from Gruber and Sarmiento (1997). To apply it, one first has to calculate R_{N_2} based on the fact that the ETS for R_{O_2} and R_{N_2} differ only in the terminal electron acceptor (Chen and Strous, 2013; Packard, 1969). This was done in Tables 2.2 and 2.3 according to Codispoti and Packard (1980) and Codispoti et al. (2001). The approach has recently been corroborated by Dalsgarrd et al. (2012). R_{N_2} in units of μmol N_2 h^{-1} m^{-3} is calculated in Table 2.2, column 2, by multiplying nanoeq min^{-1} L^{-1} by 60. The product is equivalent to μmol e^- h^{-1} m^{-3}. Then, dividing this by 105 mol e^- per mol N_2 yields R_{N_2}. The constant, 105 mol e^- per mol N_2, is the equivalent of the R_{N_2}/ETS ratio in Codispoti and Packard (1980), 2.4 μL O_2 $L^{-1}h^{-1}$/(gN_2 m^{-3} yr^{-1}). The R_{CO_2} calculation is as follows: R_{CO_2} = [106/60 mol C (mol N_2)$^{-1}$ × ETS activity (mol e^- h^{-1} m^{-3})] / [105 mol e^- (mol N_2)$^{-1}$]. The ratio, 106/60 mol C (mol N_2)$^{-1}$, is the Redfield ratio, mentioned above, for the carbon (as CO_2) produced during denitrification from NO_3^- (Gruber and Sarmiento, 1997). Note that both R_{O_2} and R_{N_2}, from Table 2.3 were converted to R_{CO_2} before being used in the E_z part of Fig. 2.2a.

2.2.4 *R* modelling

To generate *R* models as depth functions (Table 2.4), the ETS-based *R* was plotted against depths (z) normalized by the depth of the *R* maximum (z_m) as we did in Packard and Christensen (2004). From these plots, power functions of the form $R = R_m\ (z/z_m)^b$ were fitted to the data using Sigma Plot (version 12.5) according to Charland (2002). Note that R_m is the depth of the respiration maximum and b, the exponent, is always negative. The exponent b represents the maximum curvature of the respiration-depth profile. Note that *R* in the E_z of Fig. 2.2a is based directly on the ETS measurements (Table 2.3), while the *R* in the mesopelagic zone of Fig. 2.2a is based on the *R* models in Table 2.4.

Table 2.2: Step-by-step calculations of F_C from ETS activity at C-Line position C12 (station 35). Potential R (Φ), R_{O_2}, N_2 production from denitrification (R_{N_2}) and respiratory CO_2 production (R_{CO_2}) were first determined from temperature-corrected ETS activity values. Φ is stoichiometrically related to electrons by a factor of 4 ($O_2 + 4e^- + 4H^+ \rightarrow 2H_2O$). R_{O_2} is 0.26 of Φ (Packard and Christensen, 2004). R_{N_2} relates to ETS activity according to Codispoti and Packard (1980). Here, denitrifying waters occur between 93 and 233 m (values in bold). R_{CO_2} was calculated from both R_{O_2} and R_{N_2} (see Methods). Column 7 shows the modeled R_{CO_2} values below the R maximum (13 m), obtained from the depth-normalized power function ($R_{CO_2} = R_m\ (z/z_m)^b$) fitted to the data in Column 6. F_C was determined by integrating either to the bottom ($F_{t\text{-}s}$, Column 8) or to infinity (F_∞, Column 9). The first represents the C consumed by R from the E_z (21m) to the bottom, while the second includes benthic R and C burial. The difference between F_∞ and $F_{t\text{-}s}$ equals benthic R and the C burial rate (Column 10). Column 11 represents the C-flux determined by trapezoidal approximation, which relates to $F_{t\text{-}s}$ through the regression: $F_{t\text{-}s} = 0.85\ F_{C_{trap}} - 0.54$ ($r^2 = 0.99$, $p < 0.001$).

Depth z (m)	ETS Activity (neq min^{-1} L^{-1})	Φ (µmol O_2 h^{-1} m^{-3})	R_{O_2} (µmol O_2 h^{-1} m^{-3})	R_{N_2} (µmol N_2 h^{-1} m^{-3})	R_{CO_2} (µmol CO_2 h^{-1} m^{-3})	R_{CO_2} modeled (µmol CO_2 d^{-1} m^{-3})	F_C to bottom $F_{t\text{-}s}$ (mmol C d^{-1} m^{-2})	F_C to infinity F_∞ (mmol C d^{-1} m^{-2})	Benthic respiration and burial $F_\infty - F_{t-s}$	C-Flux to bottom Trap Calc (mmol C d^{-1}
0.5	37.10	556.56	144.71	-	102.74	-	-	-	-	-
3	37.81	567.14	147.46	-	104.69	-	-	-	-	-
5	35.69	535.39	139.20	-	98.83	-	-	-	-	-
9	33.65	504.68	131.22	-	93.16	-	-	-	-	-
13	39.19	587.87	152.85	-	108.52	1629.67	-	-	-	-
21	15.34	230.16	59.84	-	42.49	707.39	19.71	20.07	0.36	25.49
31	8.79	131.81	34.27	-	24.33	359.18	14.68	15.04	0.36	20.16
93	**0.44**	-	-	**0.25**	**0.44**	53.09	6.31	6.67	0.36	7.38
233	**0.35**	-	-	**0.20**	**0.35**	10.74	3.02	3.38	0.36	3.38
465	0.05	0.75	0.19	-	0.14	3.23	1.66	2.03	0.36	1.76
698	0.01	0.14	0.04	-	0.03	1.59	1.14	1.50	0.36	1.20
930	0.02	0.23	0.06	-	0.04	0.97	0.85	1.21	0.36	0.90
1395	0.01	0.21	0.05	-	0.04	0.48	0.54	0.90	0.36	0.57
1860	0.01	0.13	0.04	-	0.02	0.29	0.36	0.73	0.36	0.40
4755	-	-	-	-	-	0.06	0	0.36	0.36	0

2.2.5 F_C, NRE , and HEP calculations

The F_C was calculated (Table 2.2) from depth-normalized water column R (Packard and Christensen, 2004; Packard and Gómez, 2013; Osma et al., 2014). Power functions ($R_{CO_2} = R_m\,(z/z_m)^b$) were selected over logarithmic or exponential functions because they better described the data as previous studies found (Packard and Christensen, 2004; Packard and Codispoti, 2007). Conceptually, planktonic R_{CO_2} in a seawater cube is considered equivalent to the difference between the total F_{C_1} through the top of the cube and total F_{C_2} through the bottom of the cube, where total carbon flux refers to the sum of the DOC and the POC carbon flux. We deduce, on the basis of (Carlson et al., 2010; Craig, 1971; Hansell et al., 2012), that R based on DOC and lateral POC flux, compared to the R based on the vertical flux of labile POC, is less than 30 % of the total R. Note that if organic matter, in any form, is resistant to oxidation (Arrieta et al., 2015) its flux through the water column will not be detected by respiration measurements. The flux will be transparent to our ETS measurements. However, the dissolved organic matter in the ocean, at least, appears to be oxidizable (Arrieta et al., 2015). In all cases, to a first approximation, one can express our conceptual model using the expression, $R_{CO_2} = F_{C_1} - F_{C_2}$. In other words, in the vertical, one-dimensional case, the changes in the F_C between depths in a water column are equal to the R_{CO_2} between those depths. Extrapolating this conceptual model to the deep ocean water column, using continuous mathematics, and assuming seafloor carbon burial to be small, the F_C into the top of a water column (F_{C_t}) can be calculated by integrating all the R below the top boundary (z_t) to the ocean bottom (z_s).

$$F_{C_t} = \int_{z_t}^{z_s} R_{CO_2}\,dz \tag{2.1}$$

All F_C calculations here are based on depth-normalized power functions of R ($R_{CO_2} = R_m\,(z/z_m)^b$, Table 2.4; only if depth is normalized does the equation achieve balance with units of nmol CO_2 min^{-1} L^{-1}). For the carbon flux ($F_{f\text{-}s}$) through any depth layer in the water column (z_f) down to z_s, we use Eq. 2.2 and its integrated version in Eq. 2.3. Note that these carbon-flux calculations represent the flux at the time the CTD-Niskin cast was made. They are fine-scale calculations of C-Flux.

$$F_{f-s} = \int_{z_f}^{z_s} R_{CO_2}\,dz = \int_{z_f}^{z_s} R_m\,(z/z_m)^b\,dz \tag{2.2}$$

Table 2.3: R_{O_2} as µmol O_2 h^{-1} m^{-3} profiles in the microplankton along the C-line section in September 1976 (roman font values). At the OMZ depths (values in bold), NO_3^- was the electron acceptor and N_2 was produced during denitrification (R_{N_2} as µmol N_2 h^{-1} m^{-3}). C-Line position as well as JASON station number (in parentheses) are given. Depth (z) is in meters and R refers to either R_{O_2} or R_{N_2} depending on the font. Calculations are explained in the text.

C1 (22)		C3 (15)		C3 (21)		C5 (20)		C5 (37)		C8 (19)		C8 (36)		C10 (18)		C12 (17)		C12 (35)		C14 (16)	
z (m)	*R*	*z (m)*	*R*	*z (m)*	*R*	*z (m)*	*R*	*z (m)*	*R*	*z (m)*	*R*	*z (m)*	*R*	*z (m)*	*R*	*z (m)*	*R*	*z (m)*	*R*	*z (m)*	*R*
0.5	56.11	0.5	24.11	0.5	83.99	0.5	119.13	0.5	79.97	0.5	80.32	0.5	87.67	0.5	34.35	0.5	47.14	0.5	144.71	0.5	40.90
4	84.66	6	34.89	5	78.92	3	154.77	4	86.75	4	92.40	5	97.89	5	35.79	6	30.65	3	147.46	7	34.62
6	44.15	9	35.86	9	64.26	6	130.83	7	95.81	8	75.17	8	88.41	8	51.17	10	39.54	5	139.20	11	36.09
10	71.05	17	42.74	14	43.68	9	180.26	11	86.29	12	54.66	12	83.74	15	40.07	16	29.04	9	131.22	18	54.67
16	60.88	28	30.99	21	20.57	14	97.08	17	77.46	19	69.74	19	63.75	24	87.36	26	34.38	13	152.85	28	44.78
24	42.41	42	15.42	33	12.05	21	41.27	27	67.29	29	45.27	29	19.16	36	24.75	40	29.61	21	59.84	43	25.66
				47	**3.15**	**93**	**0.48**	40	71.55	**93**	**1.12**	44	18.08	**233**	**0.16**	**233**	**0.09**	31	34.27	100	4.51
				93	**1.80**	**233**	**0.67**			**233**	**0.48**	**93**	**0.59**	465	0.04			**93**	**0.25**	250	0.73
						465	**0.09**			465	0.62	**233**	**0.15**	1860	0.02			**233**	**0.20**	500	0.22
										930	0.36	465	0.04					465	0.19	750	0.11
										1395	0.22	698	0.03					698	0.04	1000	0.06
												930	0.05					930	0.06	2000	0.09
												1395	0.06					1395	0.05		
																		1860	0.04		

$$F_{f-s} = \{R_m/[(b+1)\, z_m^b]\}\,(z_s^{b+1} - z_f^{b+1}) \tag{2.3}$$

Note that z_f is any depth between z_t and z_s ($z_t \leqslant z_f \leqslant z_s$) and that $F_{f\text{-}s}$ is associated with the microplankton respiration, the greater fraction of water column respiration (King et al., 1978).

The NRE is equivalent to R (mol CO_2 d^{-1} m^{-3}) within an ocean layer (Δz) divided by the F_C (mol C d^{-1} m^{-2}) into the volume of that layer expressed as a percent. Note that the calculation is $(R \times \Delta z)/F_C$. Since the Redfield N/C or P/C ratio is applied to both parts of the ratio, the C, N, or P units cancel out, leaving the ratio unitless. NRE is also related to the carbon flux transfer efficiency (Buesseler and Boyd, 2009; Buesseler et al., 2007b; Burd et al., 2010) through the same layer (Packard and Gómez, 2013). For Fig. 2.2c it was calculated for 20 m layers below the E_z to the ocean bottom from the R models in Table 2.4 and the F_C models in Table 2.6.

Heterotrophic Energy Production (Fig. 2.2d, Table 2.7) was calculated from R_{O_2} and R_{N_2}, derived from the ETS measurements, from the modeled R_{O_2}, or from R_{N_2}. For oxic seawater HEP = $2 \times 2.5 \times 48 \times R_{O_2}$ where 2 represents the number of electron pairs required to reduce O_2 to $2H_2O$, 2.5 represents the ATP/$2e^-$ ratio (Ferguson, 2010), 48 is the ΔG in J per mmol of ATP (Alberty and Goldberg, 1992; Moran et al., 2012), and R_{O_2} is the respiratory O_2 consumption rate as mmol O_2 d^{-1} m^{-3}. For NO_3^-, R in anoxic waters, HEP = $5 \times 1.0 \times 48 \times R_{N_2}$, where 5 is the number of electron pairs required to reduce NO_3 to N_2, 1.0 is the ATP/$2e^-$ ratio (van Loosdrecht et al., 1997; Smolders et al., 1994), 48 is the ΔG as before, and R_{N_2} is the respiratory NO_3^- reduction rate as mmol N_2 d^{-1} m^{-3}.

2.3 **Results**

Oceanographic properties (Table 2.1) on a C-Line transect at 15° S across the Peruvian current upwelling system (Fig. 2.1a) in mid-September of the ENSO transition year, 1976, were measured on the R/V *Eastward* during the JASON-76 cruise of the CUEA-JOINT II expedition. Classic upwelling (Packard et al., 1986; Rykaczewski and Checkley, 2008; Smith, 1968) was evident during this period. Seawater density (σ_t) and NO_3^- sloped surface-ward close to the coast (Fig. 2.1b). From 25m, σ_t rose from 26.0 to 26.1 and NO_3^- rose from 12 to 16 µM. As these dense nutrient-rich waters rose, they fertilized the sunlit

surface waters at the upwelling center (C3, Brink et al., 1981; MacIsaac et al., 1985), and flowed offshore towards C5 and C8, phytoplankton bloomed to 7 mg m^{-3} chlorophyll *a* and 18 mg carbon h^{-1} m^{-3} in productivity (Table 2.1 and Fig. 2.1b). The dynamics of this process could be seen in the variability of the E_z depth. It ranged from a low of 21 m at C5, the maximum biomass and metabolism position, to twice the depth, 43 m, at the offshore position, C14 (Table 2.1). Temporal variability was exemplified at the trench position (C12) where over 1 week, the E_z depth decreased from 40 to 21 m. Minimal variability occurred at position C8, where over 6 days, the E_z depth remained at 29 m (Table 2.1). In general, a shallow E_z is caused by high plankton biomass with a high potential for metabolism and contrary conditions associated with a deep E_z.

Sea surface R_{O_2} ranged 6-fold from a low of 24.1 μmol O_2 m^{-3} h^{-1} at the upwelling center to a high of 144.7 μmol O_2 m^{-3} h^{-1}, 93 km offshore at the trench position, C12 (Table 2.1). Within days, R_{O_2} could change 3-fold both inshore and offshore (Table 2.3). During the week between C3 stations 15 and 21, R_{O_2} rose from 24.1 to 84.0 μmol O_2 m^{-3} h^{-1} and R_{O_2} at C12 rose from 47.1 μmol O_2 m^{-3} h^{-1} (station 17) to 144.7 μmol O_2 m^{-3} h^{-1} (station 35, Table 2.2). This high respiration (*R*) at station 35, occurred in a diatom bloom of *Chaetoceros compressus* and *Ch. lorenzianus*. The documentation of such temporal variability in seawater R_{O_2} has only recently begun (Fernández-Urruzola et al., 2014; Osma et al., 2014). Similar increases were seen in the chlorophyll and net productivity at C3 and C12 (Table 2.1). The co-occurrence of this rise in R_{O_2}, chlorophyll and net productivity suggests seawater R_{O_2} being driven by phytoplankton. Below the immediate sea surface, microplankton R_{O_2} usually increased to a subsurface maximum within the E_z and then decreased dramatically towards the bottom of the E_z and into the dark ocean below (Table 2.2 and Table 2.3). R_{CO_2} (Fig. 2.2a) ranged in the E_z from 0.4 mmol CO_2 m^{-3} d^{-1} in the upwelling center (C3, station 15) to 3 mmol CO_2 m^{-3} d^{-1} at C5, the shelf edge station 20. The lowest epipelagic R_{CO_2} (Table 2.5) compares with the R_{CO_2} range of 22 - 27 mmol CO_2 m^{-2} d^{-1} reported recently in eddy-upwelling in the South China Sea (Jiao et al., 2014). In the denitrifying waters R_{CO_2} was in the μmol range with a low of 4 μmol CO_2 m^{-3} d^{-1} at C5 (station 37) to 133 μmol CO_2 m^{-3} d^{-1} at C3 (station 21). In the mesopelagic waters below 500m (Table 2.5), R_{CO_2} ranged from 0.4 to 6.1 μmol CO_2 m^{-3} d^{-1} over 1 week at C-Line position C8; at other locations R_{CO_2} fell in between this range. Deeper

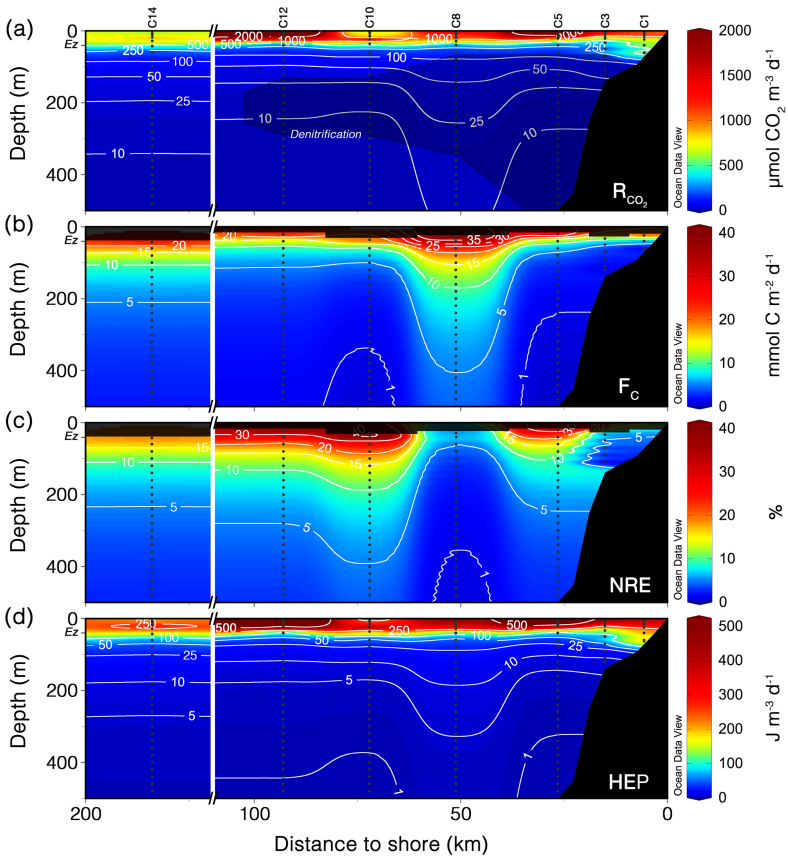

Figure 2.2: Sections for the upper 500 m along the C-line. (**a**) R_{CO_2}; the dark shadow delimits denitrification in the OMZ. In the E_z, R_{CO_2} is calculated directly from ETS-based R_{O_2} (Table 2.3). In the mesopelagic waters below, R_{CO_2} is modeled from the respiration equations in Table 2.4. (**b**) F_C is calculated by integration of the respiration models (Table 2.4) to the ocean bottom according to the Eqs. 2.2 and 2.3. (**c**) NRE, as a percentage, is determined from models in Tables 2.4 and 2.6 as $100\times(R_{CO_2}/F_C)$. (**d**) HEP is either derived directly from ETS activity in the surface waters or from calculated R_{O_2} or R_{N_2} for depths below the E_z (as in Fig 2.2a).

in the water column, over the trench and beyond, bathypelagic R_{CO_2} ranged from 0.3 µmol CO_2 m^{-3} d^{-1} at C10 over the trench to 3.7 µmol CO_2 m^{-3} d^{-1} at C8 over the continental slope (Table 2.5). Benthic R_{CO_2} and C burial (Table 2.5 and Fig. 2.3a) ranged from a high of 90 mmol CO_2 m^{-2} d^{-1} at C3, the

Table 2.4: Power functions for microplankton R (mmol CO_2 d^{-1} m^{-3}) as functions of normalized depth, $R_{CO_2} = R_m\ (z/z_m)^b$, where R_{CO_2} is the respiratory CO_2 production at any depth (z), R_m is the R maximum (mmol CO_2 d^{-1} m^{-3}) in the water column, z/z_m is the depth normalized by the depth at R_m, and b is the maximum curvature of the power function. Both z/z_m and b are unitless. Δz represents the depth range of the R values considered. The table includes the r^2 from the least-square regression analysis of the R models (Sigma Plot vs. 12.5) and the number of data considered (n). The significance level of the regressions is indicated by increasing number of stars. The last four columns represent the linear regression of the respiration model verification analysis. The slope, the intercept and the r^2 are given. The n value for each verification analysis is the same as the n used for each R model (column 7). These R models are based on ETS activity data taken during R/V *Eastward* JASON-76 expedition, along the C-Line.

CUEA C-Line Position	Δz	z_m	R_m (mmol CO_2	b	r^2	n	Modeled *vs* Calculated R_{CO_2}			
(JASON Station)	(m)	(m)	d^{-1} m^{-3})				slope	intercept	r^2	n
C1 (22)	4-24	4	1.538	-0.355	0.864	4	0.975	25.24	0.878	4
C3 (15)	17-42	17	0.783	-1.109	0.929	3	1.041	20.42	0.926	3
C3 (21)	5-93	0.5	20.659	-1.080	0.972***	7	1.095	45.37	0.905**	7
C5 (20)	9-465	9	2.796	-1.655	0.951**	6	0.890	4.25	0.996**	6
C5 (37)	7-40	7	1.596	-0.192	0.873*	5	0.875	168.87	0.902*	5
C8 (19)	4-1395	4	3.247	-1.168	0.957***	10	1.348	129.78	0.686*	10
C8 (36)	5-1395	5	4.413	-1.670	0.949***	12	0.937	-44.14	0.808**	12
C10 (18)	24-1860	24	0.946	-2.051	0.962*	5	0.638	29.3	0.976*	5
C12 (17)	0.5-233	0.5	3.172	-0.720	0.497	7	2.596	-661.42	0.339	7
C12 (35)	13-1860	13	1.630	-1.740	0.948***	10	0.627	10.56	0.998**	10
C14 (16)	18-2000	18	1.183	-1.624	0.968***	9	1.043	-19.72	0.910**	9

* Significant at level $p < 0.05$; ** $p < 0.001$; *** $p < 0.0001$

upwelling center, to a low of 0.09 mmol CO_2 m^{-2} d^{-1} at trench position, C10, with a depth of 4300 m. The R_{CO_2} section in Fig. 2.2a shows the strength of R and its associated remineralization in the upper 50 m of the water column and a tongue of high R descending deeper into the water column at position C8, 50 km off the coast. F_C along the C-Line transect is shown in Fig. 2.2b. In order to include the inshore stations, F_C, in Fig. 2.2b, only represents that part of the C-flux that supports the water column respiration. It does not include benthic R and C burial. To scale our F_C calculations, F_C at 150 m, seaward of C8, ranging from 3 to 6 mmol CO_2 m^{-3} d^{-1} (Table 2.6) are comparable to the range of 2.5 to 6.2 mmol CO_2 m^{-3} d^{-1} recently measured at 100 m by (Jiao et al., 2014).

Table 2.5: Microplankton respiration in epipelagic, mesopelagic, and bathypelagic waters along the C-Line across the Peruvian current upwelling system at 15° S. Calculations are based on the *R* models in Table 2.4. Shoreward of C5, the bottom limits the lower depth boundary. Note the 1000-fold shift in the rates expressed per area (columns 3 - 7) and per volume (columns 8 - 10).

CUEA C-Line Position (JASON station)	Ocean depth (m)	Water column *R* (mmol C m^{-2} d^{-1})	Benthic respiration and C burial (mmol C m^{-2} d^{-1})	Epipelagic 1 - 150 m (mmol C m^{-2} d^{-1})	Mesopelagic 150 - 1000 m (mmol C m^{-2} d^{-1})	Bathypelagic 1000 m - bottom (mmol C m^{-2} d^{-1})	Epipelagic 1 - 150 m (μmol C m^{-3} d^{-1})	Mesopelagic 150 - 1000 m (μmol C m^{-3} d^{-1})	Bathypelagic 1000 m - bottom (μmol C m^{-3} d^{-1})
C1 (22)	63	53.98	-	53.98	-	-	856.85	-	-
C3 (15)	117	80.32	99.23	80.32	-	-	686.50	-	-
C3 (21)	120	45.81	82.99	45.81	-	-	381.75	-	-
C5 (20)	550	252.48	2.60	248.99	3.49	-	1659.96	8.72	-
C5 (37)	607	507.91	-	162.98	344.93	-	1086.51	754.78	-
C8 (19)	1880	82.10	27.37	67.58	11.46	3.07	450.51	13.48	3.49
C8 (36)	2150	153.46	0.57	150.65	2.43	0.38	1004.36	2.85	0.33
C10 (18)	4300	1256.23	0.09	1262.18	2.72	0.34	8414.54	3.20	0.10
C12 (17)	4000	64.36	-	22.28	19.57	22.51	148.55	23.02	7.50
C12 (35)	4755	318.83	0.36	314.51	3.53	0.79	2096.75	4.16	0.21
C14 (16)	2680	318.14	1.50	310.56	6.30	1.28	2070.43	7.41	0.76

Table 2.6: Carbon flux models F_C at C-Line positions deeper than 500 m in the Peruvian upwelling system in Sep 1976. From these models, F_C at four different depths were determined. NRE and F_C Transfer Efficiency (T_{eff}) for the upper mesopelagic waters (150 - 500m) are also given. NRE was calculated as $100 \times R_{CO_2}/F_{C_{150}}$, where the R_{CO_2} represents the integrated R between 150 - 500 m; T_{eff} was calculated as $100 \times F_{C_{500}}/F_{C_{150}}$ according to Buesseler et al. (2007b).

CUEA C-Line Position (JASON Station)	Ocean depth (m)	Euphotic zone, E_z (m)	F_C models	F_C from E_z (mmol C m^{-2} d^{-1})	F_C from 150 m (mmol C m^{-2} d^{-1})	F_C from 500 m (mmol C m^{-2} d^{-1})	F_C from 1000 m (mmol C m^{-2} d^{-1})	NRE 150 - 500 m (%)	T_{eff} 150 - 500 m (%)
C5 (20)	550	21	$22.07(z/z_e)^{-0.655}$	22.07	6.09	2.77	-	54.6	45.4
C8 (19)	1880	29	$55.25(z/z_e)^{-0.168}$	55.25	41.92	34.24	30.48	18.3	81.7
C8 (36)	2150	29	$10.14(z/z_e)^{-0.670}$	10.14	3.37	1.51	0.95	55.4	44.6
C10 (18)	4300	36	$14.11(z/z_e)^{-1.051}$	14.11	3.15	0.89	0.43	71.8	28.2
C12 (35)	4755	21	$20.07(z/z_e)^{-0.740}$	20.07	4.68	1.92	1.15	59.0	41.0
C14 (16)	2680	43	$19.80(z/z_e)^{-0.624}$	19.80	5.81	2.74	1.78	52.8	47.2

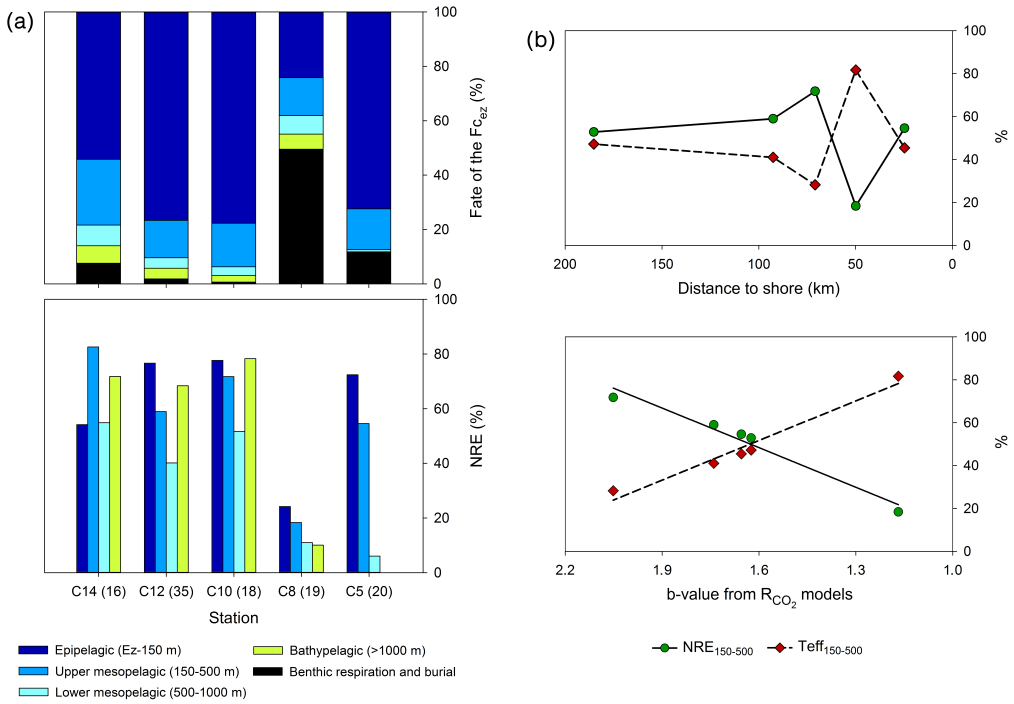

Figure 2.3: (**a**) Fate of the carbon fluxing out of the E_z ($F_{C_{Ez}}$) into the water column and seafloor below (as a percent of the total flux) along the C-Line (top panel). In the water column, the carbon is remineralized through R. In the benthos, part of the carbon is remineralized and returned to the water column above and part is buried. The bottom panel shows the different efficiencies with which carbon is remineralized through respiration in four different zones of the water column along the C-Line. (**b**) Top panel: variability of the NRE and the T_{eff} in the upper mesopelagic waters (150 - 500 m) along the C-line. Bottom panel: NRE and T_{eff} as a function of the maximum curvature b (absolute value) in the R_{CO_2} models from Table 2.4.

As one would expect with strong F_C at C8, even at 1000 m, the carbon flux transfer efficiency (T_{eff}) at this station (19) is high and the NRE low (Table 2.6, Fig. 2.3b). T_{eff} between 150 and 500 m ($T_{\text{eff}_{500}}$) is 82 and the NRE is only 18 % (Table 2.6). Unexpectedly, despite the decrease in F_C throughout the water column at C8 between 17 and 23 September, $T_{\text{eff}_{500}}$ only decreased by less than a factor of 2 to 45 % (Table 2.6). The impact on the NRE was greater,

increasing 3-fold to 55 % (Table 2.6). $T_{\mathrm{eff}_{500}}$ at other locations ranged from 28 at C10 to 47 at C14 (Fig. 2.3b). In addition to this unique documentation of the temporal variability of F_{C} from Table 2.6, Fig. 2.2b demonstrates its mesoscale spatial variability. That transect shows a maxima occurring throughout the water column, 50 km from the coast at the upper slope position, C8. As Table 2.5 and Fig. 2.3a show, the benthic R and burial are also high at this location. Fig. 2.3b highlights the importance of the maximum curvature of the respiration-depth profile. As $|b|$ increases towards 2 the NRE increases towards 70 % and the $T_{\mathrm{eff}_{150-500}}$ decreases towards 30 %.

HEP in the E_z (Fig. 2.2d and Table 2.7) ranges from a high of 555 J d^{-1} m^{-3} at the R maximum at C5 (station 20) to a low of 69 J d^{-1} m^{-3} at the bottom of the E_z at C3 (station 21). It drops slightly over the continental slope, but further offshore over the trench (C12) high values of 880 J d^{-1} m^{-3} can be found (Fig. 2.2d). In the far offshore, the E_z HEP only reaches values of 315 J d^{-1} m^{-3}. As an example of low HEP values, at 4755 m in the trench it decreases to 0.02 J d^{-1} m^{-3}. Thus the range of HEP by all the respiratory ETS and oxidative phosphorylation coupling in the microplankton of this part of the Peruvian current upwelling system spans 4 orders of magnitude from 0.02 J d^{-1} m^{-3} in the abyssopelagic waters of the trench to 880 J d^{-1} m^{-3} in the E_z above. This is the first time such calculations have been made. Integrating the

Table 2.7: HEP as ATP production in epipelagic, mesopelagic, and bathypelagic waters of the C-Line section, September 1976. Shoreward of C5 the bottom limits the lower depth boundary.

CUEA C-Line Location (JASON station)	Ocean depth (m)	Epipelagic HEP 1 - 150 m (J m^{-3} d^{-1})	Mesopelagic HEP 150 - 1000 m (J m^{-3} d^{-1})	Bathypelagic HEP 1000 m - bottom (J m^{-3} d^{-1})
C1 (22)	63	289.63	-	-
C3 (15)	117	232.05	-	-
C3 (21)	120	173.40	-	-
C5 (20)	550	977.93	1.19	-
C5 (37)	607	367.24	255.11	-
C8 (19)	1880	138.77	3.59	0.89
C8 (36)	2150	319.41	0.80	0.09
C10 (18)	4300	2609.16	0.89	0.03
C12 (17)	4000	43.60	4.56	1.23
C12 (35)	4755	535.98	1.18	0.06
C14 (16)	2680	699.88	2.51	0.26

epipelagic HEP (Table 2.7) over the upper 150 m yields a range from a low of 6.6×10^{-3} MJ d^{-1} m^{-2} to a high of 0.39 MJ d^{-1} m^{-2}, averaging 0.09 MJ d^{-1} m^{-2}. This average HEP is only 0.7 % of the average solar radiation (13.5±4.0 MJ d^{-1} m^{-2}) at the C-Line sea surface between 12 and 24 September during the JASON-76 cruise (Packard and Jones, 1976).

2.4 Discussion

Here we have demonstrated the calculation of R_{CO_2}, F_C, NRE, and HEP in an ocean section from microplankton ETS activity measurements. We have previously explained how ocean water column R_{CO_2} determines F_C of labile organic matter by oxidizing sinking POC and mineralizing phosphate and nitrate (Osma et al., 2014; Packard and Codispoti, 2007). Fig. 2.3b shows that the maximum curvature of the respiration-depth profile determines NRE as well as F_C transfer efficiency. The offshore R_{CO_2} section (Fig. 2.2a) shows the variability of R with depth and location in the upwelling area. Fig. 2.2a also shows how seawater respiration is displaced seaward to C8 from the chlorophyll maximum at C5 (Fig. 2.1b). The F_C section (Fig. 2.2b) demonstrates the power of using R to calculate spatial variability of F_C by revealing an F_C maximum over the upper part of the continental slope. The NRE section (Fig. 2.2c) reveals its inverse relationship to F_C as well as its variability in the water column. This ability of the water column to retain nutrients would not have been detected without the original ETS activity profiles. The HEP section (Fig. 2.2d), showing the energy production by the ATPases in microbial mitochondrion and plasmalemma membranes of bacteria and archaea in the water column, is a new representation of ATP production in oceanographic analysis. Because a major purpose of all forms of respiration is to make ATP, HEP should reflect R_{CO_2} in any section or profile. The similarity of the R_{CO_2} pattern in Fig. 2.2a and the HEP pattern in Fig. 2.2d confirms this.

Ocean R_{CO_2} filters sinking labile POC and should vary inversely with benthic R and carbon burial. However, the relationship between the two variables is more complicated (Figs. 2.2a and 2.3a). We can see this in the R maximum 50 km off the Peruvian coast at C-Line position C8. One might expect low benthic R and carbon burial here (Table 2.5), but that is not the case (Fig. 2.3a). From the difference between integrating the R function (Eq 2.2) to infinity and integrating it to the ocean bottom ($z = s$) we calculate a high level of benthic R and carbon burial (Fig. 2.3a). The minimum NRE at C-Line position, C8, in Fig.

2.2c explains this discrepancy. The delivery of labile POC to the bottom depends not directly on F_C, but on the ratio of the water column R (Fig. 2.2a) to F_C (Fig. 2.2b). Recent studies of the organic carbon preservation on the upper parts of the Peruvian continental slope (Dale et al., 2015) support these calculations of high carbon burial (Fig. 2.3a). They find high burial rates at depths between 200 and 400m (the upper part of the Peruvian continental slope) and attribute it to the anoxia overlying these sediments. A C-Line section of the T_{eff}, the difference between NRE and 1, would have revealed a T_{eff} maximum at C8. One can deduce this from Fig. 2.3b (lower panel).

ETS measurements can be used not only to calculate F_C, NRE, and HEP, but also to calculate biological heat production (Pamatmat et al., 1981), age, and flow rates of deep and bottom waters (Packard, 1985b). In anoxic waters, if the background chemistry (Richards, 1965) is known, ETS measurements provide proxy rate measurements for denitrification (Codispoti and Packard, 1980; Dalsgarrd et al., 2012; Packard, 1969), NO_2^- production, nitrous oxide production, and sulfide production (Packard et al., 1983), and even for iron and magnesium reduction rates (Lane et al., 2010). All of these types of microbial metabolism are different forms of R, but they are controlled by the same basic respiratory ETS with NADH dehydrogenase (Complex 1) as the common gatekeeper. Furthermore, because the energy generation of nitrification is based on a variation of this ETS, an ETS measurement is also likely a proxy for nitrification.

HEP, as ATP generation in the ocean water column, could have been calculated from R_{O_2} since 1943, the time the Nobelist Severo Ochoa first established the connection between ATP production and R (Ochoa, 1943). However, until now, calculations of biological energy production (shown in Fig. 2.2d), including HEP, in the ocean had not been made (Karl, 2014). Now the time is appropiate to make such calculations with recent research (Chen and Strous, 2013; Lane, 2002, 2005, 2009; Wilson et al., 2012) documenting the ubiquity of respiratory ETS in the biosphere, how it relates to R_{O_2}, to all other ocean respiratory processes, and to HEP as ATP production. As we have seen above, HEP and R_{CO_2} in the Peruvian upwelling system have similar time and space distributions (Figs. 2.2a and 2.2d). The small difference in the ATP/$2e^-$ relationships between oxidative phosphorylation and the rate of electron transfer in aerobic metabolism and denitrification has minimal impact. In aerobic metabolism, the ATP/$2e^-$ ratio is 2.5 and in denitrifying microbes ATP/$2e^-$ is 1.0

(van Loosdrecht et al., 1997; Smolders et al., 1994). At the rate anammox research is progressing (Dalsgarrd et al., 2012), its relative contribution will soon be known, too. In any case, less ATP should be produced in anoxic waters resulting in a lower HEP. It will be interesting in the future to look for this difference by comparing HEP offshore sections made through oxic and anoxic sectors of upwelling systems.

2.5 Conclusions

Organic carbon fluxes are critical components of reliable carbon budgets, but they are so difficult to measure that rarely can enough measurements be amassed to construct a synoptic section of F_C. Here, from plankton respiration models, we present an original mode of calculating F_C sections as well as benthic respiration and carbon burial. We reveal the importance of plankton respiration in determining the capacity of a plankton community in retaining water column nutrients, develop the concept of NRE, and demonstrate NRE variability in an ocean section. In addition, we show that the curvature of the respiration profile (the exponent b of the power function) controls both the NRE and F_C. Finally, we use respiration to calculate the heterotrophic energy production (HEP), the rate of ATP generated by plankton metabolism, and find an HEP maximum over the shelf break on the upper part of the Peruvian continental slope.

Acknowledgements. We thank, J Ammerman, RT Barber, D Blasco, RC Dugdale, N Garfield, and J Kogelschatz, for their collaboration. D. Bourgault revealed the role of depth-normalization. The challenges from the three reviewers led to many improvements in this paper and for their diligence we are thankful. NSF (USA) Grant OCE 75-23718A01 (TTP) funded JASON-76. The Basque Government (NO and I F-U), MEC (Spain) project BIOMBA, CTM2012-32729/MAR (MG), and CIE (Canary Islands):Tricontinental Atlantic Campus (TTP) funded analysis.

The scientist is not a person who gives the right answers, he/she's one who asks the right questions.

Claude Lévi-Strauss

CHAPTER

3

CAPÍTULO

Short-term patterns of vertical particle flux in northern Benguela: A comparison between sinking POC and respiratory carbon consumption

N. Osma, I. Fernández–Urruzola, T. T. Packard, L. Postel, M. Gómez and F. Pollehne (2014), Journal of Marine Systems 140 (B), 150–162.

http://dx.doi.org/10.1016/j.jmarsys.2014.01.004

ABSTRACT: Short-term variability of vertical carbon flux (C-flux) was assessed by two approaches at two stations on the Namibian shelf upwelling system (20° S). The first approach was based on modeling water-column respiratory CO_2 production (F_C) by integrating vertical profiles of the respiratory electron transport system. The second approach was based on automated sediment traps, sampling daily. In both cases, temporal variability at the same station proved to be greater than the spatial variability between stations. Comparison of the two methods yielded higher C-flux values from the sediment traps in the presence of upwelling filaments (7.85 *vs* 3.67 mmol C m^{-2} d^{-1}). Contrarily, in the post-filament stage of the upwelling system, the values from the F_C models were higher (1.43 *vs* 2.57 mmol C m^{-2} d^{-1}). This difference

was attributed to compositional changes in sinking particles and their settling velocities. In combination, both approaches served to increase current understanding of the short-term particle fluxes in this northern Benguela upwelling system. The F_C approach was further applied to zooplankton from the same area in order to quantify their importance in attenuating the particulate organic C-flux. This attenuation, as measured by fractional consumption of the primary productivity, ranged from 2 % to 20 %.

Keywords: Electron transport system (ETS); Respiratory oxygen consumption; Particulate organic carbon (POC) flux; Sediment traps; Namibian Upwelling System.

3.1 Introduction

Both loss of material from the water column and gain to the sediment are important processes in marine ecology and biogeochemistry, as the transport balance between the water and the sediment controls the biodiversity and the abundance of marine organisms on local and global scales. Upwelling systems, as hotspots of marine productivity, are particularly interesting in this concern, as pelagic and benthic process are coupled by direct feedback loops, which often affect the speciation of elements (carbon, nitrogen and phosphorus) on a basin-wide level. Both pelagic and benthic biodiversity in upwelling regions reflect these conditions, where organisms adapt to the specific environmental constraints and, at the same time, are actively involved in the production of them. Thus, the balance between sinking particles and the benthic metabolism determines the role of sediments in either accumulating elements or modifying their speciation with a direct effect on surface layer productivity, e.g., when fueling the "new production" (*sensu* Dugdale and Goering, 1967). The vertical flux of particulate organic carbon (POC) is an important driver in this network, as it is considered a key mechanism in sequestering carbon to the ocean's interior. Nutrient-rich upwelled waters in the sunlit layer favor photosynthetic organisms to convert inorganic carbon into organic carbon, which is transferred to the deep ocean by gravitational sinking processes, active transport by animals and water mixing, altogether known as the "biological pump" (Volk and Hoffert, 1985). This downward flux of POC is consumed by the water column organisms to support their metabolic requirements and, eventually, placed onto the seafloor where it is consumed by benthic organisms and buried in the sediments. The magnitude of the vertical carbon export from the

surface varies from higher values found at systems with more variable production owing to strong seasonal changes, to lower values at environments with more stable conditions (Berger and Wefer, 1990). Indeed, several authors have estimated that the biologically produced carbon export from the euphotic zone is about 25 % in high production areas, such as the coastal upwellings, whereas it drops to 10 % in the oligotrophic open-ocean areas (Berger et al., 1989; Buesseler, 1998; Martin et al., 1987; Schlitzer, 2000).

Quantification of vertical carbon fluxes (C-flux) has been the focus of international research programs during the last decades (e.g., Joint Global Ocean Flux Study, JGOFS), in which the rain of POC through the ocean water column was measured by either sediment traps or the ^{234}Th/^{238}U method. Elemental fluxes in upwelling and adjacent oligotrophic regions have been compared, for instance, by Pollehne et al. (1993a,b) with drifting traps in short term intervals. However, the number of studies that relate these fluxes to the metabolic activities of the organisms in the water column is sparse in the literature, despite the importance of respiration as the major biological process involved in POC attenuation. Steinberg et al. (2008) compared the bacteria and zooplankton metabolic requirements to the sinking POC flux by inferring their respiration and carbon demands from growth efficiencies and biomass, respectively. But to our knowledge, no study has determined the carbon flux associated with the respiration profiles of both microplankton and zooplankton and directly compared it with the sinking POC collected by the sediment traps. In this context, Packard and Christensen (2004) proposed a conceptual model to determine the C-flux from vertical profiles of plankton respiration (modeled C-flux, hereafter, F_C), and it has been recently applied to estimate the zooplankton associated F_C in waters of the Canary Islands (Packard and Gómez, 2013). The basis of this approach is the reality that plankton in the ocean water column eat and degrade sinking POC, metabolize this organic matter within their cells, and, via respiration, release it as CO_2 gas into the water column. Considering a cube of seawater, the amount of CO_2 released into the dissolved phase (into the water) equals the difference between the POC entering at the top of the cube and the POC leaving through the bottom of the cube. If each cube is 1 m^3 then the C-flux through the 100 m level of the ocean with a depth of 5000 m is the respiratory CO_2 production rate (R_{CO_2}) of every cube of seawater from 100 m to the bottom of the ocean. Mathematically, the integration of the R_{CO_2} depth profiles from any depth in the water column to the seafloor indicates the

amount of POC required to fuel the respiration of the organisms below that depth. Here, we have determined the respiration from the enzymatic activity of the respiratory electron transfer system (ETS). Since it was originally described by Packard et al. (1971), this methodology has been widely applied in the field of oceanography, as it allows a high data acquisition rate and provides sensitivity enough to quantify community respiration even in the mesopelagic and bathypelagic realms.

The present research work was accomplished at the Terrace Bay shelf off Namibia (20° S), under the influence of the northern Benguela upwelling system. This region is bordered at the north by the warm waters of the southward Angola Current and by the permanent Luderitz (26° S) upwelling cell at the south (Boyer et al., 2000). Although it is mostly perennial, it presents a pronounced seasonal peak during the austral winter and spring and an upwelling relaxation in autumn (Shannon and Nelson, 1996). The domain of the upwelled waters in this region extends further offshore than in the southern Benguela (Bakun and Nelson, 1991), mainly due to differences in the wind regimes and the shelf morphology. Moreover, this part is usually affected by the jets and filaments emerging from the main upwelling cell (Shillington et al., 1992). Therefore, the shelf off Terrace Bay is characterized by important instabilities and a high temporal and spatial variability. Previous works in this area have focused on long term patterns of vertical particle fluxes in order to study seasonality or inter-annual variability (Fisher and Wefer, 1996; Giraudeau et al., 2000; Romero et al., 2002), as well as to describe spatial patchiness in the organic matter deposition on the continental shelf (Monteiro et al., 2005), with the finest temporal scale of weeks. In our case, we decreased the sampling frequency to 24 hours, which enabled us to detect the daily variability of the particles export. The high productivity in the surface layer (Estrada and Marrasé, 1987; Carr, 2001), in turn, allowed the sediment traps to catch material enough for the analysis within this sampling time.

Accordingly, we simultaneously performed direct measurements of particle flux by daily means of sediment traps and collected ETS data for the calculation of carbon losses from the water column respiration in a comparative approach. A secondary aim was to apply the F_C determination to zooplankton samples collected along a cross-shelf transect carried out at 20° S during the same cruise, so as to quantify the impact of these organisms on the vertical carbon flux via their respiration and to show the usefulness of this approach

when high spatial resolution is needed.

3.2 Material and methods

3.2.1 Location and Sampling

Samples were collected during the SUCCESSION cruise aboard R/V *Maria S. Merian* off Terrace Bay (Namibia), from 24 August to 17 September 2011. Aside from the cross-shelf transect sampling, two stations were specifically studied (Fig. 3.1, Table 3.1): an inshore station NAM006 (20° 15.66' S, 12° 33.18' E) located on the shelf at 206 m depth and an offshore station NAM011 (20° 30.48' S, 12° 7.98' E) on the shelf break at 395 m depth. Moorings were placed successively for 13 days at NAM006 and 10 days at NAM011. Water column samples for ETS activity were taken when the sediment trap was recovered at the inshore station (NAM006R) and both times when it was deployed and recovered at the offshore station (NAM011D and NAM011R).

Seawater samples for microplankton ETS activity and chlorophyll *a* determination were taken at eight to nine discrete depths with 10-L Niskin bottles mounted on a rosette. At each cast, physical properties such as temperature, salinity and dissolved oxygen concentration were determined by the sensors of the CTD unit (SBE 911+, Seabird electronics.). Zooplankton samples were

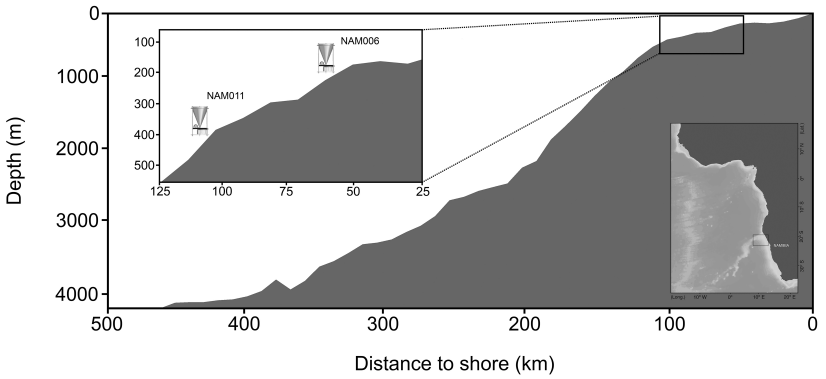

Figure 3.1: Cross-shelf section of the study area at 20° S off Walvis Bay (Namibia), showing the sediment traps moorings on the continental shelf at 150 m (NAM006) and close to the shelf-break at 320 m (NAM011). Stations position and sampling time are described in Table 3.1.

Table 3.1: Station location and seawater characteristics at inshore (NAM006) and offshore (NAM011) stations where the vertical fluxes were determined during the SUCCESSION cruise in August/September 2011. NAM006R and NAM011R represent the water column sampling when the sediment traps (STs) were recovered, while NAM011D represents the water column sampling when the ST was deployed. Temperature (Temp), salinity (S) and oxygen concentration (O_2) for each sampling are given. The euphotic zone (E_z) was set at 60 m, as the maximum chlorophyl peaks were above this depth at the three stations (Fig. 3.1). 150 m and 320 m indicate the depths at which the STs were moored at NAM006 and NAM011, respectively.

Sediment Traps		**NAM006**			**NAM011**				
	Position	20° 15.66' S, 12° 33.18' E			20° 30.48' S, 12° 7.98' E				
	Distance to shore	60 km			110 km				
	Bottom	206 m			395 m				
	STs depth	150 m			320 m				
	Deployment	24 Aug. - 6 Sept.			7 Sept. - 17 Sept.				
		NAM006R			NAM011D			NAM011R		
Water column		Temp (° C)	S	O_2 (µM)	Temp (° C)	S	O_2 (µM)	Temp (° C)	S	O_2 (µM)
	Surface	14.1	35.23	258	14.7	35.29	272	15.8	35.43	242
	60 m (Ez)	13.5	35.28	92	13.9	35.23	217	15.3	35.41	203
	150 m	12.6	35.20	41	12.9	35.22	62	12.9	35.23	43
	320 m	–	–	–	9.8	34.88	24	9.9	34.90	27

obtained from net hauls at five to six depth intervals with a 100 µm mesh MultiNet (Hydrobios GmbH, Kiel, Germany).

The stations position, sampling procedure and ETS activities of the zooplankton samples collected likewise along the four transects surveyed during this cruise are explained in Fernández-Urruzola et al. (2014). The mean ETS activity values for the four transects were used to determine the F_C at ten selected stations, which were divided into a coastal, transition and oceanic area, according to the distinct differences in geological and oceanographical properties.

3.2.2 **ETS activity and respiration**

Seawater samples for microplankton ETS activity were prefiltered through a 100 µm mesh in order to avoid the incidental inclusion of larger zooplankton. Then, four to six liters of this seawater were filtered at room temperature using Whatman GF/F 25 mm glass fiber filters. They were folded to an eighth and blotted to remove excess water, placed in cryovials and frozen in liquid N_2 (–196 °C). Zooplankton samples were split into 100 - 200 µm, 200 - 500 µm, 500 - 1000 µm and larger than 1000 µm size fractions, placed in cryovials and

frozen in liquid N_2. After 30 minutes, all the samples were transferred to an ultrafreezer and stored at –80 °C until analysis.

The ETS activity was measured kinetically by the Owens and King (1975b) method, according to the variations described in Maldonado et al. (2012). Additionally, the reagents and reaction volumes were reduced by a factor of 2.5 and the assay time was reduced to 6 minutes, depending on the linearity of the reaction and the large coefficients of determination (in most cases, $r^2 \geq 0.99$) during the reaction. The INT-formazan production rate was related to ETS activity and to potential respiration rates (Φ) as previously defined in Packard and Williams (1981). Table 3.2 shows the step-by-step procedure to calculate the respiratory oxygen consumption (R_{O_2}) from the formazan production rates. The chromogenic tetrazolium INT (2-p-iodophenyl-3-p-nitrophenyl monotetrazolium chloride) is preferentially reduced by the respiratory ETS enzymes, replacing O_2 as the electron acceptor. The INT accepts two electrons while the O_2 would accept four. Therefore, the INT- formazan production rate (µmol m^{-3} d^{-1}) is stoichiometrically related by a factor of 2 to ETS activity (µmol e^- m^{-3} d^{-1}) and by a factor of 0.5 to Φ (µmol O_2 m^{-3} d^{-1}). All the Φ rates were corrected to *in situ* temperature using the Arrhenius equation (Packard et al., 1975).

Although, in the majority of the zooplankton samples (82 %) there was no detectable contamination by phytoplankton, in a minority of the samples (18 %), phytoplankton contamination was noticeable. Principally, it was observed during zooplankton size fractionation process, mostly in the 100 - 200 µm and 200 - 500 µm sizes from the surface waters at the mid shelf. On a biomass basis, these contaminated zooplankton samples contained 35 ± 24 % phytoplankton, on average. To correct the measured zooplankton ETS activity for this, we measured the chlorophyll and protein in both the phytoplankton and the zooplankton samples. The measured protein/chlorophyll ratio in the phytoplankton samples was 4.6 mg chl *a* per mg protein (n =16, r^2 = 0.80, $p < 0.0001$). This ratio was used to estimate the phytoplankton associated-protein in zooplankton samples. After subtracting this algal contribution to the protein content, an ETS/protein ratio of 61.6 µmol O_2 d^{-1} mg−1 protein was applied to determine the zooplankton associated-ETS activity. This ratio was obtained from a regression analysis of non-contaminated zooplankton samples taken along the transect survey during this cruise (ETS = 61.6 Protein, n = 91, r^2 = 0.93).

Table 3.2: Example of the step-by-step calculation of ETS activity and water column respiration (R_{O_2}) from INT-formazan production in microplankton from NAM011D. The formazan production rate is stoichiometrically related by a factor of 2 to ETS activity and by a factor of 0.5 to potential respiration (Φ). The Arrhenius equation was applied to determine Φ at *in situ* temperature in column 5 (Packard et al., 1975). R_{O_2} was calculated from Φ in column 5 using a R_{O_2}/Φ ratio of 0.26. All these calculations are described in Packard and Christensen (2004).

Depth (m)	Formazan prod. (µmol m^{-3} d^{-1})	ETS activity (µmol e^- m^{-3} d^{-1})	Φ (µmol O_2 m^{-3} d^{-1})		R_{O_2} (µmol O_2 m^{-3} d^{-1})
			T_{assay}	T_{insitu}	T_{insitu}
5	1797	3594	898	832	216
10	1546	3093	773	751	195
50	822	1644	411	378	98
75	1111	2222	555	507	132
100	473	946	237	217	56
180	365	729	182	148	38
280	417	833	208	142	37
330	391	781	195	127	33
380	417	833	208	134	35

R_{O_2} (µmol O_2 m^{-3} d^{-1}) for microplankton and zooplankton at the sediment traps stations is presented in Fig. 3.3. It was calculated from the relationship between the Φ and R_{O_2} in the water column. The R_{O_2}/Φ value used for microplankton was 0.26 (Packard and Christensen, 2004) and for zooplankton was 0.48, both ratios are unitless. The latter was determined in parallel incubation experiments conducted onboard, in which the ETS activity and R_{O_2} were measured in organisms of different size fractions. Zooplankters were collected by vertical WP-2 net hauls and immediately fractionated into 200 - 500 µm, 500 - 1000 µm and > 1000 µm size classes. Once acclimated in filtered seawater at *in situ* temperature (15 ± 1 ° C), healthy organisms were transferred into 60 mL cap-glass bottles and incubated for two hours. This short incubation-time ensured no bias due to starvation episodes. The dissolved O_2 concentration in the bottles were continuously measured through a 6-channel Strathkelvin 928 Oxygen System® respirometer. Each batch of work included at least one control flask without organisms. Afterwards, the zooplankters were removed and frozen at –80 °C so as to analyze the ETS activity as described above. A mean R_{O_2}/Φ value of 0.48 (± 0.29, n = 19), as mentioned above, was obtained for

the mesozooplankton community, which agrees with previous values reported in the literature of 0.5 (Hernández-León and Gómez, 1996).

3.2.3 Modeled carbon flux (F_C) calculations

The respiratory CO_2 production (R_{CO_2}) was determined from R_{O_2} and a revised molar Redfield ratio for C/O_2 of 0.71 (Takahashi et al., 1985). The R_{CO_2} (µmol C m^{-3} d^{-1}) data were used to determine the respiration depth-profile (z) for microplankton and zooplankton at the three stations. According to a non-linear least-square method used in the Excel software (Brown, 2001), the best fits for each profile were the power function ($R_{CO_2} = R_0 z^b$) and the logarithmic function (R_{CO_2} = aLn(z) + c), without significant differences between them (one-way ANOVA, $p = 0.653$). Therefore, and in order to follow the approach adopted in previous studies (Martin et al., 1987; Packard and Christensen, 2004; Buesseler et al., 2007b), the power function was applied. Additionally, Packard et al. (1983) pointed out that this model fits the data better in the deeper part of the water column. The term R_0 in the equation represents the surface R_{CO_2} and the exponent b determines the curvature of the profile; more negative values indicate greater decrease of respiration with depth, and viceversa. If a layer in the water column is considered, the difference between the C-flux at the top depth and the C-flux at the bottom depth can be equated to the respiratory CO_2 production within this layer under steady state conditions. Therefore, the definite integral of the R_{CO_2} profile from the top of a water column (z_t) down to the seafloor (z_s) indicates the carbon flux into the top of that water column that is respired within this depth interval (Eq. 3.1).

$$F_{t-s} = \int_{z_t}^{z_s} R_{CO_2} dz = \int_{z_t}^{z_s} R_0 z^b dz \tag{3.1}$$

Accordingly, these calculations with the lower limit to the definite integral at z_s, do not consider either the benthic respiration or carbon burial. If the upper boundary of the integral is any depth in the water column (z_f), e.g. the sampling depths, the carbon flux from z_f to the seafloor ($F_{f\text{-}s}$) is calculated as in Eq. 3.2.

$$F_{f-s} = [R_0/(b+1)][z_s^{(b+1)} - z_f^{(b+1)}] \tag{3.2}$$

Note that these calculations should only be applied from below the E_z, due

to the high POC production in this upper layer. Thus, if z_f is the bottom of E_z, then the $F_{f\text{-}s}$ represents the carbon export from this layer that fuels the deep water-column respiration to the sediment. By resolving the Eq. 3.2 at several z_f and determining the best fit for these data, the F_C models were determined at each station. The equations of these profiles (see section 3.3) can be used to predict the carbon flux at any depth below the E_z.

3.2.4 **Sinking particles sampling**

Automatic sediment traps of the type Kiel Multitrap K/MT 234 with 0.5 m sample area, 21 collecting glasses and a sampling period of 24 hours were moored successively at NAM006 and NAM011, 50 m above ground at 150 m and 320 m respectively (Table 3.1). The sampling vials contained a salt brine of 70 per mill in order to prevent rinsing and 2 % formaldehyde for preservation of the collected material. After the recovery of the traps, the samples were kept cool (4 °C) until further treatment. Once the samples were split, aliquots were filtered on GF/F glass fibre filters for the analysis of particulate carbon, nitrogen and the isotopic composition of both by means of a Carlo Erba/Fisons 1108 elemental analyzer connected to a Finnigan Mat Delta S isotope ratio mass spectrometer. The isotope values are given in the conventional δ-notation which is related to a known isotope standard and expressed as the difference to the Pee Dee Belemnite (PDB)-standard for carbon and to atmospheric nitrogen (Mariotti et al., 1984) for nitrogen, in per mil. The analytical error for organic carbon and nitrogen determinations is less than 5 %, for the stable isotope composition less than ± 0.2 per mil. The amount of particulate biogenic silica (bSi) was determined from splits on polycarbonate filters according to procedures described in von Bodungen et al. (1991) whereas the analysis of total particulate phosphorus (TPP) was carried out after Grasshoff (1976) from splits on GF/F glass fibre filters. Aliquots of the samples were inspected under an inverted microscope and, if possible, organisms were identified up to the species level. Other aliquots of the collected material were filtered through pre-weighted Millipore Isopore membrane filters (0.45 µm pore size, polycarbonate PC) for SEM-EDX investigations and multi-element analyses, respectively. Scanning electron microscopy (SEM) and energy dispersive X-ray micro-analyses (EDX) were performed on a FEI Quanta 400 microscope connected with an EDAX-Genesis system. About 1 cm^2 of PC filters was glued on Al stubs and covered by pure carbon (vacuum sputtered) to assure electric

conductivity. Measurement parameters of the microscope system during analyses were: high vacuum; 15 kV electron beam; working distance: 10 mm; SE and BSE detector; variable enlargement. The X-ray microanalyses were done by spot analyses on selected particles taking EDX-spectra (EDAX-Econ 4 detector), identification and quantification of the elements after ZAF-correction. Peak overlapping (e.g. Mn kβ and Fe kα lines at 6.4 to 6.5 keV) was solved by holographic peak deconvolution (HPD). Besides manual single particle analyses, the system provides the opportunity of automated particle analyses. The method is based on image processing, particle recognition and element analyses of the particles on a series of different fields of the sample. On average, 2000 single particles of each sample were analyzed by this method. The resulting data set was processed for mineral (or particle group) identification and quantification (counting). Minerals and particle groups are defined by "border values" of the proven elements and calculated element concentrations (or ratios). Analyses of standard mineral samples were used to verify this method (Leipe et al., 1999).

3.3 Results

3.3.1 Sea water characteristics

Temporal variability in the hydrographic properties at the two sampling sites was greater than the spatial effect of the distance from the coast or from the core of the upwelling. These variations are described in Mohrholz et al. (2014), where they show the presence of different water masses in this area and the influence of cold water filaments arising from the south. Accordingly, during the water column sampling, both NAM006R and NAM011D exhibited similar sea water characteristics, but notably different from that of NAM011R (Table 3.1). Surface water at the first two samplings was low in temperature (14.4 ± 0.3 °C), low in salinity (35.26 ± 0.03) and high in O_2 concentration (265 ± 7 µM). Fig. 3.2 shows no strong stratification of the water column at these stations and depicts a surface chlorophyll maximum of 12 mg m^{-3} and 17 mg m^{-3} at NAM006R and NAM011D, respectively. NAM011R, in contrast, exhibited higher temperature, with higher salinity and lower O_2 concentration. The water column was more strongly stratified and the chlorophyll concentration in the surface was more than fifteen times lower than at NAM006R and NAM011D. The chlorophyll reached a maximum value of 0.78 mg m^{-3} at 50

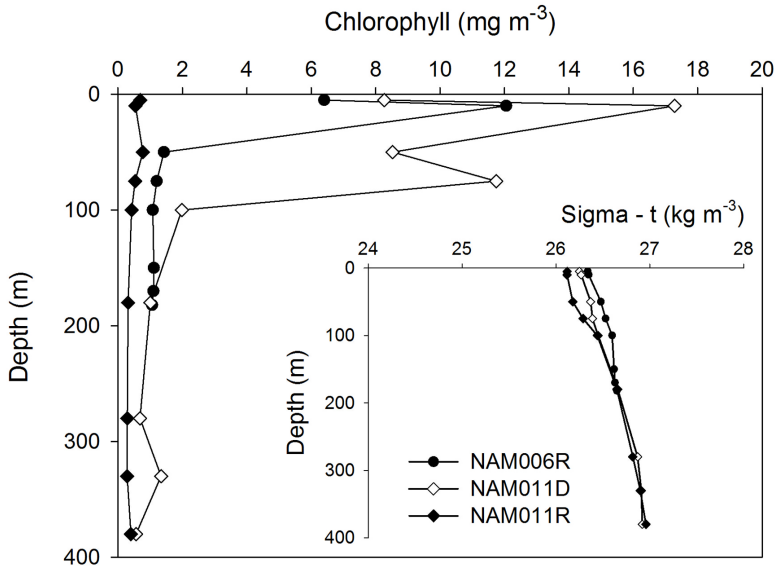

Figure 3.2: Depth-profiles of microplankton chlorophyll (mg m^{-3}) from filtered samples and seawater density as sigma-t (inset) at the sediment trap stations, during the three water column samplings.

m, which is characteristic for the transition to a deep chlorophyll maximum layer in an oligotrophic situation (Pollehne et al., 1993a).

The three water column samplings were conducted at dawn and, accordingly, on the basis of the observations, we established the euphotic zone (E_z) depth. This we defined as the 1 % light level, after considering the values from the nearby stations during the transect survey. They ranged from 23 to 58 m (see section 3.6). In order to be conservative in our calculations of the carbon flux, we decided to set the E_z depth of these three stations at 60 m which included the chlorophyll maxima in all the cases. Although NAM011D displayed a subsurface chlorophyll peak of 12 mg m^{-3} below this depth (at 75 m), it could be attributed to moribund sinking phytoplanktonic cells and, hence, not highly active. Similar events were observed in other high productive systems such as the Costa Rica Dome (Packard et al., 1977) and the Peruvian upwelling (Packard et al., 1983). For the zooplankton-associated F_C calculations of the transect survey, we used the different E_z depths measured at each station (see section 3.6).

3.3.2 Microplankton and zooplankton respiration in the water column

Step-by-step examples of the ETS activity, Φ and R_{O_2} calculations from formazan production rates for microplankton at station NAM011D are given in Table 3.2. As these parameters are related stoichiometrically by constants, changes in the ETS activity will relate linearly to change in Φ and R_{O_2}. Fig. 3.3 shows the R_{O_2} depth profiles at the three stations. Microplankton respiration in the water column followed the same profile as chlorophyll at the three stations, although the correlation between these two parameters was higher at NAM006R and NAM011D than at NAM011R. This correlation difference suggests a higher proportion of non-photosynthetic organisms at station NAM011R. Maximum R_{O_2} values were found at the surface of NAM006R and NA011D, with another subsurface R_{O_2} peak in the latter at 75 m. At NAM011R the maximum value was half (93 μmol O_2 m^{-3} d^{-1}) the values found for the other two stations.

From the four size fractions of zooplankton, the contribution of 100 - 200 μm and 500 - 1000 μm sizes to the total water column respiration was considerably lower at the three stations. The highest value of the three samplings for the 500 - 1000 μm organisms was 24 μmol O_2 m^{-3} d^{-1} at NAM011R, while for the 100 - 200 μm size fraction it was 8 μmol O_2 m^{-3} d^{-1} at NAM011D. On the other hand, the maximum respiration rates at NAM006R and NAM011D were due to the 200 - 500 μm size fraction and were found at the surface, with an average value of 178 μmol O_2 m^{-3} d^{-1}. However, the respiration value of this size fraction decreased to below 15 μmol O_2 m^{-3} d^{-1} at NAM011R. The respiration, in this case, was dominated by the largest size fraction, with a value of 734 μmol O_2 m^{-3} d^{-1} at the surface. Finally, a slight increase of respiration near the bottom was noticed at all stations, mainly due to the 200 - 500 μm and > 1000 μm size fractions.

3.3.3 Modeled vertical carbon flux, F_C

Respiratory CO_2 production rates (R_{CO_2}) were calculated from the R_{O_2} values in Fig. 3.3 and a molar Redfield ratio for C/O_2 of 0.71 (Takahashi et al., 1985). Since the conversion from R_{O_2} to R_{CO_2} only involves one constant, the shape of the depth profiles in both cases would be the same. For instance, Fig. 3.4 shows the R_{CO_2} depth profile (μmol CO_2 m^{-3} d^{-1}) for microplankton at NAM006R, with the two best mathematical descriptions of the data, the power and the logarithmic functions. As stated above, there was no statistically significant

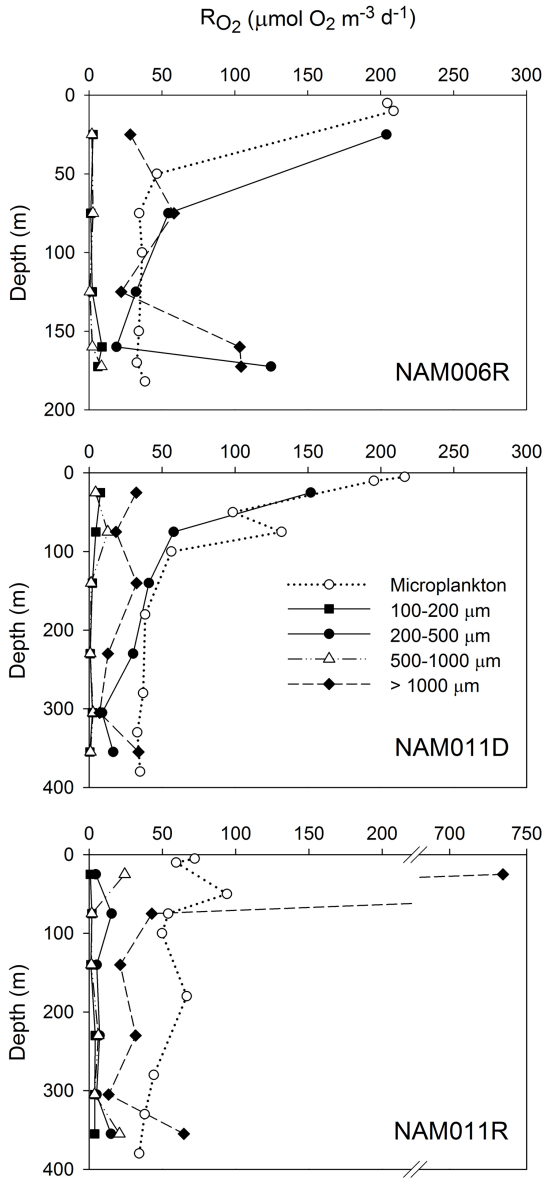

Figure 3.3: Depth-profiles of microplankton chlorophyll (mg m^{-3}) from filtered samples and seawater density as sigma-t (inset) at the sediment trap stations, during the three water column samplings.

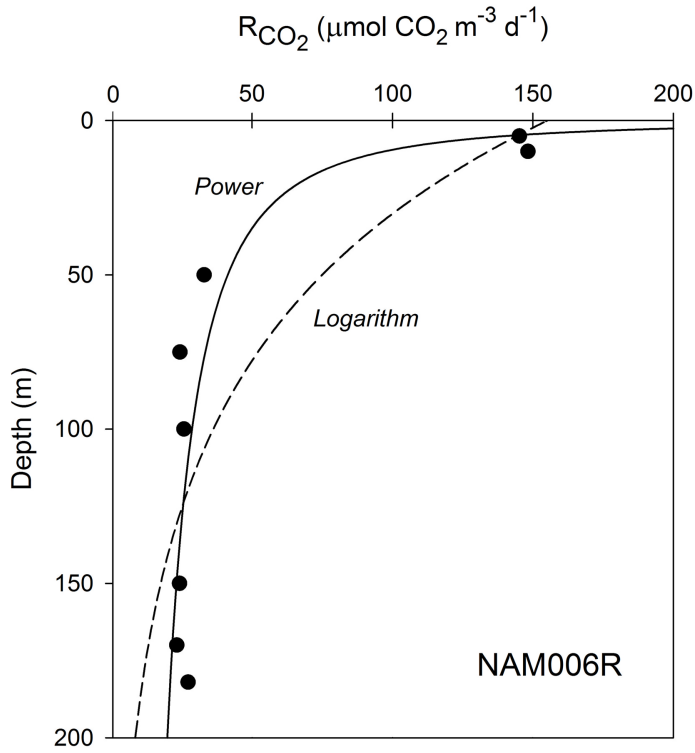

Figure 3.4: Respiratory CO_2 production (R_{CO_2}) depth profile of microplankton at NAM006R. The two best fits for the data, the power and the logarithmic functions, are given.

difference between them in all the samplings (one-way ANOVA, $p = 0.653$). Visually the power function describes the data better, and hence, the power function for R_{CO_2} was used in our calculations.

The equation parameters of Eq. 3.1 for microplankton and zooplankton at the three stations are listed in Table 3.3. R_0 refers to the calculated surface R_{CO_2} and follows the same pattern as the measured R_{O_2}: the highest values for microplankton were found at NAM006R and NAM011D, while the highest value for zooplankton was found at NAM011R. Even the b value, which reflects the curvature of the respiration depth profile, was higher (more negative) when the surface respiration values were higher, i. e., at NAM006R and NAM011D for microplankton and at NAM011R for zooplankton. Total R_{CO_2} (Table 3.3)

refers to the addition of the modeled R_{CO_2} for microplankton and zooplankton at each station. The F_C from the base of the E_z to the seafloor was calculated by the integration of this total R_{CO_2}, as described in Eq. 3.2 (Fig. 3.5). The function that best fits the carbon flux data was the logarithmic ($r^2 > 0.99$). The equations for the three profiles are as follows: $F_C = -10.47\ \mathrm{Ln}(z) + 56.37$ for NAM006R; $F_C = -12.96\ \mathrm{Ln}(z) + 77.96$ for NAM011D; and $F_C = -11.54\ \mathrm{Ln}(z) + 69.13$ for NAM011R, all in mmol C m^{-2} d^{-1} units. These equations were employed to calculate the respiration based-F_C at 150 and 320 m in order to compare them with the sediment trap-derived C-flux values.

Table 3.3: Equation parameters for the power function fit for the respiratory CO_2 production, $R_{CO_2} = R_0 z^b$. Here, R_{CO_2} represents the modeled respiration in µmol C m^{-3} d^{-1} at any depth (z) in the water column, R_0 (µmol C m^{-3} d^{-1}) is the R_{CO_2} at the surface, b is the curvature of the profile and n is the number of samples. The coefficient of determination (r^2) indicates the goodness of the fit between the modeled R_{CO_2} and the R_{CO_2} calculated from the R_{O_2}. Total R_{CO_2} (µmol C m^{-3} d^{-1}) represents the addition of the modeled R_{CO_2} for microplankton and zooplankton. The Total R_{CO_2} equations are integrated from below the E_z to the ocean bottom in order to calculate the carbon fluxes (see Fig. 3.3).

Station		R_0	b	r^2	n
NAM006R	Microplankton	433	–0.604	0.91	7
	Zooplankton	883	–0.540	0.79	4
	Total R_{CO_2}	1309	–0.558	–	–
NAM011D	Microplankton	401	–0.472	0.89	9
	Zooplankton	2077	–0.801	0.97	5
	Total R_{CO_2}	2111	–0.663	–	–
NAM011R	Microplankton	63	–0.140	0.90	7
	Zooplankton	18737	–1.254	0.97	5
	Total R_{CO_2}	8464	–0.939	–	–

3.3.4 **Particle fluxes and composition**

Vertical fluxes, mass and elemental, at both moorings can be separated into periods of high and low sedimentation (Fig. 3.6). Again, temporal variations in these fluxes from both traps were much greater than spatial effects such

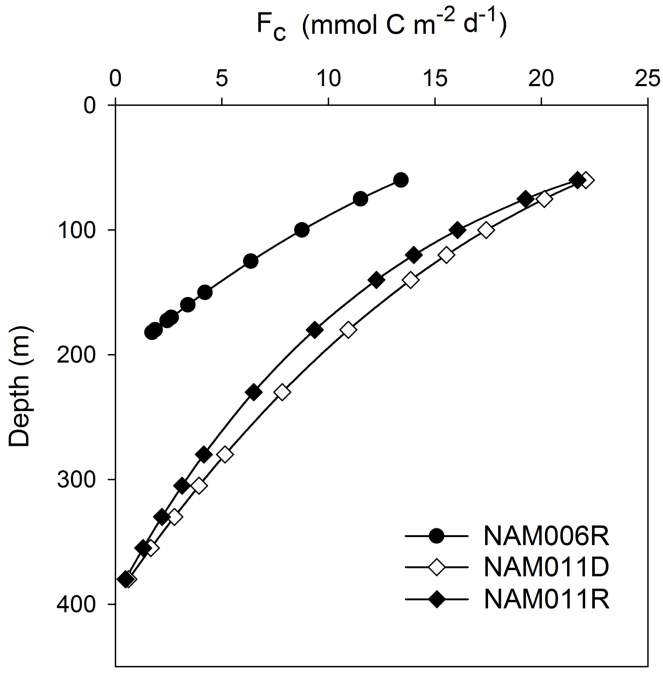

Figure 3.5: Carbon flux depth profiles measured on the shelf off Terrace Bay (Namibia). F_C represents the addition of the microplankton and zooplankton contributions to the carbon flux, via their respiration rates. The units are mmol C m^{-2} d^{-1}. Maximum depths were 206 m at station NAM006 and 395 m at station NAM011.

as differences in water depth or distance to the coast. Therefore, in an initial analysis, rather than compare the data from the two sediment traps stations, the data from the two different sedimentation regimes were compared as in Table 3.4. In this table, arithmetic means of fluxes during high (high-sed) or low (low-sed) sedimentation phases and elemental ratios derived by the division of the total accumulated masses over the respective periods are shown. The upper limit for the low range was set at 2.53 mmol POC m^{-2} d^{-1}. The two data sets are clearly distinct, as the lowest value of the high sedimentation range is more than twice this value.

High sedimentation phases (mean C-flux of 7.85 mmol POC m^{-2} d^{-1}) were characterized by 4 - 6 times higher mass and elemental fluxes, with a remark-

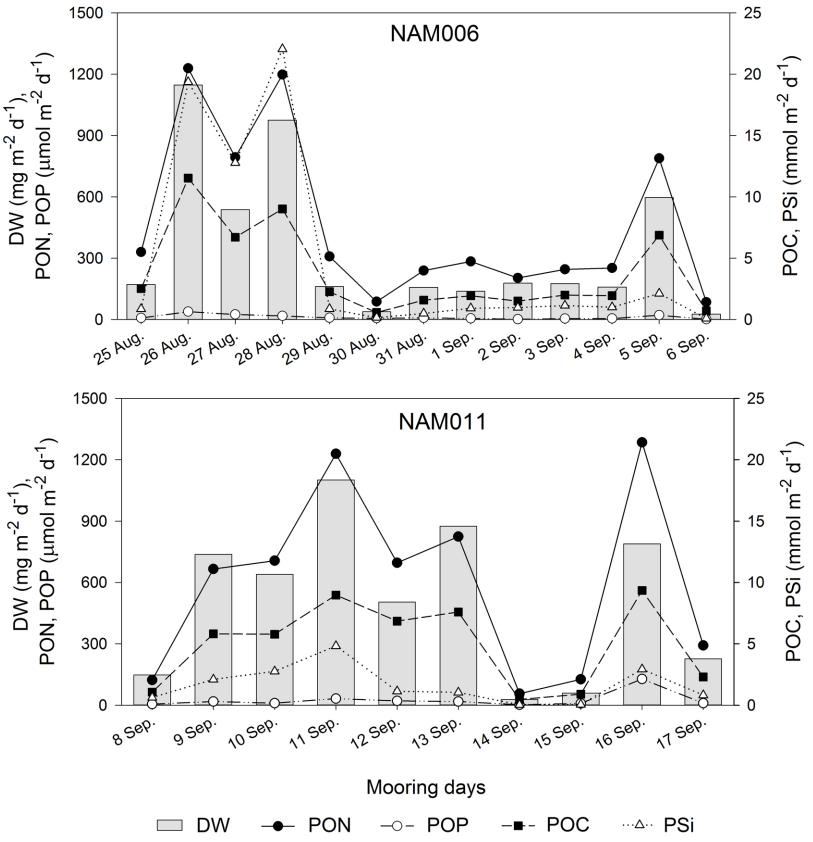

Figure 3.6: Vertical mass (bars) and elemental (lines) fluxes at NAM006 and NAM011 derived from sediment traps. Mass flux was measured as dry weight (DW), in mg m^{-2} d^{-1}. Particulate organic carbon (POC) and particulate silica (PSi) are given in mmol (C and SiO_2) m^{-2} d^{-1}, while particulate organic nitrogen (PON) and particulate organic phosphate (POP) are in µmol (N and PO_4) m^{-2} d^{-1}. The sampling time was of 13 days at NAM006 and 10 days at NAM011. The legend at the bottom applies to the two panels.

able difference in the particulate biogenic silica (PSi) in which the value was 11 times higher (Table 3.4). A great abundance of diatoms and a mineralogical composition of the inorganic material with high contributions of both opal and intermixtures of quartz and a microscopic picture of mainly diatoms, either intact or in pieces, were also recorded. Dominant diatom species were

Pseudonitzschia australis (Fig. 3.7*A*) and *Coscinodiscus walesi* (Fig. 3.7*B*) with a high proportion of debris (mainly broken diatom shells) in the material. Low sedimentation phases (mean C-flux of 1.52 mmol POC m^{-2} d^{-1}) comprised mass and element fluxes that were distinctly lower for POC, PON, POP and PSi. In these periods, coccolithophorides (Fig. 3.7*C*) increased together with carbonaceous minerals ($CaCO_3$) and $CaPO_4$ and intermixtures of feldspar (data not shown).

Elemental ratios differed between the phases (Table 3.4). Due to high diatom contents the C/Si atomic ratio in the high-sed samples was half the value found in the low-sed situation and the weight percentage of carbon against total dry mass was accordingly lower. The C/N-ratio was lower (7.5 *vs.* 8.3) in the low sedimentation periods, whereas the C/P-ratio was slightly higher (259 *vs.* 239). However, as phosphorus is involved, these ratios from particulate material may be misleading. Phosphorus is removed from cells very quickly during their first phase of sinking (Paytan et al., 2003; Faul et al., 2005) as compared to carbon, nitrogen and silica. Under our specific conditions of intercepting sinking cells (and particularly breaking or broken diatoms) close below the mixed layer we must assume, that a certain amount of dissolved material may have leached out of the vacuoles during the collecting time in the cups with a bias towards phosphorus. We, in fact, measured elevated concentrations of orthophosphate in the sampling vials which were higher than the respective silica concentrations, if normalized to the particulate phases of these elements. Due to the fixation with formalin, dissolved carbon and nitrogen species could not be reliably estimated in the supernatant water of the collecting cups and so a complete reassessment of whole input, including both particulate and dissolved elemental phases, was not possible. During the early period of cell sinking, these selective leaching processes, largely enhanced by grazing, occur in the water column as well and are, therefore, not easy to discriminate. In our case, they may have affected particularly the C/P ratio of the material, which we expected to be lower for a comparatively fresh diatom bloom.

Clear systematic differences in the isotopic composition between the two phases could not be observed (Table 3.4). Whereas the $\delta^{13}C$ signature of POC between these two situations was virtually the same (–21.96 *vs.* –22.04), the difference in $\delta^{15}N$ between high (5.07) and low (5.57) sedimentation phases may be due to a fractionation effect of nitrate between eutrophic and oligotrophic waters (Altabet et al., 1991). Without knowledge of the source compo-

Table 3.4: Average values of particles composition at NAM006 and NAM011, grouped by the sedimentation level. Tot. Flux stands for the mean values of the daily total mass flux measured at the different conditions. Note that the values for the elemental fluxes (Elem. Flux.) are in μmol m^{-2} d^{-1}. In order to simplify the reading, the atomic ratios are referred as C/N, C/P and C/Si throughout the text. The carbon content as a percentage of the dry weight (C as % DW) was estimated from the weight ratios in each case. The isotopic composition of C and N (δ^{13}C and δ^{15}N) are also given.

	Total Flux	Elemental Flux (μmol m^{-2} d^{-1})				Atomic ratios			C as % DW	δ^{15}N	δ^{13}C
	(mg m^{-2} d^{-1})	POC	PON	pP	PSi	POC/PON	POC/pP	POC/PSi	wt. ratio	per mil	per mil
All low-sed	128.3	1522	202.6	5.87	623	7.51	259	2.4	16.17	5.57	–22.04
All high-sed	790.3	7849	941.6	32.82	7110	8.34	239	1.1	12.30	5.07	–21.96
Ratio high/low sed	6.16	5.16	4.65	5.59	11.40	1.11	0.92	0.45	0.76	0.91	1.00

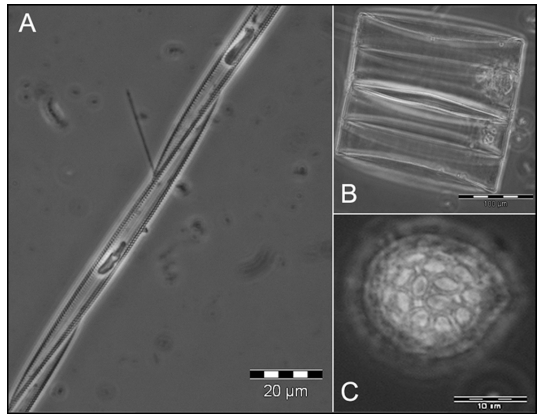

Figure 3.7: Dominant species of chain-forming diatoms during the high sedimentation period, *Pseudonitzschia australis* (A) and *Coscinodiscus walesi* (B). Coccolithophorides (C) were more abundant during the low sedimentation rates. Note that they maintained the assemblages of coccoliths covering the cell. All these photographs were taken by means of an inverted microscope.

sition of nutrients in the surface layer and consecutive trophic changes this can, however, not be substantiated.

3.3.5 Comparison of respiration based F_C *vs.* sinking POC

The main challenge of the present study was to compare the POC that is exported from the E_z and reaches the sediment traps with the calculated F_C at the same depths based on plankton respiration in the water column. Fig. 3.8 shows such a comparison.

As stated above, the sampling time of the sediment traps was divided into high and low sedimentation periods, which were attributed to high and low primary productivity events in the surface layer (Eppley and Peterson, 1979). Mean values (± SD) of POC during the high-sed periods were of 8.54 (± 2.26) at NAM006 and 7.39 (± 1.54) at NAM011, while when the particle sedimentation was low, the values decreased to 1.67 (± 0.66) at NAM006 and 1.18 (± 0.79) at NAM011, all in mmol C m^{-2} d^{-1} units. Regarding the water column samplings, they were also related to periods of high and low production, by using the chlorophyll to estimate the primary productivity as described by Brown et al. (1991). Thus, NAM006R and NAM011D coincided with periods of high production, while NAM011R was associated with lower primary

production. At the mooring depths (150 m and 320 m), the modeled F_C yielded values of 3.90, 3.43 and 2.57 mmol C m^{-2} d^{-1} at NAM006R, NAM011D and NAM011R, respectively. Then, these values for NAM006R and NAM011D were compared with the POC values obtained from the sediment traps during the high-sed period, and it turned out that the latter were more than two times higher. However, this difference was only significant for NAM011D (Student *t*-test, $p < 0.05$). The value for NAM011R, in turn, was compared with the POC concentration in the sediment traps when the particle sedimentation was low. In this case, the value from the F_C model was higher, although there was no statistically significant difference (Student *t*-test, $p = 0.11$).

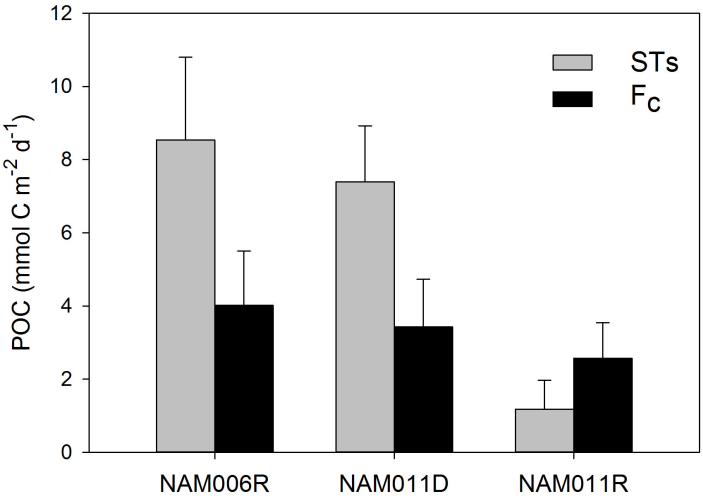

Figure 3.8: Comparison of carbon fluxes measured by sediment traps (STs) and by respiration-based models (F_C) at 150 m (NAM006R) and 320 m (NAM011D and NAM011R). Differences are only significant ($p < 0.05$) for NAM011D. Error bars on the ST approach correspond to the standard deviation of the measurements, while on the F_C approach reflect the maximum uncertainty in the carbon flux calculations (38 %).

3.3.6 Application of F_C approach to zooplankton

The zooplankton contribution to the vertical carbon flux was also determined from ETS activities in water column profiles from the cross-shelf transect (20° S) during the SUCCESSION cruise. For further information about the zo-

oplankton biomass distribution and metabolic activities along this transect see Fernández-Urruzola et al. (2014). We determined the respiratory CO_2 production as a function of depth and integrated it from the base of the E_z to the seafloor by applying, as before, Eq. 3.2. Table 3.5 shows the logarithmic, exponential and power fits to the F_C profiles for ten stations along the transect. The data from the two stations of sediment traps are also included. The best fit at the coastal and transition stations was the logarithmic function. It was significantly different from the power and exponential functions for the transition stations (two-way ANOVA, $p < 0.05$). In the oceanic area, however, the best fit was the exponential equation, although no significant differences were found between it and the logarithmic fit. It is noteworthy that the coefficient of correlation (r^2) for the power function is consistently lower than the r^2 for the other two functions at all the stations (Table 3.5).

The calculated carbon loss associated with zooplankton respiration for the entire water column yielded mean values of 17.32, 39.72 and 16.63 mmol C m^{-2} d^{-1} at the coastal, transition and oceanic areas, respectively. These values represent the zooplankton respiratory carbon demands for the entire water column. With these F_C models, one could also estimate some key values (Table 3.6), such as the zooplankton associated carbon export ratio from the E_z (*e*-ratio), the carbon transfer efficiency (T_{eff}) and the nutrient retention efficiency (NRE). Here, the *e*-ratio stands for the percentage of the primary productivity that is consumed by the zooplankton respiration below the E_z. Note that, in this calculations, the microplankton contribution is not taken into account. These values varied distinctly from about 2 to 13 % at the three regions, mainly with higher *e*-ratios found at the oceanic area. The T_{eff} (Buesseler et al., 2007b) is defined as the ratio between the F_C at 500m to F_C at 150m, multiplied by 100 when is expressed as a percent. Higher values indicate higher efficiency of the system in transferring the carbon from the surface to deep waters. Contrary to the *e*-ratio, we estimated a practically constant T_{eff} value of 60 % at the stations from the oceanic area, the only ones deep enough for this determination. The NRE, which was recently proposed by Packard and Gómez (2013), refers to the capability of the plankton community to retain the nutrients in the upper layer of the water column ($z \leq 500$ m) and equals $(F_{C_{150}} - F_{C_{500}})/F_{C_{150}} \times 100$. In fact, it reflects the opposite concept of the T_{eff} and the *e*-ratio. It should correlate directly with regenerated production and correlate inversely with new production (*sensu* Dugdale and Goering, 1967). We obtained values for NRE

Table 3.5: Carbon flux depth profiles associated with zooplankton respiration along the transect. The best fits for the data are given, the logarithmic (F_C = a Ln(z) + F_0), the exponential ($F_C = F_0\ e^{bz}$) and the potential ($F_C = F_0\ z^b$) functions. F_0 is the estimated F_C at the surface, i. e., when z = 0 for the logarithmic equation and z = 1 for the exponential and potential equations. Units are mmol C m^{-2} d^{-1} for the three functions, z is in meters (m). These equations should only be applied to calculate the F_C at any depth from below the E_z to the seafloor. The data for the sediment traps stations (NAM006 and NAM011) are also included.

Area	Station	Logarithmic equation	r^2	Exponential equation	r^2	Power equation	r^2
Coastal	NAM002	-2.29Ln(z) + 10.71	0.999	$10.06e^{-0.036z}$	0.982	$10000z^{-2.233}$	0.956
	NAM003	-3.02Ln(z) + 14.77	0.999	$11.72e^{-0.029z}$	0.966	$2000z^{-1.688}$	0.881
	NAM004	-5.34Ln(z) + 26.49	0.996	$20.02e^{-0.026z}$	0.962	$5000z^{-1.785}$	0.916
	Average		0.999		0.970		0.918
Transition	NAM006 [a]	-7.69Ln(z) + 41.41	0.996	$30.06e^{-0.016z}$	0.967	$10000z^{-1.702}$	0.929
	NAM007	-4.52Ln(z) + 26.15	0.992	$15.00e^{-0.010z}$	0.994	$167.31z^{-0.798}$	0.912
	NAM009	-9.89Ln(z) + 58.66	0.987	$32.46e^{-0.009z}$	0.972	$1000z^{-1.054}$	0.877
	NAM011 [a]	-5.46Ln(z) + 32.64	0.999	$22.95e^{-0.010z}$	0.931	$20000z^{-1.722}$	0.820
	Average		0.994		0.966		0.885
Oceanic	NAM014	-3.67Ln(z) + 29.52	0.954	$16.25e^{-0.002z}$	0.999	$63.48z^{-0.355}$	0.896
	NAM017	-2.38Ln(z) + 19.17	0.988	$9.88e^{-0.001z}$	0.996	$78.87z^{-0.504}$	0.893
	NAM018	-1.56Ln(z) + 12.34	0.999	$6.35e^{-0.001z}$	0.995	$78.29z^{-0.625}$	0.914
	NAM022	-0.86Ln(z) + 6.79	0.994	$3.09e^{-0.001z}$	0.969	$41.99z^{-0.602}$	0.969
	NAM026	-1.40Ln(z) + 15.31	0.935	$9.52e^{-0.0004z}$	0.999	$23.38z^{-0.212}$	0.880
	Average		0.974		0.992		0.910

[a]From the zooplankton values at the ST stations.

of around 40 % (Table 3.6), except for the station NAM026, where the downward transmission of carbon was higher.

3.4 Discussion

3.4.1 Temporal variability in the community structure and sinking particle composition

Sinking particle composition and vertical fluxes have been described here, as well as the planktonic contribution to the heterotrophic POC degradation via respiration. The variability of the hydrological properties during the sampling time impacted both approaches. The sediment trap data from the two successive moorings at different water depths and distances from the coastal core of the upwelling (Fig. 3.1) displayed similar patterns. Peaks and means of C-flux were in the same range in both the deeper offshore and the shallower onshore traps (Fig. 3.6). Note that the latter was situated closer to the core of the upwelling. Depth profiles of community respiration, in turn, also reflected this pattern. The shape of R_{O_2} profiles at station NAM011D was more akin to NAM006R than it was to NAM011R (Fig. 3.3). This was because the two samplings at the NAM011 were made ten days apart, whereas NAM011D and NAM006R were sampled within a day of each other. Thus, we observed that temporal variability in this area was stronger than the spatial variability. Although this does not fit into the general scheme of a system that ages strictly with distance from the center of the upwelling, it fits well into the complex spatial pattern of the Benguela upwelling characterized by filaments and eddies as can be seen in satellite images of color and temperature as well as in modeling results (Mohrholz et al., 2014).

On a general level, the pattern of vertical particle export represented an image of the structure and state of the pelagic system in the surface mixed layer. Independent of geographical position and depth, we found two states that differed both in quality and quantity of the material and which alternated on a daily basis. One was the result of particle loss from an eutrophic upwelling filament (Mohrholz et al., 2014). It originated farther south and was characterized by high phytoplankton biomass due to strong diatom growth (Hansen et al., 2014). The other, by contrast, derived its particle load from a mixed layer, that contained elements of both upwelling and oligotrophic Atlantic waters. Here, the oligotrophic state can be described as the late temporal phase

Table 3.6: Application of respiration based-carbon flux model (F_C) to zooplankton samples collected along the transect. Carbon fluxes at the euphotic zone (E_z), 150 m and 500 m were determined from the logarithmic equations in Table 3.5. Carbon export (*e*-ratio) and the efficiency of the biological pump in the carbon transfer (T_{eff}) and in the nutrient retention (NRE) from 150 m to 500 m were also determined. Net primary productivity (NPP) in this layer was estimated from chlorophyll and ^{14}C incubation measurements made on board; the calculations followed the procedure given in (Brown et al., 1991) for the Benguela system, with the regression model of best fit to the data being $^{14}C = 3.75$ Chl $a^{0.653}$ (n = 24, $r^2 = 0.60$, $p = 0.001$). It comprises the integrated NPP in the E_z. The *e*-ratio stands for the percentage of the NPP that is consumed by zooplankton respiration from the base of the E_z to the seafloor. Gaps indicate no determination due to insufficient water column depth.

Zone	Station	Depth (m)	E_z depth (m)	F_C (mmol C m^{-2} d^{-1})			NPP (mmol C m^{-2} d^{-1})	*e*-ratio (%)	T_{eff} (%)	NRE (%)
				Ez	150 m	500 m				
Coastal	NAM002	107	39	2.34	–	–	123.0	1.9	–	–
	NAM003	132	26	4.94	–	–	123.7	4.0	–	–
	NAM004	133	38	7.06	–	–	169.7	4.2	–	–
Transition	NAM006 [a]	206	60	9.94	2.90	–	357.7	2.8	–	–
	NAM007	266	23	11.99	3.53	–	215.2	5.6	–	–
	NAM009	308	58	18.52	9.13	–	210.8	8.8	–	–
	NAM011 [a]	395	60	10.32	5.28	–	211.5	4.9	–	–
Oceanic	NAM014	871	52	14.53	11.77	5.55	109.4	13.3	47.1	52.9
	NAM017	2159	46	9.31	8.12	5.13	154.1	6.0	63.2	36.8
	NAM018	2611	40	6.02	5.19	3.25	110.0	5.5	62.6	37.4
	NAM022	3775	50	2.92	2.61	1.76	106.1	2.8	67.3	32.7
	NAM026	4339	50	9.32	8.92	7.68	72.9	12.8	86.0	14.0

[a] From the zooplankton values at the ST stations.

of an upwelling system, which after a period of warming, mixing and reduction of free nutrients is transformed from a typical "new" into a "regenerating" production system. Nevertheless, the material collected in the traps itself did, in no way, reflect a growth limited or senescent biological community. Similar C/P, lower C/N and higher C/Si ratios (Table 3.4) indicated a shift in the community towards smaller and probably to a higher percentage of heterotrophic cells, which corresponded to our microscopic observations. Mass transfer was, however, quite different between the two basic states and whereas the high-sed values of C, N and P flux with means of 7850, 940 and 33 μmol m^{-2} d^{-1} formed the trophic base of the highly productive Benguela Upwelling System, the low-sed values of 1500, 200 and 6 μmol m^{-2} d^{-1} of C, N and P respectively, constituted the transition to oligotrophic open ocean conditions. In fact, our POC values for the two sedimentation situations are comparable to fluxes measured in other eastern upwelling systems, such as the California Current (Pilskaln et al., 1996) and Humboldt Current (González et al., 2009). Pilskaln et al. (1996) reported values in Monterey Bay of 0.8 - 2.5 mmol C m^{-2} d^{-1} during non-upwelling situation and of 4 - 15 mmol C m^{-2} d^{-1} when the upwelling was active. Values from González et al. (2009), were relatively higher, ranging from 3 - 87 mmol C m^{-2} d^{-1}, likely due to a shallower sample collection. Therefore, the basic difference in our short term measurements is related to the suspension of the traps either beneath a comparatively young upwelling filament or beneath water between these filaments.

An interesting, although at the moment just descriptive, finding is that the mineralogical loads of the two sedimentation regimes revealed not only different biogenic minerals, like carbonates or opal, but lithogenic minerals, like quartz or feldspars and different clay minerals as well. If this dichotomy is related to changes in particle sizes, forms or stickiness of the organic load or to different input terms of aeolian dust it is not known and still has to be resolved.

Similarly, the respiration profiles also reflected a change in the structure of the communities between the two basic situations. While the water column respiration associated with the filament of mature water was dominated by the microplankton and the 200 - 500 μm size fraction zooplankton, the highest respiration rates in the more oligotrophic waters were due to > 1000 μm size fraction zooplankton, with a significantly lower contribution from the microplankton (Fig. 3.3). If, as stated above, the oligotrophic state here refers to a later temporal phase of an upwelling system, this pattern agrees with that

modeled by Vinogradov et al. (1972). They predicted that the small-sized herbivores would peak right after the maximum of phytoplankton, followed by the maximum of large-sized herbivores and carnivores with a delay of days. Accordingly, the > 1000 μm organism in the more oligotrophic waters of the NAM011R were predominantly salps. Maximum values of microplankton respiration during the most productive period (200 μmol O_2 m^{-3} d^{-1}) were around 4-fold lower than others found farther south in the same northern Benguela upwelling region (Chapman et al., 1994). However, it is not surprising as they reported greater productivity rates and ~ 3 fold higher chlorophyll concentration values, indicating higher phytoplankton biomass as compared to our findings. Few studies have paid attention to the respiratory metabolism of the entire zooplankton community in this region, although recently various researchers have described the metabolic rates of the dominant species of mesozooplankton (Bode et al., 2013; Huenerlage and Buchholz, 2013). Our zooplankton respiration rates at the sediment traps stations compare well with the mean values for the different size fractions reported in Fernández-Urruzola et al. (2014) for other stations in this transition area, but they are higher than previously published values in other upwelling systems (Packard et al., 1974; Hernández-León et al., 2002; Isla and Anadón, 2004). This is likely related to the higher primary productivity in our case.

On a general level, this study is embedded in a large scale investigation of the aging process of a coastal upwelling system. On small temporal and spatial scales, like those inherent in distinct water samples or characteristics of daily sampling intervals of sediment traps, the patchiness affected our measurements much more than did the overlying general spatial pattern. In this regard, the long term development in the surface water masses after upwelling, determines what will sink out of the these overlying waters in the long run. Therefore, in order to detect these consecutive stages of an aging upwelling system, more time series sampling along an Eulerian approach, integrated with more spatial coverage, would be required.

3.4.2 Comparing and combining the sinking POC and the F_C approaches

The comparison of conceptually different methods of estimating vertical carbon transfer in the water column in such a heterogeneous system revealed the pros and cons of each method. Whereas the sediment trap approach collects

integrated amounts of sinking matter irrespective of the system interactions in the water column, the plankton respiration approach describes the system interactions with higher depth resolution. In addition, the F_C method, because of its high data acquisition rate, allows wider temporal and spatial ocean coverage than the stationary trap approach. Nonetheless, because it is a near-instantaneous measurement, it lacks the temporal integration if not performed in a highly elaborate large scale effort. Accordingly, this differs from the sediment trap approach. F_C from ETS activities are based on minute-to-hour scale changes while the C-flux from sediment traps are based on a day-to-month scale changes. Here, the POC value from sediment trap data for the high-sed and low-sed periods comes from the average of 4 - 9 days, while the F_C profiles represent a snapshot of the water column characteristics at the sampling time. However, by operating on different scales of integration, the two approaches are meant to complement one another by placing recent measured fluxes into the context of the wider field of vertically resolved respiration.

When the two approaches are to be compared, one should also consider the intrinsic uncertainty of each determination. Several reviews concerning the sediment trap efficiency (Gardner, 2000; Buesseler et al., 2007a; Burd et al., 2010) pointed out that factors such as the hydrodynamic processes, the incidental presence of zooplankton swimmers, and the solubilization of labile biogenic components in the cups can bias the collection of sinking particles, specially at the shallower depths. From our results, we showed evidence of the selective solubilization process of organic phosphorus, as this element leaches from breaking cells faster than carbon, nitrogen or silica (Paytan et al., 2003; Faul et al., 2005). All things considered, the sediment trap-based carbon flux estimations vary by a factor of 3 to 10 (Buesseler, 1991). On the other hand, the uncertainty in the prediction of R_{CO_2} from ETS measurements is dictated by the errors associated with all the conversion steps. Thus, the Φ has an uncertainty of ± 16 % (Packard et al., 1977). The recalculated CO_2/O_2 ratio from Takahashi et al. (1985) has an standard error of ± 18 % (Martin et al., 1987). Still, the overall variability lies in the R_{O_2}/Φ ratios, namely ± 12 % for microplankton (Packard and Christensen, 2004) and ± 23 % for zooplankton (King and Packard, 1975). Considering all sources of errors during the calculations, the resultant uncertainty in the F_C determination ranges from 31 to 38 % (Packard et al., 1988; Packard and Gómez, 2013).

Apart from the uncertainties in each determination, the comparison of the

two approaches distinguished two different scenarios (Fig. 3.8). Regardless of the distance to shore, during the high-sed period, the POC flux values obtained in the sediment traps were higher than those estimated by the respiration based-F_C method, while when the sedimentation rate was lower, the value from the F_C approach were twice as high the value from the sediment traps. This discrepancy can be explained by basic differences in the plankton community structure in the surface layer, as the phytoplankton size would directly influence their settling velocities (Boyd and Newton, 1995; Guidi et al., 2009). Thus, the high-sed scenario was dominated by large diatoms (Fig. 3.7*A* and *B*) that easily aggregate forming fast-sinking particles and producing a rapid flux of particulate organic matter from the surface to the deep sea, with rates that could exceed 100 m day^{-1} (see Thornton, 2002, and references therein). In addition, the relatively high presence of lithogenic material ($\sim$ 45 %) might have contributed to this flux by the ballast effect (Armstrong et al., 2001). These rapidly settling particles are presumably less influenced by either lateral advection or organisms consumption and, therefore, the material collected in the cups is in phase with the production at the surface. During the low-sed period, in contrast, the abundance of diatoms substantially decreased while the occurrence of coccolithophorides increased. Although these organisms were also present within the cups during the high-sed period, their presence was masked by the high peak pulses of fast-sinking particles. Coccolithophorides can form aggregates that settle even faster than the diatom formed-aggregates, but they would require more time, higher cell densities and the release of coccoliths after the cell lysis (Iversen and Ploug, 2010). Contrarily, our results during this low-sed period showed a considerably low phytoplankton biomass, low contribution of lithogenic material and indicated a non-senescent community, which revealed no significant aggregate formation of these organisms. This hypothesis was strengthened by microscopic observations of the material that indicated intact coccolithophorides cells (Fig. 3.7*C*). All these data suggest that this period was dominated by slow-sinking particles with an increased probability to be consumed by zooplankton in the midwater layers. Additionally, a portion of slow-sinking particles, that originated from a previous upwelling filament could still be present in the deeper water layers and contribute to enhance respiration rates (Packard et al., 1977). Giving the observed fluctuations between the high- and low-production phases in surface waters of a few days to a week and sinking speeds of only few meters per day for slow-

sinking particles, the surface production patterns and the deeper water particle inventory for this group of particles can easily be out of phase. This is different for fast-sinking aggregates and fecal pellets, which over the first few hundreds of meters in the water column are more or less synchronized with their surface production. Therefore, what we observe in deeper layers is always a mixture of particles with different production histories. Whereas the presence of light particles will enhance midwater respiration, fast-sinking particles will tend to escape this process by sinking. The persistence of slow-sinking particles in deeper layers from previous phases of high surface production and their respiration can then lead to the observed imbalance in flux rate estimations between our two methods. Besides, these particles are more susceptible to lateral transport, decreasing the collection efficiency of sediment traps. In agreement with our findings during this period, recent works have reported a greater metabolic carbon demand for the plankton community as compared to the measured vertical POC supply (Steinberg et al., 2008; Baltar et al., 2009). They recorded a contribution of slowly settling particles to the total mass flux considerably high, and hence, the consumption of this POC pool not sampled by the sediment traps could explain the mismatch (Alonso-González et al., 2010). In addition to this, considering the contribution of the dissolved organic carbon (DOC) to the microheterotroph respiration, which has been estimated to be as high as 15 % for the global ocean (Arístegui et al., 2002), could help lessen the difference between the two measurements. In any case, Alonso-González et al. (2010) suggested that if the fast-sinking particles dominated the flux, the imbalance between the metabolic carbon demand and the vertical POC flux would be lower. Here, we have demonstrated that for the specific case of the high productive system of the Benguela upwelling and when the fast-sinking particles dominated in the water column, the vertical POC flux exceeded the respiration associated carbon flux. Whether this pattern holds for other productive systems and/or sinking particle characteristics needs further research. Overall, our results agree with Gust and Kozerski (2000), who asserted that particle settling velocity is a key factor controlling the hydrodynamic biases affecting sediment traps.

The F_C approach has previously been applied in waters of the Gulf of Maine (Packard and Christensen, 2004) and, more recently, the Canaries (Packard and Gómez, 2013). This method has proved to be a useful tool to determine the vertical carbon flux in these sites that are characterized by more oligo-

trophic waters, where the sediment respiration and carbon burial is negligible. In our case, due to the high productivity of the northern Benguela system, we might be partially underestimating total sinking carbon flux by the F_C approximation. However, the combination of this approach together with the sediment trap data serve the requirements for both integrated balanced flux estimates and layer- and sizeclass- resolving assessments of driving forces for the particle loss in the water column. This fosters the concurrent comprehension of both quantitative and qualitative aspects of system functioning and delivers both the process-understanding and the quantitative information. Thus, assuming a mean primary productivity (PP) value of 201 mmol C m^{-2} d^{-1} for the surface waters in this transition area (Fernández-Urruzola et al., 2014), 20.2 % of this PP was consumed on average from below the E_z to the sediment traps depth via plankton respiration. The mean POC value that arrived to the sediment traps during the entire sampling time was 4.7 mmol C m^{-2} d^{-1}, which represented 2.3 % of the PP. This rate agrees with previous values reported for carbon accumulation on the sediments of Atlantic and Pacific continental margins (Walsh et al., 1981; Anderson et al., 1994; Pilskaln et al., 1996). The addition of both values reflected the percentage of PP that was exported at the base of the E_z , i.e. the *e*-ratio (Buesseler et al., 2007b), namely ~ 23 %. These values compare reasonable well with others found in the literature for similar high productive systems (Martin et al., 1987; Schlitzer, 2000; Buesseler and Boyd, 2009).

3.4.3 Changes in F_C with distance to shore

The variation of POC flux with depth is commonly estimated by regression equations taken from the literature rather than by *in situ* measurements (Sarmiento et al., 1993; Baltar et al., 2009). One of the most used regression is that proposed by Martin et al. (1987), which relates the flux at any depth to the known flux at 100 m. However, this power law is sensitive to shallow depths and therefore, it biases the comparison of the POC flux in the upper mesopelagic waters between sites of different depths (Primeau, 2006; Buesseler and Boyd, 2009). Other published regressions related the POC flux with the PP in the surface (Suess, 1980; Betzer et al., 1984; Pace et al., 1987), although Berelson (2001) demonstrated that these models overestimated the actual POC flux when the PP > 40 mmol C m^{-2} d^{-1}. Therefore, there is still a controversy about the best model to estimate the POC flux. In our case, we have applied the best fit to model the POC flux associated with zooplankton respiration. The regres-

sion equation for the coastal and transition areas was the logarithmic function while for the oceanic area the best fit was the exponential function (Table 3.5). Although it seems to be in disagreement with previous applied models, we suggest that it is not. In the shallow, high productive waters of the shelf and continental slope, the zooplankton is widespread throughout the water column and so will be the POC consumption to sustain their metabolic requirements. Indeed, if we compare our results with those obtained in Martin's work for their coastal station (Fig. 2, Martin et al., 1987) and we consider the first 400 m of their profile so as to compare with our maximum depth of the northern Benguela shelf, the shape of the curve would reasonably resemble our logarithmic curves described for the transition zone (Fig. 3.5). In the deep, less productive waters of the oceanic area, in turn, the zooplankton is mainly found in the upper layer of the water column and, therefore, the POC consumption will be major at surface and will decrease rapidly with depth, depicting a typical exponential curve. We propose that in the case of having more sampling depths in the mesopelagic and bathypelagic waters, the best profile might have been a power function, as it fits the data better at depth (Packard et al., 1983).

From the F_C profiles, we estimated the zooplankton associated *e*-ratio, T_{eff} and NRE in order to characterize the system (Table 3.6). Here, the *e*-ratio represents only the export production that sustains the zooplankton metabolism below the E_z. It does not consider the POC consumption by the microplankton and the eventual carbon accumulation in the sediments and, therefore, it falls at the low end of the range given by other trap-derived and model-based studies (Berger et al., 1989; Schlitzer, 2000; Buesseler et al., 2007b). In the oceanic area, the contribution of zooplankton to the POC attenuation was remarkably variable as was its distribution (Fernández-Urruzola et al., 2014). At NAM014, the zooplankton respiration was higher, which increased the POC remineralization and the NRE but decreased the T_{eff}. In contrast, the respiration values at NAM026 were lower and therefore, most of the POC was not remineralized and was transferred to the depth below 500 m, decreasing the NRE in this upper mesopelagic layer. For the stations in between, the T_{eff} stayed relatively constant, even though the *e*-ratio varied by a factor of 3, which suggests that most of the POC consumption occurred above 150 m in this area.

3.5 Conclusions

The short term assessments of vertical particle fluxes accomplished here revealed the major influence of the temporal variability rather than the effect of distance to the core of the coastal upwelling, mainly due to the important instabilities that upwelling filaments caused in this region. Two basic situations were distinguished during the study: one was influenced by mature waters of the upwelling filament, characterized by higher respiration rates of microplankton and small zooplankton as well as by high particle sedimentation rates. The predominance of diatoms during this period together with the higher contribution of lithogenic material promoted particle aggregation and led to the formation of fast-sinking particles. Thus, the remineralization by the water column plankton did not account for all the sinking POC and consequently, estimates of carbon flux from the sediment traps exceeded that of respiration-based values. The other distinct situation corresponded to a later temporal stage of the upwelled waters, with the predominance of respiration by large zooplankton, an increase of coccolitophorides and low particle sedimentation rates. In this case, the rain of POC from the surface was mainly constituted by slow sinking particles, which probably originated during a high production period and that supported asynchronously midwater respiration. Thus, in regions of oscillating surface productivity, the inventory of slow sinking particles in deeper strata from previous production peaks might have a certain compensation effect on the respiratory activities. Accordingly, the carbon flux values from the respiration-based model were larger than those from the sediment traps during this low-sed situation. In view of the results, we have shown that the previously reported mismatch in the carbon flux estimations between the sediment trap data and the metabolic carbon requirements of the organisms decreases or even disappears depending on the productivity rates, the nature of the sinking particles and, eventually, on their settling velocities. We encourage future studies to see whether this pattern holds for other highly productive systems, such as other eastern boundary currents, coastal waters or equatorial upwellings, with different community structures in the water column.

In the highly productive waters of the northern Benguela upwelling, the combination of the two approaches has served to obtain a global picture of particle fluxes. However, in oligotrophic waters, where the sediment respiration and carbon burial is negligible as compared to the water column respiration, the F_C approach itself is a useful tool to estimate the vertical carbon flux

due to heterotrophic POC consumption. In the same way, the conceptual basis of the F_C approach can be applied to describe other biogeochemical processes, such as the contribution of zooplankton to the vertical PON flux attenuation, from GDH activity measurements (Fernández-Urruzola et al., 2011).

Acknowledgements. We would like to thank to R. Hansen, I. Liskow and T. Leipe for analytical work on the sediment trap material. The microphotographs were also provided by R. Hansen. We are grateful to A. Herrera for her collaboration in collecting the biological samples as well as to the anonymous reviewers for contributing valuables suggestions which notably improved the manuscript. This work was founded by a DFG cruise support, and by the BIOMBA project (CTM2012-32729/MAR) awarded to M. Gomez by the Spanish Economy and Competitivity Ministry. N. Osma and I. Fernández-Urruzola received finantial support from the Formation and Perfection of the Researcher Personal Program from the Basque Government.

An experiment is a question which science poses to Nature, and a measurement is the recording of Nature's answer.

Max Planck

CHAPTER

4

CAPÍTULO

Variability of respiration and pyridine nucleotide concentration in oceanic zooplankton

N. Osma, F. Maldonado, I. Fernández-Urruzola, T.T. Packard and M. Gómez,
Submitted to Journal of Plankton Research.

ID: JPR-2015-277

ABSTRACT: We have studied the *in vivo* respiratory oxygen consumption (R_{O_2}) and the potential respiration rates (Φ), measured by the enzymatic activity of the electron transport system (ETS), in epipelagic marine zooplankton from several marine systems. Furthermore, we have determined the intracellular concentration of the ETS substrates, i.e., the pyridine nucleotides (PN), in these organisms . Both the R_{O_2} and Φ, as well as the relationship between them (R_{O_2}/Φ), showed a major dependency on habitat temperature, with significantly higher values in the warm waters of North Atlantic. Conversely, the pattern described by the PN concentration was mainly associated with the productivity regime, that ultimately determined the food availability for the zooplankton. The largest spatial changes in PN corresponded to the nicotinamide adenine dinucleotide (NAD) concentration, which ranged from a high of 887.5 nmol mg prot^{-1} in the upwelling waters to a low of 346.8 nmol mg prot^{-1} in the more oligotrophic waters. We further studied seasonal varibility of the R_{O_2}, Φ and PN concentrations in the coastal waters of the Canary Islands. In this

case, the fluctuations in all these variables were mainly attributed to changes in the productivity level of the seawater. Larger values were measured during the late winter bloom period whereas they decreased between 30 - 40 % with the stratification of the water-column. Shedding light on the processes that drive the respiratory control at the physiological level will help in understanding the variability of the respiration rates in marine organisms as well as the impact that these rates have in the remineralization of the organic matter.

Keywords: Electron transport system (ETS); Respiratory metabolism; nicotinamide adenine dinucleotide (NAD); nicotinamide adenine dinucleotide phosphate (NADP); trophic conditions.

4.1 Introduction

Carbon flux in the ocean is closely linked to remineralization processes through the water column. The efficiency of a system to sequester in the deep ocean the organic carbon produced in the sunlit layer is inversely proportional to the respiration rates (R_{O_2}) of the water-column biota. During respiration, both the dissolved and particulate organic carbon are degraded into CO_2, O_2 is consumed in oxic waters and the energy needed for other metabolic processes (i.e., growth, reproduction, etc.) is produced. On this basis, the carbon flux associated with this respiratory consumption, the nutrient retention efficiency of the system and the heterotrophic energy production can be estimated from R_{O_2} measurements (Osma et al., 2014; Packard and Christensen, 2004; Packard and Gómez, 2013; Packard et al., 2015). However, R_{O_2} in the ocean is not constant and, therefore, it becomes necessary to understand its spatio-temporal, biological, and ecological variability.

Acquiring enough R_{O_2} data to provide the high temporal and spatial resolution that oceanography requires, is unaffordable by the classic incubation methodology. To overcome this problem, Packard et al. (1971) proposed an assay based on measuring the activity of the electron transport system (ETS), the major enzymes involved in the intracellular oxygen consumption (Packard, 1985a,b). This method consists of saturating the ETS with substrates, so that the reaction yields the maximum velocity, i.e., the potential respiration (Φ). Since then it has been routinely used as a biochemical proxy for respiratory metabolism (e.g., Agatova et al., 2011; Ikeda, 2011; Minutoli and Guglielmo, 2012; Naqvi et al., 1996). However, organisms in the marine environment are unlikely to be under substrate-saturation conditions and, there-

fore, Φ measurements need to be converted into the actual *in vivo* R_{O_2}. In theory, the *in vivo* R_{O_2} should be close to half the maximum velocity of the ETS (Segel, 1993). Still, in the actual conditions, this value may vary and should be checked for the different experimental situations. Accordingly, empirically determined R_{O_2}/Φ ratios have been traditionally applied in biological oceanography, based on the good correlation exhibited by the two parameters (Finlay et al., 1983; Packard, 1985a; del Giorgio, 1992). Nevertheless, it has been well-documented that these ratios exhibit variability with ecological and physiological factors (King and Packard, 1975; Bamstedt, 1979; Hernández-León and Gómez, 1996), which precludes the use of a single universal value. Hernández-León and Gómez (1996) discussed the influence of body size, temperature, chlorophyll *a* and primary productivity on the variability of the R_{O_2}/Φ ratios in zooplankton. They identified R_{O_2} to be the principal parameter causing that variability. Thus, this process responds to changes in the quantity and/or quality of the food. Still, how this effect is explained at the intracellular level in zooplankton is unclear.

R_{O_2} depends directly on the regulatory mechanisms that control the ETS activity. As these enzymes obey Michaelis-Menten kinetics, the most quantitative regulatory factor is the substrate concentration (Packard et al., 1996; Aguiar-González et al., 2012). The major substrates of the ETS in the zooplankton are the pyridine nucleotides (PNs), namely nicotinamide adenine dinucleotide (NAD) and its phosphorylated form (NADP) (Savenkoff et al., 1995). These molecules are one of the most important electron-carrying cofactors. They donate electrons in a wide variety of reduction reactions in biosynthesis, whereas they are constantly regenerated (reduced) by catabolic reactions, e.g. the glycolysis (Lehninger et al., 2005). Among all the functions they play in the cells, the most important is to provide reducing equivalents to the ETS which is coupled to the ATPase, the enzyme responsible for the energy production (Lehninger et al., 2005). In spite of their key role, the information about their concentration in microorganisms is sparse in the literature (Andersen and von Meyenburg, 1977; Karl, 1980; London and Knight, 1966; Wimpenny and Firth, 1972, *Chapter 5*), and there are practically no reports about their levels in marine zooplankton, but some information in meroplankton (Schomer and Epel, 1998). Setlow and Setlow (1977) reported an increase in the PNs concentration during the growth phase in bacteria cultures. Accordingly, one can presume that the intracellular NAD and NADP levels

of metabolically active zooplankton would be higher than the levels found in organisms with a basal metabolism, due to their higher energy requirements. Consequently, it is also plausible to expect higher NAD and NADP concentrations in well-fed organisms than in organisms grown under food-limitation.

In the present study, we have focused on the respiratory metabolism of the zooplankton. This group of organisms plays a key role in the remineralization of the organic matter in the ocean as they consume about 17 - 32 % of the photosynthetic carbon produced in the surface layer (Hernández-León and Ikeda, 2005). Therefore, understanding the variability of their respiration rates in the ocean is essential when global carbon budgets are pursued. We have described the spatial variability of the biomass-specific Φ and R_{O_2} rates, as well as the $R_{O_2}/\ \Phi$ ratios in zooplankton from contrasting productivity areas. Moreover, we have determined the intracellular concentration of NAD and NADP in the marine zooplankton community and we have observed how they vary under these different trophic conditions. Additionally, we have addressed the variability of these rates and concentrations that is associated to environmental factors, such as temperature and chlorophyll-*a* concentration, the latter used as an index of the productivity of the waters. Finally, the seasonal variability was studied in a coastal station off Canary Islands. These waters are rather oligotrophic during most of the year, with low nutrient concentrations and low phytoplankton biomass due to the stratification of the water-column (De León and Braun, 1973). However, during a short period of time the cooling of the surface waters erodes the seasonal thermocline and allows the deep, nutrient-rich waters to reach the sunlit layer, which promotes the so-called late winter bloom (Menzel and Ryther, 1961). The patterns described by the planktonic community during this period have been well-documented in the last years (Arístegui et al., 2001; Schmoker et al., 2012, 2014). Nevertheless, our focus was to compare, for the first time, both the respiratory metabolism and PN concentration in zooplankton between the late winter bloom and the stratification periods.

4.2 Material and methods

4.2.1 Sample collection and processing

The zooplankton samples were collected during three oceanographic cruises that covered areas as different as nutrient-rich upwelled waters and oligo-

trophic subtropical gyres (Fig. 4.1). All the cruises were conducted between February and October 2011 (Table 4.1). Zooplankton samples were obtained by vertical WP-2 net hauls (UNESCO, 1968) in the epipelagic waters (0 - 200 m), at a speed no faster than 0.2 - 0.3 m s^{-1} as recommended by Sameoto et al. (2000) for physiological studies on live organisms. The net consisted of a single 60 cm-diameter ring equipped with a 100 μm or 200 μm size mesh, depending on the cruise, and with a large cod-end to prevent damage of the organisms. Once on deck, organisms were screened into 100 - 500 μm (200 - 500 μm in Benguela), 500 - 1000 μm and > 1000 μm size-fractions. Then, in order to reduce stress, they were placed in filtered seawater for a short time, prior to analysis.

Healthy organisms were gently transferred to 60 mL glass-capped bottles for incubation. Special care was taken when filling the bottles to avoid the presence of large phytoplankton. Incubation times ranged between 60 - 90 min, depending on the abundance of organisms within the bottles, and they were all carried out in darkness. When the incubation was finished, the organisms were collected on a 50 μm mesh, placed in cryovials and shock-frozen in liquid N_2. Afterwards, the samples were stored at –80 °C for subsequent determination of the biochemical parameters.

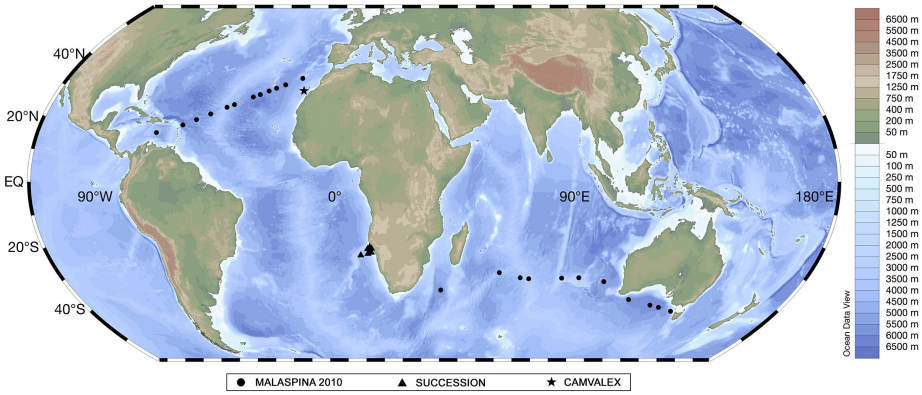

Figure 4.1: Station positions of the three oceanographic cruises where the zooplankton samples were taken. All the cruises were conducted between February and November in 2011. The average temperature and chlorophyl for each location are described in Table 4.1. Organisms were collected by vertical net hauls from the epipelagic waters (0 - 200 m) at all the stations.

4.2.2 Respiration measurements

The O_2 consumption rate (R_{O_2}) was determined as the change in the dissolved O_2 concentration during the incubation time. These values were corrected for the signal obtained in bottles with only filtered seawater (blanks). The dissolved O_2 concentration was continuously monitored by a 6-channel Strathkelvin 928 Oxygen System ® respirometer that was coupled to a refrigerated recirculator in order to maintain a stable temperature during the incubation. Previously, the respirometer was calibrated according to the Strathkelvin 928 manual, with O_2-saturated water as the maximum value and Na_2SO_4 treated-water as zero.

4.2.3 Chlorophyll-*a* determination

All chlorophyll-*a* measurements were carried by extracting the pigments in acetone. However, the samples from Malaspina 2010 cruise were analyzed onboard fluorometrically according to Yentsch and Menzel (1963) whereas the samples from Camvalex and Succession cruises were analyzed in the lab by the spectrophotometric method described by Parsons et al. (1984).

4.2.4 Biochemical parameters

(i) ETS activity. The ETS activity was measured kinetically by the Owens and King (1975a) method, considering the modifications described in Packard et al. (1996). The absorbance increase of the INT-formazan at 490 nm was continuously monitored for 6 minutes in 1 cm path length-cuvettes at the average temperature of each cruise (see Table 4.1). The regression line of absorption versus time was used to estimate the ETS activity and potential respiration rates (Φ) after Packard and Williams (1981). The tetrazolium, INT (2-p-iodophenyl-3-p-nitrophenyl monotetrazolium chloride) was reduced by the respiratory ETS enzymes, replacing the O_2 as the electron acceptor. The INT accepts two electrons whereas the O_2 would accept four. Thus, the INT-formazan production rate is stoichiometrically related by a factor of 2 to ETS activity and by a factor of 0.5 to Φ. Blanks were run without the ETS substrates in order to subtract the contribution of the non-enzymatic reduction of the INT (Maldonado et al., 2012). All the Φ rates were corrected to *in situ* temperatures using the Arrhenius equation and an activation energy of 15 kcal mol^{-1} (Packard et al., 1975).

(ii) Protein content. Biomass was estimated as the protein concentration in the samples by the Lowry method (Lowry et al., 1951) with the modifications described by Rutter (1967). Calibration curves were made from standard solutions of bovine serum albumin (BSA).

(iii) Pyridine nucleotides concentration. The pyridine nucleotides were determined by a modification of the method described by Wagner and Scott (1994). We introduced an additional step for the homogenization of the zooplankton samples by sonication, followed by a centrifugation of 2 minutes at 4000 rpm and 0 °C. We then discarded the pellet and analyzed the supernatant. This assay is based on a single-extraction procedure that distinguishes between the oxidized and reduced forms by means of heat. An incubation of the extract for 30 min at 60 °C destroys the oxidized forms while has no effect on the reduced forms. Accordingly, the total amount of PNs in the sample is determined from the unheated extract whereas the reduced fraction is determined from the heated extract. The oxidized forms are calculated as the difference between these two values. The phosphorylated (NAD(P)H) and non-phosphorylated (NAD(H)) forms of the pyridine nucleotides were differentiated by the cycling buffer involved in each assay.

NAD(H) determination. One hundred microliters of the heated/unheated extracts were added to 800 µL of ice-cold, freshly prepared NAD cycling buffer and incubated in the dark at 37 °C for 5 min. The NAD cycling buffer contained 100 mM Tris-HCl (pH 8.0), 0.5 mM thiazolyl blue (MTT), 1 mM phenazine ethosulfate (PES), 0.2 mg mL^{-1} alcohol dehydrogenase (ADH) and 1 % bovine serum albumin (BSA). Following temperature equilibration, 100 µL of ethanol were added to start the reaction. Before measuring the MTT-formazan production in the spectrophotometer, a quick centrifugation (16000g, 30 s) was necessary to remove any insoluble material. Afterwards, the change in absorbance at 570 nm was monitored over 3 min at 37 °C in a thermoregulated cuvette holder. The reactions in the NAD cycling buffer were as follows:

$$Ethanol + NAD^+ \xrightarrow{ADH} Acetaldehyde + NADH + H^+ \tag{4.1}$$

$$NADH + PES_{ox} \xrightarrow{non-enzymatic} NAD^+ + PES_{red} \tag{4.2}$$

$$PES_{red} + MTT \xrightarrow{non-enzymatic} PES_{ox} + MTT - formazan \quad (4.3)$$

NADP(H) determination. One hundred microliters of the heated/unheated extracts were added to 800 µL of ice-cold, freshly prepared NADP cycling buffer and incubated in the dark at 37 °C for 5 min. The NADP cycling buffer contained 100 mM Tris-HCl (pH 8.0), 0.5 mM thiazolyl blue (MTT), 2 mM phenazine ethosulfate (PES), 5 mM Na_4EDTA and 1.3 IU mL^{-1} of glucose-6-phosphate dehydrogenase (G6PDH). Following incubation, 100 µL of 10 mM glucose-6-phosphate (G6P) were added to start the reaction. In this case, no centrifugation step was required. The change in absorbance at 570 nm was monitored over 3 min at 37 °C in a thermoregulated cuvette holder. The reactions in the NADP cycling buffer were as follows:

$$Glucose-6-phosphate + NADP^{+} \xrightarrow{G6PDH} 6-phosphogluconate + NADPH + H^{+} \quad (4.4)$$

$$NADPH + PES_{ox} \xrightarrow{non-enzymatic} NADP^{+} + PES_{red} \quad (4.5)$$

$$PES_{red} + MTT \xrightarrow{non-enzymatic} PES_{ox} + MTT - formazan \quad (4.6)$$

The slope of the MTT-formazan production rate in each case was used to quantify the amount of PNs present in the samples. To accomplish this, standards of NADH and NADPH were prepared (ranging from 0 - 1000 nM) and were assayed as stated above. A standard curve for each nucleotide was determined by the regression line of formazan production rate versus concentration. Fig. 4.2 shows an example for the NADH.

4.2.5 **Statistical analysis**

The variability of the biological parameters (R_{O_2}, Φ, NAD and NADP) at the different sampling sites and between the three size fractions was studied by a two-way ANOVA test. A pairwise comparison procedure based on the Holm-Sidak method (with 999 permutations) was applied to reveal the differences between the significant factors. Previously, the normality of the data was analyzed by the Shapiro-Wilk test and, as a result, they were log trans-

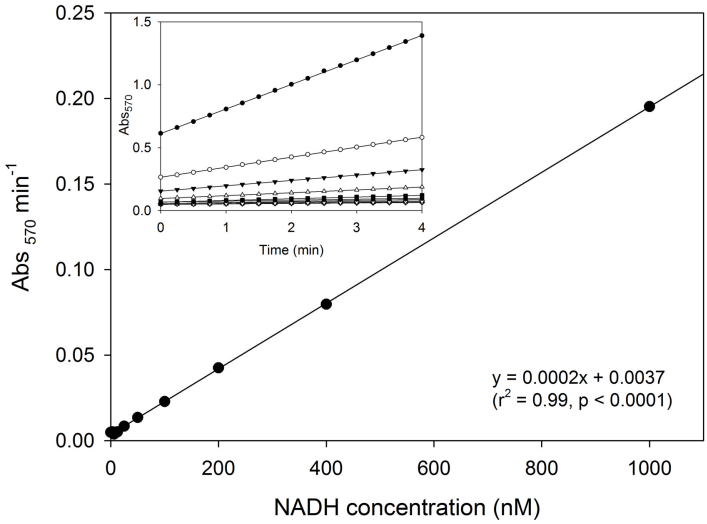

Figure 4.2: Construction of the standard curve for the NADH determination. Each data point represents the slope of the MTT-formazan production-rate per minute obtained at the different NADH concentrations (inset). The resultant regression line is used to estimate the NADH concentration present in the zooplankton samples. The standard curve for the NADPH was constructed in the same way.

formed. Furthermore, a multiple regression technique was adopted to analyze the relationship of the biological parameters (dependent variables) with the habitat temperature and chlorophyll-*a* concentration (independent variables). Finally, in order to detect significant differences in the variables between the two samplings conducted off Canary Islands, a Student *t*-test was applied. All these analysis were performed with the statistical software Sigma plot version 12.5.

4.3 Results

The hydrographic characteristics of the four sampling regions were considerably different among them (Table 4.1). Highest surface temperature (25.1 °C) and lower chlorophyll-*a* concentration (0.08 mg m^{-3}) corresponded to the North Atlantic (NA) waters. Conversely, the nutrient-rich waters from the

Table 4.1: Sampling regions and dates (all in 2011) surveyed during the three oceanographic cruises where the zooplankton samples were collected. Mean values and ranges (in parentheses) of surface temperature and chlorophyll at each location are also given. Inc. number represents the number of incubations performed during each cruise. See Fig. 4.1 for station positions.

Cruise	Location	Date (2011)	Surface Temp. (°C)	Surface chlorophyll (mg m^{-3})	Inc. number
Malaspina 2010	North Atlantic	Jun. - Jul.	25.1 (28.8 - 21.1)	0.08 (0.27 - 0.04)	57
	Indian Ocean	Feb. - Mar.	21.5 (25.9 - 16.5)	0.18 (0.52 - 0.04)	23
Camvalex	Canary Islands	Apr.	19.3 (20.8 - 18.2)	0.34 (0.36 - 0.33)	83
		Oct.	22.1 (23.3 - 20.6)	0.24 (0.26 - 0.22)	52
Succession	Benguela Upwelling	Aug. - Sep.	14.6 (16.2 - 12.8)	3.18 (14.34 - 0.75)	32

Benguela Upwelling (BU) presented the lowest surface temperature (14.6 °C) and a chlorophyll-*a* concentration more than 10-fold higher as compared to the other sampled regions (3.18 mg m^{-3}). The Indian Ocean (IO), in turn, was characterized by an average surface temperature of 21.5 °C and a chlorophyll-*a* concentration of 0.18 mg m^{-3} during the austral summer. Finally, although a seasonal change was observed in seawater features off the Canary Islands (CI, Table 4.1), the average values of surface temperature and chlorophyll-*a* concentration for this location were 20.4 °C and 0.29 mg m^{-3}, respectively.

4.3.1 **Spatial variability of respiratory metabolism in zooplankton**

As expected, the highest protein-specific Φ and R_{O_2} rates were measured in the smallest size fraction whereas the lowest rates were found in the zooplankton over 1000 μm (Table 4.2). Indeed, a more detailed examination of the differences between the size fractions and the sampling locations by two-way ANOVA test (Table 4.3) revealed that specific Φ rates were significantly higher in the 100 - 500 μm size zooplankton in all regions, except in the BU where no significant differences between sizes were found. Here, the specific Φ rates were rather constant, ranging from 1.12 μmol O_2 mg $prot^{-1}$ h^{-1} in large zooplankton to 1.18 μmol O_2 mg $prot^{-1}$ h^{-1} in the small zooplankton. The largest difference between size fractions were measured in organisms from the NA, where the values varied from a low of 1.75 μmol O_2 mg $prot^{-1}$ h^{-1} in large zooplankton to a high of 3.30 μmol O_2 mg $prot^{-1}$ h^{-1} in the smallest size frac-

Table 4.2: Mean values ± SD of the protein-specific potential respiration (Φ), respiration (R_{O_2}), and NAD and NADP concentrations measured in three size fractions of zooplankton from the different oceanic regions. Note that the small zooplankton in the Benguela upwelling ranged between 200 and 500 µm, in contrast to the 100 - 500 µm range considered in the other regions. The values in parentheses represent the number of samples analyzed for each parameter and size. Gap indicates no data available.

	Φ (µmol O_2 mg $prot^{-1}$ h^{-1})	R_{O_2} (µmol O_2 mg $prot^{-1}$ h^{-1})	NAD (pmol mg $prot^{-1}$)	NADP (pmol mg $prot^{-1}$)
North Atlantic				
100 - 500 µm	3.30 ± 1.23 (39)	2.60 ± 1.14 (19)	423.96 ± 87.26 (4)	139.73 ± 73.14 (10)
500 - 1000 µm	2.40 ± 0.86 (34)	1.86 ± 0.97 (16)	281.33 ± 117.37 (6)	119.06 ± 35.13 (6)
> 1000 µm	1.75 ± 0.68 (15)	1.79 ± 0.57 (4)	933.82 (1)	193.90 (1)
Canary Islands				
100 - 500 µm	1.79 ± 0.84 (153)	1.42 ± 0.77 (44)	668.58 ± 196.75 (27)	173.39 ± 55.90 (34)
500 - 1000 µm	1.47 ± 0.76 (50)	1.18 ± 0.80 (22)	645.46 ± 233.83 (15)	179.11 ± 51.49 (13)
> 1000 µm	1.10 ± 0.51 (15)	0.98 ± 0.49 (10)	500.49 ± 146.24 (3)	180.44 ± 91.22 (4)
Benguela Upwelling				
200 - 500 µm	1.18 ± 0.34 (13)	0.98 ± 0.54 (21)	-	157.77 ± 51.38 (7)
500 - 1000 µm	1.15 ± 0.53 (27)	0.99 ± 0.61 (36)	879.16 ± 292.10 (5)	305.80 ± 126.32 (8)
> 1000 µm	1.12 ± 0.66 (15)	0.89 ± 0.52 (11)	895.81 ± 326.69 (5)	340.50 ± 185.86 (5)
Indian Ocean				
100 - 500 µm	1.61 ± 0.52 (18)	1.43 ± 0.61 (15)	299.54 ± 67.97 (4)	205.35 ± 57.57 (4)
500 - 1000 µm	1.71 ± 0.42 (15)	1.11 ± 0.54 (12)	319.76 ± 70.50 (5)	185.59 ± 84.27 (8)
> 1000 µm	1.01 ± 0.48 (13)	0.93 ± 0.38 (6)	454.77 ± 99.04 (3)	257.52 ± 97.59 (4)

Table 4.3: Results of 2-way ANOVA testing for differences in the potential respiration (Φ), respiration (R_{O_2}), and NAD and NADP concentrations between sampling locations (Lo) and zooplankton size (Si). A logarithmic transformation was applied to all the variables to achieve the normality of the data. Location acronyms corresponds to the North Atlantic (NA), the Canary Islands (CI), the Benguela Upwelling (BU) and the Indian Ocean (IO). The three size fractions considered are 100 - 500 μm (100), 500 - 1000 μm (500) and larger than 1000 μm (1000). All pairwise multiple comparisons were obtained by the Holm-Sidak method with a significance level of 0.05.

	df	MS	F	*p*	Pairwise comparison
Φ					
Location	3	3.04	34.91	***	NA: 100 > 500 > 1000*
Size	2	1.42	16.32	***	CI: 100 > 500*; 100 > 1000***
Lo × Si	6	0.19	2.13	*	BU: n.s.
Residual	392	0.09			IO: (100 = 500) > 1000*
Total	403	0.13			
					100: NA > (CI, BU, IO)***; CI > BU*
					500: NA > CI***; NA > BU***
					1000: NA > (CI = BU = IO)*
R_{O_2}					
Location	3	1.30	13.55	***	NA > (CI = BU = IO)***
Size	2	0.51	5.31	**	
Lo × Si	6	0.81	0.85	0.532	100 > (500 = 1000)*
Residual	201	0.10			
Total	212	0.13			
NAD					
Location	3	311.38	18.55	***	CI > (NA = IO)***
Size	2	16.60	0.99	0.377	BU > (NA = IO)***; BU > CI*
Residual	72	16.79			
Total	77	28.79			
NADP					
Location	3	38.43	5.63	***	NA: n.s.
Size	2	21.44	3.14	*	CI: n.s.
Lo × Si	6	16.54	2.43	*	BU: (500 = 1000) > 100**
Residual	90	6.82			IO: n.s.
Total	101	9.40			
					100: n.s.
					500: BU > NA***; BU > CI**; BU > IO*
					1000: BU > CI*

*Significant at a level $p < 0.05$, ** $p < 0.01$, *** $p < 0.001$; n.s.: not significant.

tion. Similar results were achieved by the specific R_{O_2} rates, which showed higher values for the small zooplankton in all the locations (Table 4.2). However, no significant difference between 500-1000 μm and > 1000 μm size fractions was noted in the specific R_{O_2}. When average protein-specific rates for the total zooplankton were compared (Fig. 4.3), we observed that Φ and R_{O_2} rates of organisms from the NA were significantly higher ($p < 0.001$) than the values measured in the other sampling sites (Table 4.3). Average values in the CI, the BU and the IO, however, were not significantly different between them. Still, the small zooplankton from the CI, presented a Φ rate of 1.79 μmol O_2 mg $prot^{-1}$ h^{-1} that was significantly higher ($p < 0.05$) than its counterpart in the BU (1.18 μmol O_2 mg $prot^{-1}$ h^{-1}).

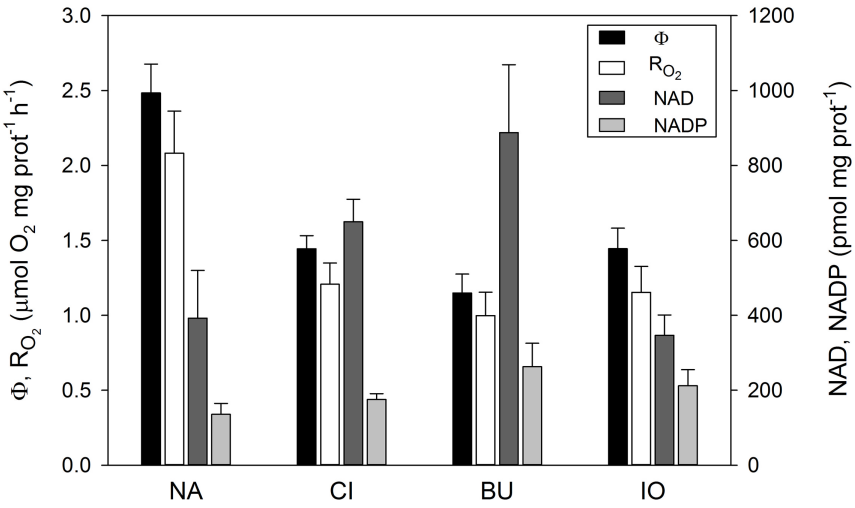

Figure 4.3: Comparison of the protein-specific potential respiration (Φ) and respiration (R_{O_2}) rates, as well as protein- specific concentration of the pyridine nucleotides (NAD, NADP) in the zooplankton from the different sampling sites. The location acronyms from the *y*-axis stands for the North Atlantic (NA), the Canary Islands (CI), the Benguela Upwelling (BU) and the Indian Ocean (IO). Bars represent average values for the zooplankton ranging from 100 μm to larger than 1000 μm, except for the BU where the lower end of the range corresponded to 200 μm size. Error bars indicate the 95 % confidence limits.

The R_{O_2}/Φ ratios have been routinely used to calculate the physiological O_2 consumption rates from enzymatic activity measurements. Fig. 4.4 shows the ratios determined for the mixed zooplankton community at the different

sampling sites. The highest values corresponded to organisms from the NA waters, with a mean value (± SD) of 0.73 (± 0.05). However, this ratio was only significantly different ($p < 0.001$) from the one obtained in the zooplankton from the BU region, which presented the lowest values (0.43 ± 0.05). The ratios measured in the organisms from the CI and the IO were of 0.57 ± 0.04 and 0.61 ± 0.05, respectively.

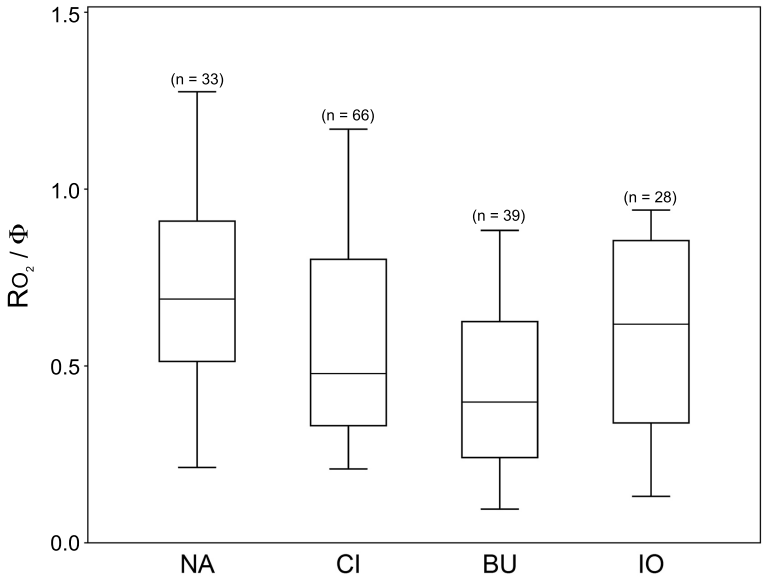

Figure 4.4: Box plot showing the differences between the respiration/potential respiration ratios (R_{O_2}/Φ) in the zooplankton collected in the North Atlantic (NA), the Canary Islands (CI), the Benguela Upwelling (BU) and the Indian Ocean (IO). Lower and upper boundaries of the box correspond to the first and third quartiles, respectively, while the line in the box indicates the median. Error bars represent the 95 % confidence limits and n the number of incubations considered at each sampling site.

The PN concentration did not parallel the pattern depicted by R_{O_2} and Φ rates (Table 4.2). We determined the oxidized and reduced forms of these coenzymes separately but, unfortunately, we could not quantify the relative proportion of the reduced forms due to methodological problems during the analysis. Accordingly, the values of NAD and NADP presented here refers to the sums of the oxidized and reduced forms. The NAD levels showed significant differences between regions but not between size fractions (Table 4.3). The

highest concentrations for each size fraction were obtained in organisms from the BU, with the exception of the value reported for the large zooplankton in the NA waters which can be, however, attributed to the scarcity of data (n = 1). The average concentration for the entire zooplankton community was higher in the samples from the BU ($p < 0.001$, Table 4.3), with a value of 887.49 nmol NAD mg prot^{-1} (Fig. 4.3). The lowest value, in turn, was measured in organisms from the IO (346.77 nmol NAD mg prot^{-1}), although it was not significantly lower than the concentration of 392.52 nmol NAD mg prot^{-1} determined in the NA ($p = 0.66$). The average NAD levels of the zooplankton from the CI (649.67 nmol NAD mg prot^{-1}) was higher than the value found in both the NA and the IO ($p < 0.001$). On the other hand, the NADP levels were 2 - 4 times lower than the NAD concentration (Table 4.2). In this case, there were only significant differences between the size fractions in the BU ($p < 0.01$), where the zooplankton larger than 500 μm presented a higher concentration of NADP than the small zooplankton. When average values for the total zooplankton community were considered (Fig. 4.3), we observed significant differences between sampled regions, mainly due to the zooplankton larger than 500 μm (Table 4.3). Thus, NADP levels in zooplankton from the BU were significantly higher (262.67 nmol mg prot^{-1}) than the levels measured in the NA (135.62 nmol NADP mg prot^{-1}), the CI (175.40 nmol NADP mg prot^{-1}) and the IO (211.96 nmol NADP mg prot^{-1}).

Multiple and simple regression analysis were determined for each size fraction to study the dependency of the rates and concentrations studied above on the environmental factors (Table 4.4). In the present work, we have used the chlorophyll-*a* concentration as a relative index of the productivity of the waters (Lorenzen, 1970). Thus, R_{O_2}, Φ, NAD and NADP were included as the dependent variables and temperature and chlorophyll-*a* as the continuous independent variables. Temperature accounted for around 26 % of the variability of the Φ rates in zooplankton ranging from 100 - 1000 μm whereas it dropped to 7.5 % in larger zooplankton. In contrast, chlorophyll-*a* could not explain more than 13 % of the variability of these rates. However, the combination of these two parameters explained from a low of 14 % in large zooplankton to a high of 29 % in organisms below 1000 μm. Similar effect of both temperature and chlorophyll-*a* was observed in R_{O_2}, although in this case the mayor dependency on temperature was only observed in the small zooplankton (100 - 500 μm). Additionally, no significance was attained between chlorophyll-*a* and

Table 4.4: Variance of the size-fractionated potential respiration (Φ), respiration (R_{O_2}), as well as NAD and NADP concentrations that is explainable by habitat temperature (Temp), chlorophyll-*a* (Chl *a*) concentration and a combination of both (Temp × Chl *a*). Data represent the adjusted r^2 of the multiple or simple regression analysis applied in each case and are expressed as percentages. The *n*-value represents the number of samples.

		n	Temp	Chl *a*	Temp × Chl *a*
100 - 500 µm	Φ	225	25.5 ***	6.6 ***	28.7 ***
	R_{O_2}	96	25.9 ***	12.4 ***	30.5 ***
	NAD	35	15.8 **	31.3 ***	42.2 ***
	NADP	55	n.s.	n.s.	n.s.
500 - 1000 µm	Φ	121	25.8 ***	13.2 ***	28.8 ***
	R_{O_2}	86	10.0 **	5.2 *	12.3 **
	NAD	31	42.7 ***	23.9 **	42.8 ***
	NADP	33	42.0 ***	36.4 ***	40.3 ***
> 1000 µm	Φ	58	7.5 *	n.s.	14.2 **
	R_{O_2}	31	9.8 *	n.s.	17.1 *
	NAD	12	n.s.	29.6 *	45.3 *
	NADP	14	n.s.	n.s.	n.s.

*Significant at a level $p < 0.05$, ** $p < 0.01$, *** $p < 0.001$; n.s.: not significant.

both Φ and R_{O_2} rates in large zooplankton. The variance of the NAD concentration attributable to temperature differ between size fractions and was maximum for 500 - 1000 µm size zooplankton (43 %), whereas the chlorophyll-*a* accounted for 24 - 31 % of the NAD variation. When the two environmental parameters were considered together the percentage of the variance explained by them arose to 42 - 45 %. Contrarily, the NADP concentration did not appear to have any dependency on either temperature or chlorophyll-*a* as no significance was obtained, except for the 500 - 1000 µm size fraction where the two parameters explained around 40 % of its variance.

4.3.2 **Temporal variability of zooplankton respiration and pyridine nucleotides off the Canary Islands**

Both the environmental parameters and the biological variables evidenced a temporal variability between the samplings in April and October off the Canary

Islands (Table 4.1, Fig. 4.4). The average surface temperature increased from the 19.3 °C measured during the late winter bloom (CI-LWB) in April, to the 22.1 °C recorded in October, when the water column was more stratified (CI-ST). At the same time, the chlorophyll-*a* at the surface waters was significantly lower in October than in April (Student *t*-test, $p < 0.01$).

Fig. 4.5 shows a general decline in the biological variables for the two smaller size fractions between CI-LWB and CI-ST. No data are available for large zooplankton (> 1000 μm) in April. The small zooplankton displayed a significant decrease (Student *t*-test, $p < 0.001$) of 29 % and 35 % of the Φ and R_{O_2} rates, respectively, from April to October. Parallel decline was recorded for the 500 - 1000 μm size zooplankton, although the decrease of the R_{O_2} was greater (65 %) in this organisms. Likewise, we observed a significant reduction of the NAD concentration in 500 - 1000 μm size fraction at CI-ST to half the value at CI-LWB (Student *t*-test, $p < 0.001$), whereas it remained virtually constant in the smaller zooplankton. The NADP concentration, in turn, did not showed a diminution between the two samplings in any size fraction. The R_{O_2}/Φ ratio resembled the decrease in the NAD concentration, with a significantly lower value at CI-ST for the 500 - 1000 μm organisms while no variation in the ratio for the 100 - 500 μm size fraction was observed. Values of each variable determined in the larger zooplankton (> 1000 μm) did not differ to those reported for smaller organisms (< 1000 μm).

4.4 Discussion

4.4.1 Spatial variability of respiratory metabolism in zooplankton

Carbon flux in the ocean depends directly on the respiration rates of the water-column biota. Accordingly, variations in these rates would impact the efficiency of the organic matter remineralization and, eventually, the sedimentation rate of the refractory compounds (Osma et al., 2014; Packard et al., 2015). Here, we have reported the respiratory metabolism of zooplankton collected from various oceanographic systems with contrasting productivity regimes. The highest metabolic rates and enzymatic activities were found in the smallest zooplankton (Table 4.2), which agrees with observations by Ikeda and Mitchell (1982). Averaged specific R_{O_2} varied from a low of 0.99 μmol O_2 mg prot^{-1} h^{-1} in the BU waters to a high of 2.08 μmol O_2 mg prot^{-1} h^{-1} in the NA region. These values are considerably higher than the specific R_{O_2} range (0.37

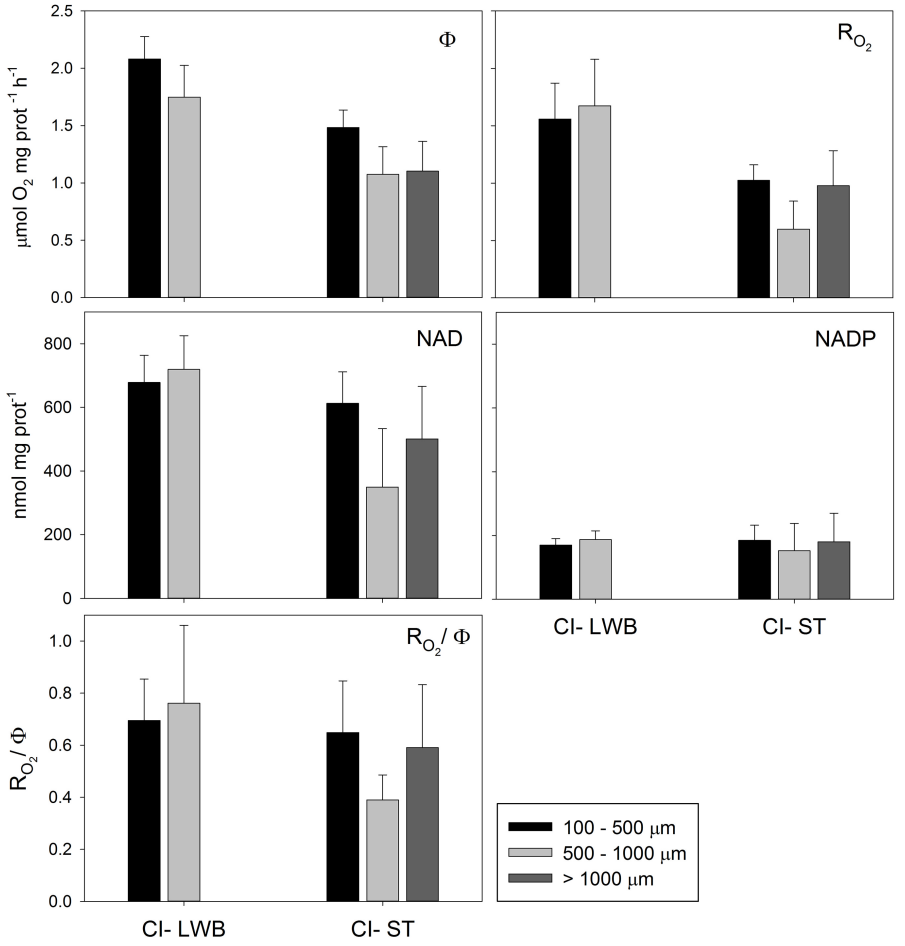

Figure 4.5: Comparison of the protein-specific potential respiration (Φ), respiration (R_{O_2}), pyridine nucleotides (NAD, NADP) concentration and the R_{O_2}/Φ ratios determined in three size fractions of zooplankton from a station off the Canary Islands that was sampled twice in 2011. The first sampling was conducted on April and corresponded to a late winter bloom (LWB) situation characterized by high-nutrients, low-temperature waters. The second sampling was conducted on October and corresponded to a more stratified (ST) situation, characterized by warmer waters and lower chlorophyll-*a* concentration (Table 4.1). No data are available for > 1000 μm zooplankton in April due to their exceptional appearance in the collected samples. Bars represent average values for each size fraction whereas error bars indicate the 95 % confidence limits.

- 0.62 μmol O_2 mg $prot^{-1}$ h^{-1}) predicted by the equations of Ikeda (1985), but they are within the range of 0.90 - 1.86 μmol O_2 mg $prot^{-1}$ h^{-1} reported by Hernández-León and Ikeda (2005) for the same latitudes. A dry mass to protein conversion factor of 1/0.192 was applied in both cases for the data comparison (Postel et al., 2000). The reasons for the relative difference between our values and Ikeda's may be two-fold. On the one hand, our averaged values may be biased to some extent as the number of samples considered from the smallest size fraction (n = 99) tripled that of the largest zooplankton (n = 31). However, the major reason is likely that they included a large proportion of data from high latitudes and from extremely low habitat temperatures to obtain their equations, which are characterized by lower metabolic rates. In this light, the temperature has been identified as the most influential factor on the metabolic rates of marine zooplankton, together with body mass (Ikeda, 1985; Ikeda et al., 2001; Ivleva, 1980). Our results reflected this influence, as the minimum R_{O_2} for all size fractions was measured in the cold waters of the BU (Fig. 4.3), despite it being the most productive system of this study (Table 4.1). Furthermore, the temperature explained a higher percentage of the R_{O_2} variability in the ocean than did the chlorophyll-*a* concentration, being maximum for the small zooplankton (26 %, Table 4.4). If a Q_{10} value of 1.8 (averaged value from Ikeda, 1985) is applied and the R_{O_2} is standardized to the highest temperature (25.1 °C), the specific rate in the BU (1.85 μmol O_2 mg $prot^{-1}$ h^{-1}) would be close to that obtained in the NA. A comparable effect of the habitat temperature on the enzymatic activity of the ETS was described by Packard et al. (1975), and is also evidenced in our results (Table 4.2, Fig. 4.3). On the other hand, the influence of temperature on the R_{O_2}/Φ ratios of zooplankton has also been described before in the literature (Hernández-León and Gómez, 1996; King and Packard, 1975). Thus, Hernández-León and Gómez (1996) observed higher ratios at lower temperatures, which they attributed to the indirect effect of the relationship between primary production and mixing in the water column. King and Packard (1975), in turn, did not attain any significance between the R_{O_2}/Φ ratios and the temperature, although the regression line that they determined between the two variables indicated a positive and exponential increase of the ratio with increasing temperature, which agrees with our results (Fig. 4.4). Furthermore, these authors measured a significantly lower ratios for gelatinous zooplankton as compared to the R_{O_2}/Φ for the non-gelatinous zooplankton. Accordingly, a difference in the species composition may explain

the lower R_{O_2}/Φ values registered in the BU despite being the most productive system, as these waters were characterized by a high abundance of gelatinous zooplankton by the sampling time (Fernández-Urruzola et al., 2014).

The biomass-specific PN concentrations measured in zooplankton ranged between 281 - 933 pmol mg prot^{-1} for NAD, and between 119 - 340 pmol mg prot^{-1} for NADP (Table 4.2). These values constitute one of the first determinations of the PN in the marine zooplankton and, consequently, there is virtually no information available to be compared with in these organisms. Schomer and Epel (1998) measured the PN concentration in marine invertebrate eggs, although they focused on the redox ratios between the reduced and oxidized forms and do not present any concentration on a biomass basis. Still, the ranges measured here are in good agreement with the values reported for a cultured marine dinoflagellate (*Chapter 5*) as well as for other several species of bacteria (Andersen and von Meyenburg, 1977; Karl, 1980; London and Knight, 1966; Wimpenny and Firth, 1972). By contrast, they are slightly lower than those determined in other more complex eukaryotes (for instance, Agius et al., 2001; Umemura and Kimura, 2005, in plant and animal cells, respectively). We expected to obtain the highest NAD and NADP values in high productive areas, and viceversa, provided that *(i)* the PNs concentration is directly proportional to the food availability and, *(ii)* food availability is proportional to the productivity of the system. Our results support this hypothesis as the zooplankton from the BU showed significantly higher average concentrations whereas the lowest values were obtained in organisms from the more oligotrophic waters of NA and IO (Fig. 4.3, Table 4.3). When the size fractions were considered separately, the NADP concentration showed similar values in all the regions, except in the BU where the values of the zooplankton over 500 μm doubled that of the small zooplankton. This is likely explained by the key role of NADP on the anabolic reactions and growth processes. Thus, these waters were characterized by a complex interplay of water masses that encompasses exponential growing populations, with the highest biomass observed in larger zooplankton (Fernández-Urruzola et al., 2014). The NAD concentration, in turn, did not present any significant difference between the size fractions (Table 4.3), albeit it showed differences between regions. This evidences a parallel response of the intracellular NAD levels in the three size fractions to food availability. As commonly occurs in other organisms (Pollak et al., 2007), the NAD levels were higher than the NADP levels in all the

cases. Hence, the NAD/NADP ratios obtained here for oceanic zooplankton ranged from 2 to 5, which is consistent with the range of 0.8 - 8 reported for several bacteria species (Brody, 1972; Manlapaz-Fernandez and Olivera, 1973; Setlow and Setlow, 1977). Although in the present work it was not possible to determine the reduced and the oxidized forms of NAD and NADP separately, it would be interesting to study short-term changes of the relative contribution of each form to the total pool, as the oxidized/reduced ratios are involved in the regulation of the intracellular redox state and in the control of many metabolic enzymes (Mathews et al., 2000).

An aim of the present work was to explore the relationship of the R_{O_2} and the PN concentration in the zooplankton from different oceanic regions. On the basis of the work accomplished by Packard et al. (1996) and Aguiar-González et al. (2012), we expected to record a parallel pattern of the R_{O_2} and PNs concentration through the sampled regions, with the peaks of R_{O_2} coinciding with the peaks of NAD and NADP concentrations. However, this was not the case (Fig. 4.3). While the highest R_{O_2} rates were observed in the warmer waters of the NA, the highest values of PNs were measured in the high productive waters of BU. This discrepancy is likely due to a distinct effect of the habitat temperature and the water productivity on the two variables (Table 4.4), which masks their relationship at the intracellular level. Furthermore, other factors such as the specie composition might also affect in a different way the R_{O_2} and PNs concentration, contributing to the mismatch observed between their patterns in the ocean. All in all, it is clear that experiments on monospecific cultures at constant temperatures are needed in order to isolated the response of the respiratory metabolism and intracellular NAD and NADP concentrations to changing food conditions (see *Chapter 5*).

4.4.2 **Temporal variation in coastal waters**

Substantial temporal change in the respiratory metabolism of zooplankton was found between the two compared periods around the Canary Islands (Fig. 4.5). Highest rates were measured during the late winter bloom when the disruption of the seasonal thermocline allows the entrance of nutrients into the surface waters and an increase in the primary productivity is promoted (Menzel and Ryther, 1961). During this time, the zooplankton biomass and metabolic rates were observed to peak with a short delay with respect to the chlorophyll maximum (Arístegui et al., 2001; Hernández-León et al., 2004; Schmoker et al.,

2012). Our average biomass-specific Φ rates for the zooplankton (2.0 μmol O_2 mg $prot^{-1}$ h^{-1}) are in accordance with previous observations in these waters by Hernández-León et al. (2004). These authors reported average rates, for the same zooplankton range, of around 2.2 μmol O_2 mg $prot^{-1}$ h^{-1} for the beginning of April, the time of our sampling.

As the surface waters get warmer, a restoration of the thermocline occurs which impedes the vertical flux of nutrients and limits the phytoplankton growth. Under this situation, we observed an average decrease for both the specific-Φ and R_{O_2} rates of 32 % and 40 %, respectively, which agrees with the decline reported for the zooplankton biomass in these waters between these two periods (Arístegui et al., 2001; Schmoker and Hernández-León, 2013). The fact that R_{O_2} dimished at a higher rate than Φ entailed a drop in the R_{O_2}/Φ (Fig. 4.5). Similarly, Hernández-León and Gómez (1996) showed a seasonal decrease of the ratio from a high of 0.77 during the late winter mixing period to a low of 0.5 during the stratification conditions, which agrees with the averaged decline reported here. On the view of the results, it can be presumed that food availability is a major factor affecting both the metabolic rates and enzymatic activities, although the latter presented a more mitigated response, as observed by Bamstedt (1980). In this case, the slight increase of surface temperature in November (Table 4.1) does not affect the metabolic rates and enzymatic activities more than does the productivity of the water. Other studies in the North Atlantic have likewise shown seasonal changes in the metabolic rates of copepods associated with the phytoplankton production cycle (Conover and Corner, 1968; Marshall and Orr, 1958).

Here, we have used the chlorophyll-*a* concentration as an index of the phytoplankton biomass and productivity of the system. In the coastal waters of the Canary Islands, 60 % of the primary production is due to picoplanktonic cells (<2 μm, Arístegui et al., 2001), which is far below the food preference by zooplankton (Calbet and Landry, 1999). However, these organisms promote the growth of other non-pigmented nano- and microheterotrophs that, in turn, constitute the 35 - 80 % of the zooplankton diet in these waters (Hernández-León et al., 2004). Therefore, although chlorophyll-*a* is not a commonly employed parameter to study the effect of food availability on the respiration rates in zooplankton, it can indirectly put into context the nutritional conditions in which these organisms are living. In this light, and in agreement to what we showed above for the spatial variability, the intracellular NAD concentration

mirrored the productivity pattern of the waters whereas the NADP concentration remained fairly constant between the two samplings (Fig. 4.5). Larger values of NAD for each size fraction were measured during the late winter bloom period whereas they decreased in the stratification period, mainly in the 500 - 1000 μm size fraction. Indeed, the temporal pattern depicted by the R_{O_2} and the NAD concentration resembled each other, which supports the hypothesis that the R_{O_2} is controlled by the substrate concentration (Packard et al., 1996; Aguiar-González et al., 2012). Still, as discussed above, further research is required to understand the short-term changes in the intracellular concentration of PNs and to explore their role in the control of the respiration at the cellular level with changing food conditions (see *Chapter 5*). On the other hand, the lack of data on PN concentration in marine zooplankton impides the verification of whether these changes in the NAD levels are strictly reliant upon the food quantity or whether there are other factors, such as species composition or food quality, that could contribute to the observed seasonal variability. These two aspects are addressed in *Chapters 5* and *6* of this thesis, respectively.

4.5 Conclusions

Both the metabolic rates and enzymatic activities displayed significant differences between the sampling sites, which were mainly attributed to the influence of the habitat temperature. This dependency was further observed in the R_{O_2}/Φ ratios but not in the PNs concentration, which appeared to be directly dependent on the productivity of the system. Consequently, the expected correlation between the R_{O_2} and PNs at different oceanic regions was not detected, as it was masked by the distinct effect of the environmental parameters on the two variables. When the temporal variability was studied, in contrast, the R_{O_2} and PNs concentration depicted a parallel pattern. In this case, the change in the habitat temperature exerted a lower effect and a major influence of the food availability was observed. The NAD and NADP concentrations reported here constitute the first determination of these compounds in marine zooplankton. Needless to say, further research is required to understand how they vary with food quantity and /or quality, as well as within different organisms. This is essential to understand the control of the respiratory metabolism associated with the substrate availability at the cellular level.

Acknowledgements. We wish to thank the crews of the BIO Hespérides, BIO Atlantic Explorer and RV Maria S. Merian for their expert and enthusiastic support during the cruises. We are grateful to C. M. Duarte and L. Postel for providing the opportunity to collect samples during the Malaspina 2010 (CSD2008-00077) and Succession cruises (German Research Foundation, DFG), respectively. M. Estrada and P. Mozetic are also thanked for providing the chlorophyl data from the Malaspina 2010 cruise. This work was founded by the BIOMBA project (CTM2012-32729/MAR) awarded to M. Gomez by the Spanish Ministry of Economy and Competitiveness. T. Packard was supported by Canary Islands CIE: Tricontinental Atlantic Campus (CEI10/00018). N. Osma and I. Fernández-Urruzola received financial support from the Formation and Perfection of the Researcher Personal Program from the Basque Government.

Science, my lad, is made up of mistakes, but they are mistakes which it is useful to make, because they lead little by little to the truth.

Jules Verne

CHAPTER

5

CAPÍTULO

Influence of starvation on respiratory metabolism and pyridine nucleotide levels in the marine dinoflagellate *Oxyrrhis marina*

N. Osma, M. Aristizabal, I. Fernández–Urruzola, T. T. Packard and M. Gómez, Submitted to Protist

ID: PROTIST-D-15-00037R1

ABSTRACT: Respiratory oxygen consumption rate (R_{O_2}) and potential respiration (Φ) has been monitored during a food deprivation period in the heterotrophic dinoflagellate *Oxyrrhis marina*. Φ was determined by measuring the activity of the enzymes from the electron transport system (ETS), the major contributor to the oxygen consumption in the cells. Additionally, we have quantified for the first time the pyridine nucleotides concentration in this organism, both in their oxidized ($NAD(P)^+$) and reduced forms (NAD(P)H). These molecules are the main electron donors at the beginning of the ETS. We observed a dramatic decrease in R_{O_2} within the first days, whereas Φ steadily, but more gradually declined during the entire experiment. This led to a decrease of the R_{O_2}/Φ with time. The intracellular total pool of NAD and NADP concentration, in turn, dropped exponentially in a manner parallel to the R_{O_2}. This

strong decrease was mainly driven by a reduction in the concentration of the oxidized forms. The present work constitutes a first step in clarifying the role of intracellular NAD and NADP concentrations and redox status in the control of *in vivo* R_{O_2} in marine organisms.

Keywords: Electron transport system (ETS); Respiration; Nicotinamide adenine dinucleotide (NAD); Nicotinamide adenine dinucleotide phosphate (NADP); Food deprivation; Microzooplankton.

5.1 Introduction

Knowing respiration rates in the water column is essential to quantify the remineralization of both dissolved and particulate organic matter as well as to describe the energy and carbon fluxes in marine food webs. Still, the magnitude of respiration in the ocean at a global scale remains uncertain (del Giorgio and Duarte, 2002), mainly due to the difficulty in measuring the *in situ* rates throughout different areas and depths with currently available techniques. Most methodologies are based on determining the respiratory oxygen consumption rate (R_{O_2}) on incubated organisms. These rates will be inevitably affected by manipulation, starvation and overcrowding effects during the incubation time (Bidigare, 1983). Moreover, these are tedious and time consuming procedures that diminishes the raw data acquisition rate.

Alternatively, Packard et al. (1971) proposed a biochemical assay to estimate the R_{O_2} by measuring the activity of the key enzymes involved in this process, i. e., the respiratory electron transport system (ETS). The ETS is composed of pyridine nucleotide dehydrogenases, flavin nucleotide dehydrogenases and cytochrome oxidoreductases arranged in four complexes, which together account for more than 95 % of all aerobic and anaerobic respiration (Nelson et al., 2008). This enzymatic system is embedded in the inner mitochondrial membrane in eukaryotic cells and in the plasma membrane in prokaryotic cells. The ETS assay of Packard et al. (1971) was designed to measure, under substrate saturation, the maximum activity of these enzymes or, in other words, the potential respiration (Φ) of the organisms. The significant linear relation between R_{O_2} and ETS activity holds for all organisms from bacteria to large zooplankton, with a size range over 10 orders of magnitude (Christensen et al., 1980; Finlay et al., 1983; King and Packard, 1975). Accordingly, measurements of ETS activity has been systematically applied in field research to describe respiratory processes in a variety of oceanic areas, such as deep-sea

sediments (Christensen and Packard, 1977) and upwelled waters (Fernández-Urruzola et al., 2014). Besides, the ETS activity has also been measured in laboratory experiments to characterize the respiratory metabolism of bacteria (Christensen et al., 1980; Romero-Kutzner et al., 2015), protozoa (Finlay et al., 1983), phytoplankton (Kenner and Ahmed, 1975b; Packard, 1971), zooplankton (Herrera et al., 2011; Owens and King, 1975a) and benthic organisms (Cammen et al., 1990).

But, how does the respiration of an intact organism relate to an *in vitro* measurement of potential respiration at the enzymatic level? Due to the strong causal biochemical relationship between the physiological R_{O_2} and the ETS activity (Nelson et al., 2008), the rate in the former should be determined by the control in the latter. This was the raison d'être behind the original development of the ETS assay (Packard et al., 1971). Later, Packard et al. (1996) explained how a Michaelis-Menten based enzyme kinetic mechanism could control the *in vivo* ETS and respiration during changes in an organism's nutritional state. More recently, Aguiar-González et al. (2012) demonstrated that a model based on substrate concentration (Packard and Gómez, 2008) better predicted respiration rates than a biomass-based model. The ETS substrates are pyridine nucleotides and succinate, although it has been demonstrated that in marine organisms the pyridine nucleotides contribute the most (Savenkoff et al., 1995). They occur in oxidized and reduced forms as nicotine adenine dinucleotide (NAD^+, NADH) and as nicotine adenine dinucleotide phosphate ($NADP^+$, NADPH). Both molecules are ubiquitous in living cells and play a key role in providing reducing equivalents for hundreds of cellular reactions. Since the seminal work of Chance and Williams (1955), where they correlated the mitochondrial metabolic state with the oxidation-reduction levels of nucleotides, there has been a substantial amount of information on the concentration of these coenzymes in animal tissues. Owing to the recognition of additional functions of these molecules in cells signaling, antioxidation and oxidative stress, as well as in cell death, (Berger et al., 2004; Moller and Rasmusson, 1998; Pollak et al., 2007; Ying, 2008; Ziegler, 2005), the study of their concentration and redox status has gain attention in the last years. Still, the knowledge about their concentration and behavior in microorganisms is limited (London and Knight, 1966; Wimpenny and Firth, 1972) and, to our knowledge, is virtually inexistent in marine protozoans. Furthermore, no study has described the intracellular levels of both NAD(H) and NADP(H) in marine organisms and

has compared them with respiration rates.

The importance of microzooplankton as an essential group in the marine microbial food webs has become apparent in the last decade (Landry and Calbet, 2004; Sherr and Sherr, 2002). They are mostly constituted by heterotrophic protists that form an important trophic link between phytoplankton and mesozooplankton, not only by competing for the primary producers with higher trophic levels, but also by becoming the major food source for them (Gismervik, 2006). Understanding the physiology of the microzooplankton would help in the construction of the carbon and energy transfer models throughout the marine food chain. Here, we have focused on the respiratory metabolism of the heterotrophic marine dinoflagellate *Oxyrrhis marina*. It is a cosmopolitan species often found in intertidal pools (Johnson, 2000), with tolerance to highly variable environmental conditions (Lowe et al., 2011; Watts et al., 2011). Moreover, it is an omnivorous organism that can feed in a wide range of particle sizes, either by filtering or by raptorial grazing (Jeong et al., 2008). Although it has also been observed to be cannibalistic under certain ambient conditions (Flynn et al., 1996), Martel and Flynn (2008) reported that the cannibalistic cells seldom amount to more than 2 % of an experimental population. All in all, *O. marina* has traditionally served as a model organism to examine the response of the marine protozoan grazers to a variety of factors (Montagnes et al., 2011). For instance, among the latest works on *O. marina* (Calbet et al., 2013; Hantzsche and Boersma, 2010; Meunier et al., 2012), the common thread has been to determine the influence of the food quality on the biochemical composition and metabolism of this organism, with the subsequent improvement in the food quality for the consumers at higher trophic levels.

In the present work, we have focused on the ETS, the biochemical driver that controls and steers the respiratory processes in *O. marina* and we have shown how this enzymatic activity and the physiological R_{O_2} vary distinctly during a starvation period. Furthermore, we have quantified the intracellular pyridine nucleotide concentration in a marine dinoflagellate for the first time and we have discussed its relation with the respiration rates.

5.2 Material and methods

5.2.1 Culture conditions

The microalga *Rhodomonas salina* and the heterotrophic dinoflagellate *O. marina* were obtained from the microalgal culture collection of the Institute of Marine Sciences in Barcelona (ICM-CSIC, Spain). Batch cultures of *R. salina* (ESD 6.3 - 6.5 μm) were grown in autoclaved 0.2 μm filtered seawater enriched with f/2 medium (Guillard, 1975) and they were kept under exponential growth conditions at 18 °C ± 0.5 °C, 38 PSU, 31.5 μmol photons m^{-2} s^{-1} and 12:12 h light:dark cycle. *O. marina* was cultured at the same temperature and salinity conditions but at lower light intensity (0.8 μmol photons m^{-2} s^{-1}), and was fed on *R. salina*. Both organisms appeared stressed when bubbled with air or when the flasks were agitated continually. So, all experimental flasks were capped with cotton plugs in order to allow gas exchange and were gently swirled several times per day to maintain high levels of oxygen and to keep the cells in suspension. When samples were taken for respiration measurements the initial oxygen concentrations were always above 80 % saturation.

5.2.2 Experimental design

The time-course experiment was conducted in triplicated 2 l Pyrex flasks filled with a well-fed *O. marina* stock culture at a concentration of ~12000 cells mL^{-1}. In order to start with a similar initial concentration of the triplicates, the suspension was gently mixed before filling the flasks. A single pulse of *R. salina* was then added at a concentration of ca. 500000 cells mL^{-1} to assure saturated food conditions, and no more food was supplied during the experimental time. The sampling began once the dinoflagellates had consumed all the food and before the prey were entirely digested inside the *O. marina* cells, i.e. 2 days, as verified by microscope observations. At this moment, a similar procedure to that described by Almeda et al. (2011) was followed in order to reduce the number of bacteria in the cultures during the experiment. First, the cultures were filtered through a 25 μm mesh to remove cell aggregates and other debris. Second, organisms were exposed to low temperatures (10 °C) to promote their settling and the water was carefully removed from the surface by reverse filtration using a 10 μm-meshed siphon. Filtered seawater was then added to resuspend the organisms. After repeating this procedure two times, the cultures were acclimated to the culturing temperature before starting the

sampling. Afterwards, cell samples were taken every second day to determine cell abundances, protein content, ETS activity, levels of pyridine nucleotides and respiration for a total period of 17 days. Except for respiration measurements and cell abundances, the samples were filtered through a 25 mm GF/F filters, immediately frozen in liquid nitrogen and stored at –80 °C until analysis. The optimal sample volume for each parameter was determined in previous experiments to ensure a good signal during the analysis. Aliquots for cell abundance were fixed with lugol (4 %) and counted using a double counting chamber (Neubauer).

5.2.3 Respiration measurements

The O_2 consumption rate (R_{O_2}) was determined as the slope of the linear regression that relates the dissolved oxygen concentration and the incubation time. These values were corrected for the signal obtained in bottles with only filtered seawater (blanks). All the incubations were performed in triplicate bottles, in darkness and for 2 hours. A 6-channel oxygen sensor (mod 928, Strathkelvin Instruments®) was used to record changes in the dissolved O_2 concentration, which was coupled to a refrigerated recirculator in order to keep a stable temperature at 18°C. Oxygen levels were maintained above 50 % saturation. The R_{O_2} is given in μmol O_2 d^{-1} L^{-1} units on a volume basis (Fig. 5.1), as well as in μmol O_2 d^{-1} mg^{-1} prot units for protein-specific rates and in pmol O_2 d^{-1} $cell^{-1}$ units for cell-specific rates (Table 5.1).

5.2.4 Biochemical parameters

Filters were homogenized by tissue grinding for 2 min in an ice-cold water bath, and then centrifuged for 2 min at 4000 rpm and 0 °C. These experimental settings were determined specifically for *O. marina* in previous laboratory experiments. The following biochemical parameters were determined in aliquots of the same homogenate.

(i) ETS activity. The ETS activity was measured kinetically by the Owens and King (1975a) method, considering the modifications described in Packard et al. (1996) and Packard and Christensen (2004). The absorbance increase of the INT-formazan at 490 nm was continuously monitored for 8 minutes in 1 cm path length-cuvettes at 18 °C. The regression line of absorption versus time was used to estimate the ETS activity and potential respiration rates

(Φ) according to Packard and Williams (1981). The tetrazolium INT (2-p-iodophenyl-3-p-nitrophenyl monotetrazolium chloride) is preferentially reduced by the respiratory ETS enzymes, replacing the O_2 as the electron acceptor. The INT accepts two electrons whereas the O_2 would accept four. Hence, the INT-formazan production rate is stoichiometrically related by a factor of 2 to ETS activity and by a factor of 0.5 to Φ. Blanks were run without the ETS substrates in order to subtract the contribution of the non-enzymatic reduction of the INT (Maldonado et al., 2012). Results are reported on a per volume basis as μmol O_2 d^{-1} L^{-1} (Fig. 5.1), or on a per cell basis as pmol O_2 d^{-1} $cell^{-1}$ (Table 5.1).

(ii) Protein content. Biomass was determined in terms of protein concentration by the Lowry method (Lowry et al., 1951) as modified by Rutter (1967), and is given in mg L^{-1}. Bovine serum albumin (BSA) was used as a standard.

(iii) Pyridine nucleotides concentration. The pyridine nucleotides were measured with a modification of the method described by Wagner and Scott (1994). The major change concerned the nucleotide extraction procedure, where we had to introduce a step for filter homogenization and a subsequent centrifugation, as stated above. Briefly, the method consists on a single- extraction procedure that distinguishes between the oxidized/ reduced forms and the phosphorylated/ non-phosphorilated forms of the nucleotides by means of heat and cycling buffers, respectively. Based on the fact that heat destroys the oxidized forms while has no effect on the reduced forms, the total pool of NAD and NADP (NADt and NADPt) was determined in the unheated extracts whereas the reduced forms (NADH, NADPH) were determined in an aliquot that was incubated at 60 °C for 30 minutes. The cycling buffer for both NAD(H) and NADP(H) quantification consisted of three serial reactions that yielded as the end-product the formazan of MTT (thiazolyl blue). The difference between the two buffers was the enzyme involved in the first reaction. The enzyme used in the NAD(H) determination was alcohol dehydrogenase whereas the one used in the NADP(H) determination was glucose-6-phosphate dehydrogenase (see *Chapter 4* for the detailed serial reactions). The change in absorbance at 570 nm was monitored for 3 minutes and the slope of the MTT-formazan production rate was used to quantify the amount of pyridine nucleotides present in the samples. To accomplish this, standards of NADH and NADPH were pre-

pared (ranging from 0 - 200 nM) and were assayed as explained before for the samples. A standard curve for each nucleotide was determined by the regression line of formazan production rate versus concentration. To further ascertain the validity of this method in dinoflagellates, the recovery of both NAD(H) and NADP(H) was previously determined in separate experiments. Known amounts of NAD^+, NADH, $NADP^+$ and NADPH were added to an extract which was then analyzed as stated above. On average, the destruction of the oxidized forms was of 103.3 % (± 8.5 %), whereas the recovery of the reduced forms was of 105.8 % (± 4.8 %).

5.2.5 **Statistical analysis**

The statistical software Sigma plot version 12.5 was used to obtain the regression equations on the time profiles of all the variables, as well as to confirm the normality of the data by the Shapiro-Wilk test. To study the correlation between respiration, Φ, NAD and NADP during the starvation experiment Pearson correlation coefficients were determined using the program SPSS statistics version 22. A percentile bootstrap was applied to the correlations according to Davison and Hinkley (1997).

5.3 **Results**

5.3.1 **Respiratory metabolism during starvation**

We observed a significant decrease in cell number, protein content, potential respiration, and respiration in *O. marina* during the food deprivation period (Fig. 5.1). On a culture volume basis, R_{O_2} and cell abundance decreased exponentially with starvation, whereas protein and Φ exhibited a linear decrease. Cell mortality rate was high (5 % of daily decrease in the abundance) during the first nine days and diminished 5-fold to the end of the experiment. Likewise, R_{O_2} dropped on average from a high of 166 μmol O_2 d^{-1} L^{-1} to a low of 36 μmol O_2 d^{-1} L^{-1} in the first nine days, with an attenuation of the decline in the following 8 days. On the other hand, the protein content in the culture decreased at a constant rate of 0.13 mg d^{-1} L^{-1} while Φ decreased at a comparatively higher rate of 3.77 μmol O_2 d^{-1} L^{-1}. When cell- and protein- specific R_{O_2} rates were considered (Table 5.1), we observed a significant exponential decrease (non-linear regression, $r^2 = 0.99$, $p < 0.0001$) in both cases, although it was 10 % larger for the protein-normalized R_{O_2} rates. Protein- and cell-

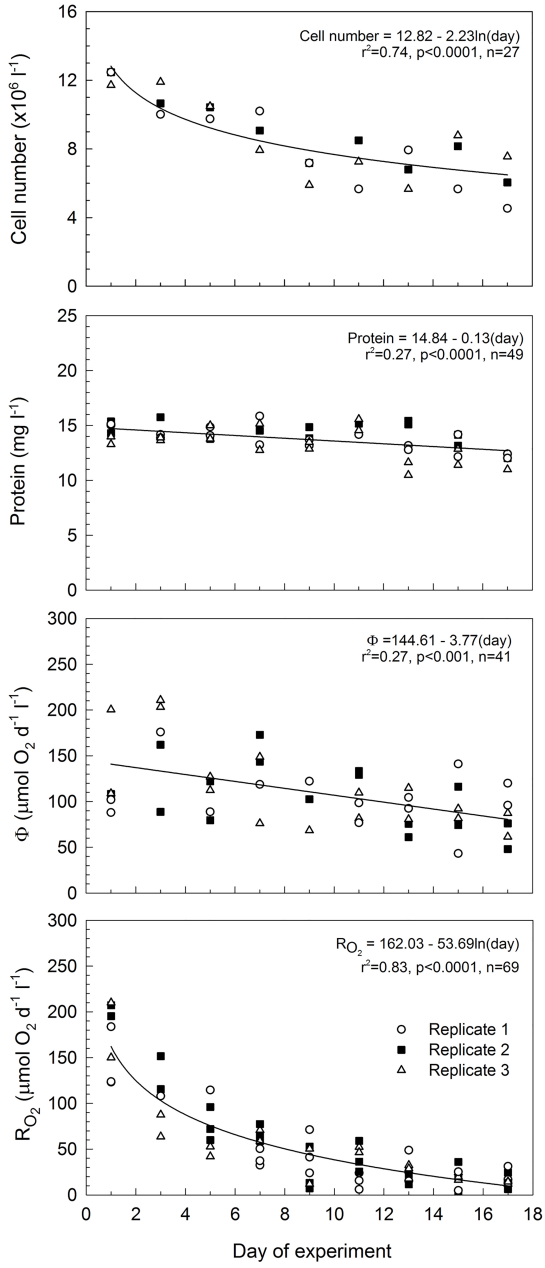

Figure 5.1: Time profiles of cell number, protein content, potential respiration (Φ) and respiratory oxygen consumption (R_{O_2}) in the culture during starvation (from the top panel to the bottom panel). Data for separate triplicate bottles are shown. When possible, duplicate or triplicate measurements were performed in each bottle. All regressions were significant, at least, at $p < 0.001$ level.

Table 5.1: Cell-specific and protein-specific rates of respiration (R_{O_2}) and potential respiration (Φ) during the starvation experiment. Mean values (±SD) of three replicates are given. Notice the change in units between cell-specific rates (pmol O_2 d^{-1} $cell^{-1}$) and protein-specific rates (μmol $O_2 d^{-1} mg\ prot^{-1}$).

Starvation	Cell-specific rates		Protein-specific rates	
(days)	R_{O_2} (pmol O_2 d^{-1} $cell^{-1}$)	Φ (pmol O_2 d^{-1} $cell^{-1}$)	R_{O_2} (μmol O_2 $d^{-1} mg^{-1}$ prot)	Φ (μmol O_2 $d^{-1} mg^{-1}$ prot)
1	13.65±1.96	9.83±2.97	11.52±1.85	8.31±2.67
3	9.89±3.19	14.30±5.43	7.39±1.87	9.65±4.25
5	7.85±3.64	10.06±1.21	5.61±2.52	7.24±0.97
7	6.57±2.29	14.42±2.92	4.18±1.41	7.94±2.33
9	5.37±2.25	14.31±2.71	2.64±1.12	7.12±1.72
11	4.74±2.06	14.70±1.31	2.31±1.18	6.93±1.54
13	3.69±1.49	13.24±3.66	1.91±0.75	6.85±1.82
15	2.63±0.53	12.61±3.28	1.49±0.16	7.05±0.26
17	2.85±1.45	13.76±6.41	1.34±0.28	6.59±1.35

specific Φ rates, in turn, remained fairly constant during the same period (Table 5.1), with average values (± SD) of 7.52 (± 0.97) μmol O_2 d^{-1} mg $prot^{-1}$ and 13.03 (± 1.86) pmol O_2 d^{-1} $cell^{-1}$, respectively.

The R_{O_2}/Φ ratio has been traditionally employed in biological oceanography to estimate respiration rates from ETS measurements. Fig. 5.2 documents the variability in this ratio with starvation in triplicates cultures of *O. marina*, showing a mean decrease of 60 % of the initial value of 1.4 in the first week, and of 85 % to 0.25 by the end of the experiment.

5.3.2 **Concentration of pyridine nucleotides and response to starvation**

The protein-specific concentration of NAD and NADP in their reduced (NADH, NADPH) and oxidized (NAD^+, $NADP^+$) forms as well as the total pool (NADt, NADPt) during the starvation experiment are given in Fig. 5.3. The intracellular level of NADt was 3 times to 7 times higher than that of NADPt, under well-fed conditions and after 17 days of starvation, respectively. The total concentration of nucleotides depicted a logarithmic decay during this time, represented by NADt = 620.43 − 66.42 Ln(day) ($r^2 = 0.71$, $p < 0.005$), and NADPt = 177.67 − 46.82 Ln(day) ($r^2 = 0.97$, $p < 0.0001$), both in pmol mg

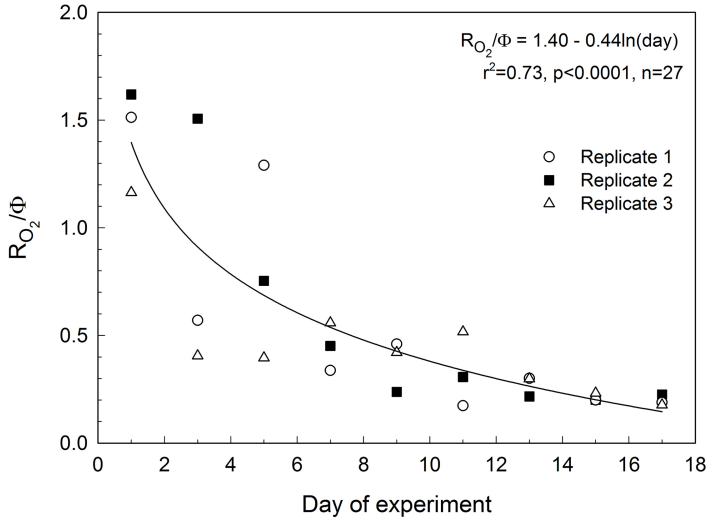

Figure 5.2: Relationship between respiration (R_{O_2}) and potential respiration (Φ) during the starvation period. The R_{O_2}/Φ ratio is unitless. Data for three replicate bottles are shown.

prot^{-1} units. This decrease was driven by a descent in the concentration of the oxidized forms, as the reduced forms remained virtually constant, with no clear pattern of increase or decrease ($p > 0.05$).

On average, NAD^+ concentration of the triplicates ranged from 353.34 to 87.57 pmol mg prot^{-1}, whereas $NADP^+$ ranged from 117.98 to 7.82 pmol mg prot^{-1} in the same period. Conversely, mean values (± SD) for the total experimental time for NADH were of 295.51 (± 41.38) pmol mg prot^{-1} and for NADPH were of 49.89 (± 6.65) pmol mg prot^{-1}.

Table 5.2 summarizes the concentration of pyridine nucleotides in its various forms during starvation, standardized by the number of cell in the culture at each sampling time. The cell-specific NADt maintained constant levels throughout the experiment, with a mean value of 8.16×10^{-4} pmol cell^{-1}. However, a significant linear decrease of NAD^+ was observed (slope = -0.14 $\times 10^{-4}$ pmol d^{-1} cell^{-1}, $r^2 = 0.71$, $p < 0.005$), although it was dampened by a parallel increase of NADH concentration with time (slope = 0.24×10^{-4} pmol d^{-1} cell^{-1}, $r^2 = 0.81$, $p < 0.001$). Conversely, cell-specific NADPt concentration showed a decline of 0.07×10^{-4} pmol d^{-1} cell^{-1} ($r^2 = 0.85$, $p <$

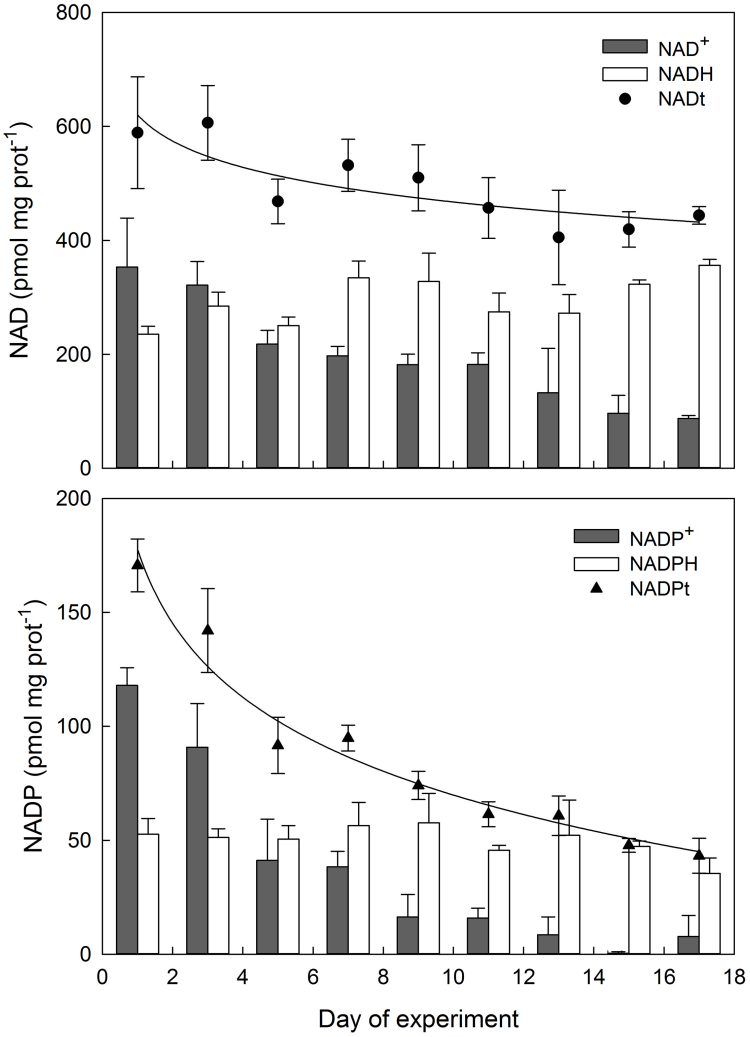

Figure 5.3: Protein-specific NAD concentrations (top panel) and NADP concentrations (lower panel) during the food deprivation period. Bars represent the concentration of the oxidized forms (NAD^+, $NADP^+$; grey bars) and reduced forms (NADH, NADPH, white bars), whereas symbols correspond to the total pool of NAD and NADP (NADt, NADPt). Mean values for three replicates are given for each parameter (n = 27). Error bars indicate the standard deviation of the mean.

0.0005), that was due to a concurrent decrease in the $NADP^+$ concentration (slope = -0.08 $\times$ 10^{-4} pmol d^{-1} $cell^{-1}$, r^2 = 0.85, $p < 0.0005$). Intracellular NADPH level in turn presented a slight increase with time, although it was not significant ($p = 0.25$).

The NAD^+/NADH and $NADP^+$/NADPH ratios are indexes of the intracellular redox state, which in turn is a paramount determinant of cellular functioning and metabolism. After 17 days of starvation, NAD^+/ NADH and $NADP^+$/ NADPH ratios decreased to 10 % and 17 % of their initial levels, respectively (Table 5.2). Hence, there was an increase in the proportion of the reduced forms as compared to the oxidized forms with time. Similarly, the NADt/ NADPt ratio increased from a value of 3 at well-fed conditions to a value of 10 at the end of the experiment.

5.3.3 **Relationship between pyridine nucleotides and respiratory metabolism**

A comparison of the respiration, potential respiration, NADt and NADPt profiles during starvation is shown in Fig. 5.4. They were determined by standardization of the data to the initial values, expressed as a percentage. Contrary to the relatively low decrease observed for Φ and NADt, R_{O_2} and NADPt exhibited a sharp parallel decline. Indeed, the latter two variables dropped to less than 60 % of their initial values in the first week, whereas potential respiration and NADt fairly decreased 10 % within the same period. Table 5.3 includes the Pearson correlation coefficients (r) of R_{O_2} and Φ with the oxidized and reduced forms as well as with the total pool of each nucleotide. The standard error and the confidence intervals at 95 % level are also given.

Both R_{O_2} and Φ presented a stronger correlation with the oxidized forms than with the reduced forms, the highest values being obtained for R_{O_2}. In fact, the maximum r value corresponded to the correlation between R_{O_2} and $NADP^+$ (r = 0.981, $p < 0.0001$). Except with the reduced forms, Φ correlated in a similar manner with every form of the two nucleotides, with no significant differences between the r values, as determined by the Fisher's r-to-z transformation.

Table 5.2: Cell-specific pyridine nucleotides levels in *O. marina* during the food deprivation period. The oxidized forms (NAD^+, $NADP^+$), reduced forms (NADH, NADPH) as well as the total pool (NADt, NADPt) of each nucleotide are given. Data corresponds to mean values (± SD) of three replicate cultures. The ratios from columns 5 and 9 reflect the redox state of the cell and they are unitless.

Starvation	Cell-specific NAD ($\times 10^{-4}$ pmol NAD $cell^{-1}$)			NAD^+/NADH	Cell-specific NADP ($\times 10^{-4}$ pmol NADP $cell^{-1}$)			$NADP^+$/NADPH
(days)	Oxidized (NAD^+)	Reduced (NADH)	Total (NADt)		Oxidized ($NADP^+$)	Reduced (NADPH)	Total (NADPt)	
1	4.21±1.09	2.80±0.22	7.01±1.29	1.49±0.28	1.40±0.10	0.63±0.09	2.03±0.17	2.27±0.32
3	4.26±0.79	3.77±0.59	8.03±1.36	1.13±0.05	1.20±0.30	0.67±0.02	1.87±0.30	1.78±0.45
5	3.04±0.38	3.49±0.26	6.52±0.65	0.87±0.04	0.57±0.25	0.70±0.08	1.28±0.18	0.85±0.47
7	3.08±0.10	5.21±0.06	8.29±0.14	0.59±0.02	0.60±0.07	0.89±0.20	1.49±0.14	0.71±0.27
9	3.34±0.72	5.98±1.36	9.31±1.95	0.56±0.09	0.32±0.18	1.19±0.38	1.51±0.22	0.31±0.21
11	3.90±1.05	5.86±1.49	9.75±2.53	0.66±0.01	0.33±0.05	0.97±0.21	1.30±0.19	0.35±0.09
13	2.55±1.48	5.26±0.67	7.81±1.55	0.49±0.29	0.16±0.15	1.01±0.30	1.17±0.17	0.21±0.22
15	1.76±0.74	5.79±1.58	7.55±2.21	0.30±0.10	0.02±0.01	0.85±0.24	0.86±0.23	0.03±0.01
17	1.81±0.62	7.32±2.33	9.13±2.95	0.25±0.01	0.12±0.13	0.75±0.36	0.87±0.25	0.24±0.28

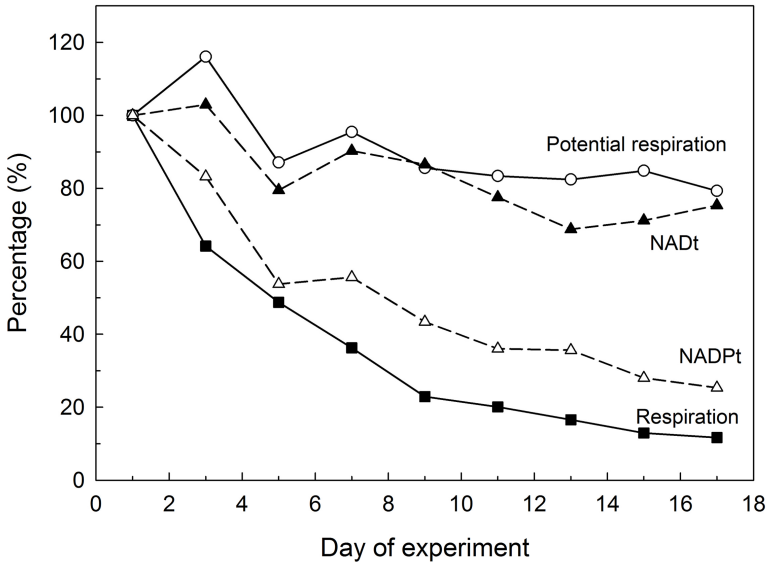

Figure 5.4: Relative decrease of respiration, potential respiration and total pool of each nucleotide (NADt, NADPt) with starvation. The data are standardized to the initial values and expressed as percentage. Correlation coefficients between these variables are given in Table 3.

5.4 Discussion

5.4.1 Effect of starvation on respiratory metabolism

We have described here a distinct effect of long-term starvation on the R_{O_2} and on the enzymatic machinery that drives this consumption, i.e. the enzymes from the ETS, on the marine dinoflagellate *O. marina*. R_{O_2} showed a rapid decrease in the first nine days, to then weaken towards the end of the experiment, whereas Φ presented a lower steady decrease during the entire period (Fig. 5.1). A rapid reduction of metabolic rates constitutes a survival strategy in times of food shortage in microorganisms. Indeed, starved protozoans can lessen their metabolic rates to 2 - 10 % of that characteristic for normal growing conditions (Fig. 5.4, this study; Fenchel, 1990). Such a trait allows them to face starvation, in some cases, for more than a month (Menden-Deuer et al., 2005; Strom, 1991). At the same time, however, they conserve cellular resources, such as respiratory capacity, structural proteins, enzymes,

Table 5.3: Pearson correlation coefficients (r) between respiration (R_{O_2}) and potential respiration (Φ) with the nucleotides in their oxidized forms (NAD^+, $NADP^+$) and reduced forms (NADH, NADPH), as well as with their total intracellular pool (NADt, NADPt) are given. The p-value represents the two-tailed significance levels and n = 9 in all the comparisons. A percentile bootstrap was applied to determine the standard error (SE) and to construct the 95 % confidence intervals (95 % CI).

		NAD			NADP		
		NAD^+	NADH	NADt	$NADP^+$	NADPH	NADPt
R_{O_2}	r	0.946***	-0.661	0.825 *	0.981 ***	0.354	0.977 ***
	SE	0.037	0.231	0.116	0.019	0.254	0.020
	95 % CI	0.822-0.988	-0.917-0.005	0.473-0.963	0.944-0.998	-0.303-0.758	0.915-0.997
Φ	r	0.835 *	-0.301	0.890 **	0.832 *	0.391	0.842 *
	SE	0.096	0.278	0.103	0.104	0.269	0.076
	95 % CI	0.573-0.971	-0.764-0.356	0.609-0.971	0.655-0.988	-0.185-0.831	0.732-0.991

*Significant at a level $p < 0.01$, ** $p < 0.001$, *** $p < 0.0001$.

etc., as evidenced by the constant specific Φ rates (Table 5.1), which would benefit them in highly variable habitats. Once the new energy source appears, they could start immediately making use of it, without the need to wait for a *de novo* synthesis of the enzymatic pool (Finlay et al., 1983; Packard et al., 1996). A similar response of the respiratory metabolism to food limitation has been described in other marine organisms (Herrera et al., 2011; Packard et al., 1996), as well as in other physiological processes, like ammonium excretion (Fernández-Urruzola et al., 2011; Mayzaud, 1976).

Our cell-specific R_{O_2} values for well-fed and starved organisms (Table 5.1) are within the range of those measured in other protozoa (Fenchel and Finlay, 1983). They are likewise fully consistent with the respiration rates reported in *O. marina* during similar starvation experiments (Hantzsche and Boersma, 2010; Meunier et al., 2012), and more specifically, with the recently described values in the same strain of this dinoflagellate (Calbet et al., 2013). In this light, Meunier et al. (2012) suggested that the metabolism of nitrogen-rich *O. marina*, during food limitation, mainly relied on proteins. In contrast, Calbet et al. (2013) observed that comparable nitrogen-rich *O. marina* presented a decrease in the fatty acid concentration with starvation, which indicated that these molecules were probably being metabolized and used as an energy source during this period. Our fairly constant protein concentration (Fig. 5.1) appears to support the observations from Calbet et al. (2013).

The ratio of respiration to potential respiration (R_{O_2}/Φ) is an index of physiological state (Christensen et al., 1980). Very often in the literature, there are found R_{O_2}/Φ ratios higher than 1 (Hernández-León and Gómez, 1996; Herrera et al., 2011; King and Packard, 1975; Martínez et al., 2010). Since the theoretical maximum value of 1 indicates that the organisms are respiring at their maximum capacity, ratios higher than 1 are surprising and suggest additional investigation. Similar to what has been described for other species (Herrera et al., 2011; Martínez et al., 2010), we observed the highest R_{O_2}/Φ ratios in well-fed organisms (Fig. 5.2). One could tackle this controversy from two different perspectives. The first is that there may be other metabolic pathways that consume O_2 besides the ETS and that we do not consider in our assay. Although there are oxygenases, hydroxylases, and other oxidases in a cell, the enzymes of the ETS are responsible of the 95 % of all biological O_2 consumption (Nelson et al., 2008) and the other 10 % could not account for the difference in R_{O_2} in ratios as high as 1.5 - 2. The second perspective is that there may be additional mechanisms other than substrate concentration that controls the *in vivo* activity of the ETS enzymes. In this light, previous research in higher organisms (Chance and Williams, 1955; Kasimova et al., 2006, among many others) have shown that the respiration started to increase after the addition of substrates in isolated mitochondria preparations. However, the R_{O_2} was greatly enhanced when a certain amount of ADP was added (i.e., respiratory state 3, *sensu* Chance and Williams, 1955). This evidences that the electron transport and the ATP synthesis are closely coupled in the inner mitochondrial membrane at *in vivo* conditions. To ascertain if this additional control of respiration is also found in marine organisms, it is necessary to determine the intracellular ADP concentration and to study its behavior under different metabolic situations.

5.4.2 **Role of pyridine nucleotides in the regulation of respiratory processes**

Despite the importance of pyridine nucleotides as key molecules involved in energy metabolism and oxidation-reduction reactions of cells, little is known about their concentration, intracellular distribution and behavior in marine microorganisms. Here, we have quantified the NAD and NADP concentration in the heterotrophic dinoflagellate *O. marina* and we have monitored their levels during starvation. Under well-fed conditions, the protein-specific NAD and

NADP concentrations averaged 0.589 nmol mg prot^{-1} and 0.171 nmol mg prot^{-1}, respectively (Fig. 5.3). These concentrations are slightly lower as compared to the ones observed for other eukaryotes, such as the 4 nmol NAD mg prot^{-1} measured in mouse cell monolayers (Umemura and Kimura, 2005), or the range of 0.93 - 3.70 nmol NAD mg prot^{-1} determined in isolated mitochondria from various plant species (Agius et al., 2001). However, the agreement between our findings and the figure observed in several species of aerobic bacteria is closer. In these organisms, average values for the total amount of coenzyme were of 0.728 nmol mg prot^{-1} for NAD and of 0.481 nmol mg prot^{-1} for NADP (London and Knight, 1966; Wimpenny and Firth, 1972), assuming a mean protein:dry weight ratio of 0.63 (Simon and Azam, 1989). Regardless of the cell type, the intracellular levels of NAD are commonly higher than those of NADP (Pollak et al., 2007), which is also reflected in our results (Table 5.2). Furthermore, some authors have suggested that in bacteria the NAD:NADP ratio is thoroughly controlled by intracellular mechanisms at a constant value of 3:1 (Brody, 1972; Manlapaz-Fernandez and Olivera, 1973). In our case, this value was true for well-fed *O. marina* cells, but afterwards the ratio rose up to 10:1. Similar increase in the ratio was observed in *Pseudomonas sp.* cultures with decreasing the dilution rate (Matin and Gottschal, 1976).

One of the most interesting observations of the present work is the relative constancy of the reduced forms during starvation (Fig. 5.3). NADH is mostly regenerated in catabolic reactions including glycolysis and the tricarboxylic acid (TCA/Krebs) cycle (Mathews et al., 2000), whereas NADPH is restored in the oxidative phase of the pentose phosphate pathway (Kruger and von Schaewen, 2003). If the NADH and NADPH levels were to be strictly proportional to the ingested food, one would expect to detect a decrease in their concentration as the substrate availability becomes limiting. In contrast, the decay was recorded in both NAD^+ and $NADP^+$ instead of in their reduced forms during our experiment (Fig. 5.3). In addition, we observed a decrease in the $NAD(P)^+$/NAD(P)H ratios with starvation (Table 5.2). From these findings, it can be presumed that (*i*) oxidation-reduction pathways in the cells may be geared towards maintaining a constant NAD(P)H pool rather than a constant $NAD(P)^+$/NAD(P)H ratios and that, consequently, (*ii*) the $NAD(P)^+$ pool would account for the fluctuations of the $NAD(P)^+$/NAD(P)H ratios. The first suggestion is in accordance with previous findings in bacterial cultures, where constant NADH levels were reported under different growth environ-

ments (Matin and Gottschal, 1976; Wimpenny and Firth, 1972). More recently, it has also been observed that the free NADH concentration (i.e., the fraction of the NADH pool that is not bound to proteins) is kept constant under different metabolic situations in plant mitochondria (Kasimova et al., 2006). On the other hand, it is worth mentioning that the $NAD(P)^+$/NAD(P)H ratios play a key role in the regulation of the intracellular redox state as well as in the control of many metabolic enzymes (Mathews et al., 2000). It has also been well documented that they fluctuate in response to changes in metabolism. Therefore, if the second suggestion is correct and NAD^+ and $NADP^+$ are metabolic regulators, the values of $NAD(P)^+$/NAD(P)H should be close to 1. As suggested by Lin and Guarente (2003) for NAD, if the value was higher (e.g., 500), the ratio would be very sensitive to changes in the concentration of NADH and not NAD^+.Our results agree with this statement in that the values ranged between 1.49 - 0.25 (Table 5.2). A similar rationale can be applied in the case of NADP, as the NAD pool and NADP pool are closely related (Noctor et al., 2006).

We have further explored the relationship between nucleotide concentration and respiratory metabolism (Fig. 5.4). The Φ was positively correlated with nucleotides, but the highest correlation coefficients corresponded to the relation of R_{O_2} with the oxidized forms of NAD and NADP (Table 5.3). This means that when R_{O_2} is higher under well-fed conditions, we expect to have higher $NAD(P)^+$ concentrations, whereas when R_{O_2} decreases due to starvation we will find lower $NAD(P)^+$ concentrations. One can compare these findings with those of several works conducted on plant mitochondria (Agius et al., 2001; Kasimova et al., 2006), being mindful that our study refers to a larger temporal scale (i.e., minutes *vs* days). For instance, Kasimova et al. (2006) reported higher NAD^+ concentrations and lower reduction levels of NAD (%NADH) when the R_{O_2} was maximum. Conversely, when the R_{O_2} decreased, the NAD^+ values decreased and the %NADH increased, which is consistent with our results. From the higher correlation coefficients between R_{O_2} and NADP levels (Table 5.3), it can likewise be suggested that respiration in *O. marina* is mainly driven by this nucleotide. To ensure this, it is necessary to know the K_m (Michaelis-Menten half-saturation constant) for both NADH and NADPH of Complex I from the ETS. If the K_m is lower for NADH than for NADPH, as occurs in plant mitochondria (Moller and Rasmusson, 1998), the complex I would preferentially oxidize NADH. At present, however, this

statement can only be a subject of speculation as no information about the K_m nor other kinetic constants are available for the ETS enzymes in marine dinoflagellates.

5.5 Conclusions

Understanding the mechanisms that regulate the oxygen consumption in the respiratory chain as well as the control of other metabolic enzymes, such as the ones involved in the TCA cycle, will help in understanding, for instance the variability in the respiratory quotient (Romero-Kutzner et al., 2015) or in the R_{O_2}/Φ ratios (Hernández-León and Gómez, 1996; King and Packard, 1975, this study). Both factors are of special interest in biological oceanography. With the present work, we have started to shed light on this regard, as we have addressed for the first time the pyridine nucleotide concentration in a marine dinoflagellate. The protein-specific levels of both NAD(H) and NADP(H) (Fig. 5.3) are within the range of those reported for bacteria and slightly lower than those measured for other eukaryotes. We have further revealed a close relationship between the pyridine nucleotides, especially with the oxidized forms, and the respiration rates during starvation (Table 5.3). Accordingly, Φ and NADt retained 80 % of their original values while R_{O_2} and NADPt dropped to around 20 % of their original value (Fig. 5.4). Whether the regulation process of the R_{O_2} in marine organisms relies on pyridine nucleotides levels and redox status, ADP concentration, or a combination of both, has still to be elucidated. Likewise, further research is needed to verify if the patterns described in the present work holds for other more complex marine organisms. In addition to this, we have shown that *O. marina* presented fairly constant specific-Φ rates during starvation (Table 5.1), which confers on this organism an adaptive advantages to live in environments that are highly patchy in resources.

Acknowledgements. We would like to thank to A. Calbet for providing the cultures of *O. marina* and *R. salina* from their collection in Barcelona. This work was founded by the BIOMBA project (CTM2012-32729/MAR) awarded to M. Gomez by the Spanish Ministry of Economy and Competitiveness. N. Osma and I. Fernández-Urruzola received financial support from the Formation and Perfection of the Researcher Personal Program from the Basque Government.

The most erroneous stories are those we think we know best and, therefore, never scrutinize or question.

Stephen Jay Gould

CHAPTER

6

CAPÍTULO

Predicting *in vivo* oxygen consumption rates from ETS activity and bisubstrate enzyme kinetics in cultured marine zooplankton

N. Osma, I. Fernández–Urruzola, M. Gómez, S. Montesdeoca-Esponda, and T. T. Packard

Submitted to Marine Biology

ID: MABI-S-15-00764

ABSTRACT: Oxygen consumption rates (R_{O_2}) in the rotifer *Brachionus plicatilis* and the mysid *Leptomysis lingvura* during both well-fed conditions and starvation have been modeled using the electron transport system (ETS) activity, bisubstrate kinetics and intracellular concentration of NADH and NADPH. Furthermore, the influence of the food quality on the respiratory metabolism and metabolites levels has been explored. The highest values of all variables both in rotifers and mysids were mainly found on organisms grown on the lipid-rich diet, although no differences were determined between treatments in the response to starvation. Time courses of the R_{O_2} and the concentration of pyridine (NAD and NADP) and adenine (ADP and ATP) nucleotides evidenced a sharp decrease during food shortage and a fast recovery with food restoration,

whereas the potential respiration (Φ) remained fairly constant. In general, the modeled R_{O_2} (V_{O_2}) predicted with a high degree of success the *in vivo* R_{O_2}, even though it yielded relatively lower values. Nonetheless, the correlation of the measured R_{O_2} with V_{O_2} during starvation was much better than with the R_{O_2} estimated from ETS measurements and a fixed R_{O_2}/Φ ratio. Finally, the observed relationship between the measured R_{O_2} and ADP suggests that the contribution of this nucleotide should be included in future applications of this model.

Keywords: Respiration; Enzyme kinetic model; Nicotinamide adenine dinucleotide (NAD); Nicotinamide adenine dinucleotide phosphate (NADP) ; *Brachionus plicatilis* ; *Leptomysis lingvura*.

6.1 Introduction

In the ocean, respiration constitutes the principal process by which organic matter is remineralized in the water column. In cells, in turn, respiration is the process responsible for most of the oxygen consumption. Accordingly, the control mechanisms of the respiratory oxygen consumption rates (R_{O_2}) at the intracellular level will ultimately affect the contribution that the marine plankton has on the biogeochemical cycles through its respiration. At constant temperature, R_{O_2} is a direct result of the enzymatic activity of the electron transport system (ETS), which is embebed in the inner mitochondrial membrane in eukayoriotic cells. At the end of the ETS, cytochrome oxidase reduces O_2 to H_2O. At the beginning of the system, NADH and succinate dehydrogenases accept reducing equivalents from the Krebs Cycle and other reactions of intermediary metabolism (Mathews et al., 2000). The electron flux between the two ends is controlled by the dehydrogenases, not by cytochrome oxidase. On this basis, Packard et al. (1971) proposed an assay that measures the maximum activity (V_{max}) of the dehydrogenases from the ETS by adding a surplus of substrates. Because of the stoichiometry between the O_2 consumption and the electron flux through the ETS, this assay yields the respiratory capacity of the ETS or, in other words, the potential respiration (Φ). As organisms are unlikely to be under substrate-saturating conditions in the ocean, the potential rates need to be converted into *in vivo* R_{O_2}. This can be accomplished by applying either an empirically determined R_{O_2}/Φ ratio or bisubstrate enzyme kinetics (Packard et al., 1996). The first approach has been commonly used in oceanography to

estimate respiration from ETS activity, when direct measurements of *in vivo* R_{O_2} through the incubation technique were unfeasible (i.e., in cruises where high data-acquisition rates are required, in deep-sea waters, etc.). Its application is supported by the good correlation that exists between the ETS activity and the R_{O_2} (del Giorgio, 1992; Maldonado et al., 2012; Packard, 1985a). However, factors such as species composition and trophic conditions, have been observed to generate variability on these ratios (*Chapters 4* and *5* in this thesis; Hernández-León and Gómez, 1996; Packard, 1985a) and, therefore, the use of a universal value could lead to a inaccurate estimations of the actual respiration rates.

The second approach consists of a model based on the bisubstrate control of the *in vivo* ETS activity. This model was originally introduced by Packard et al. (1996) and it is based on the assumptions that (*i*) the R_{O_2} is the direct result of the ETS activity, (*ii*) these enzymes are controlled by the availability of their substrates and, (*iii*) the reaction obey the rules of enzyme kinetics. Accordingly, the bisubstrate kinetic equation that determines the predicted R_{O_2} (V_{O_2}) takes the form:

$$V_{O_2} = \frac{A_{ETS}\,[\mathrm{NADH}]\,[\mathrm{NADPH}]}{K_\beta + [\mathrm{NADH}]\,[\mathrm{NADPH}]} \tag{6.1}$$

$$K_\beta = K_{ia}\,K_{NADPH} + K_{NADPH}\,[\mathrm{NADH}] + K_{NADH}\,[\mathrm{NADPH}]$$

Here, A_{ETS} is the potential rate of the process and it is equivalent to the V_{max} but expressed in the same units as the physiological rate. K_{NADH} and K_{NADPH} are bisubstrate Michaelis constants for NADH and NADPH. K_{ia} is the dissociation constant for the enzyme-NADH complex, and [NADH] and [NADPH] are the intracellular ETS substrate concentrations. The contribution of succinate in the reaction was neglected due to its relatively minor role as compared to the role of the pyridine nucleotides (Savenkoff et al., 1995). The model built this way successfully predicted the *in vivo* R_{O_2} in the marine bacterium *Pseudomonas nautica* (Packard et al., 1996), as well as in other species grown on a different carbon source (Aguiar-González et al., 2012). However, both studies constituted heuristic applications of the model as they used intracellular substrate concentrations estimated from the carbon sources and bacterial biomass. Furthermore, the kinetic constants included in their models were obtained by the optimization through successive iterations of measurements made on other organisms. Accordingly, the predictive capacity of the model still needs to be

verified by using measured values instead of estimated values.

Besides the control that the substrates exert according to the bisubstrate kinetics, the *in vivo* activity of the ETS is affected by the relative intracellular concentration of enzyme modulators, such as adenosine-5'-diphosphate (ADP) and adenosine-5'-triphosphate (ATP). In fact, Chance and Williams (1955) observed that when the mitochondria were exposed to an excess of the ETS substrates, the oxygen consumption was stimulated to its maximum capacity by the addition of ADP. Furthermore, the concentration of ADP and ATP, as well as the ratio between them, have been proposed as fundamental regulatory parameters controlling both the activity of certain enzymes (Karl, 1980) and the redox state of pyridine nucleotides (Stubbs et al., 1972).

In this study, we have tested the ability of a bisubstrate kinetic model (Eq. 1) to predict the *in vivo* R_{O_2} in two species of marine zooplankton, during a food deprivation period. Even though this model has only been applied in bacteria, similar rationale may be expected for the more complex metazoans (Packard and Gómez, 2008). Here, we chose the rotifer *Brachionus plicatilis* and the mysid *Leptomysis lingvura* to study the implications of different structural complexities on the predictive capability of the model for respiratory O_2 consumption rates. We monitored their R_{O_2} and Φ, as well as the intracellular concentration of the ETS substrates (NADPH and NADPH) and modulators (ADP and ATP) during starvation. The Michaelis (K_{NADH} and K_{NADPH}) and the dissociation (K_{ia}) constants were likewise measured. In addition, we provided two types of food with different nutritional composition to further ascertain the influence of food quality on both the metabolic rates and the intracellular concentration of metabolites. Our results demonstrated that the predicted V_{O_2} compared successfully with the R_{O_2} time course in both organisms, irrespective of the food quality.

6.2 Material and methods

6.2.1 Cultures

Our work was conducted on two marine species of zooplankton, the rotifer *Brachionus plicatilis* and the mysid *Leptomysis lingvura*, to provide a range of variability in organisms of different sizes. Furthermore, both organisms were fed with two diets that differed in their fatty acid composition, in order to detect the effect of food quality.

B. plicatilis was grown in two plastic tanks that contained 20 L of 0.2 μm-filtered and diluted (23 PSU) seawater. Both tanks were maintained at 25 °C, in darkness and with a gentle aeration to ensure saturating oxygen conditions. A fraction of the total water volume as well as the debris deposited in the bottom was daily removed in order to avoid the NH_4^+ concentration exceeding 0.1 mg L^{-1} in the culture. The rotifers from one of the tanks were fed with the microalgae *Nannochloropsis* sp. (ESD 2 - 3 μm) at a concentration of 1.2 $\times$ 10^5 cells $rotifer^{-1}$ d^{-1}, corresponding to the fatty acid-rich diet (Lubzens et al., 1995). Accordingly, batch cultures of this microalgae were likewise grown in autoclaved and filtered seawater, enriched with f/2 medium (Guillard, 1975). They were maintained under exponential growth conditions in a culture chamber at 20 °C, with a light intensity of 54.1 μmol photons m^{-2} s^{-1} and a light:dark cycle of 16:8 h. The other tank of rotifers was fed with a lower lipidic diet that consisted of 0.8 μg dry yeast $rotifer^{-1}$ d^{-1}, that was re-hydrated with diluted and filtered seawater. Continuous feeding allowed densities of $\sim$ 200 rotifers mL^{-1} to be achieved in each tank.

The mysid *L. lingvura* was collected at sea according to the procedure described by Fernández-Urruzola et al. (2011). Afterwards, the organisms were immediately transferred to the culture facilities in the laboratory and they were maintained at 18.2 ± 0.1 °C (*in situ* temperature) on a 14:10 h light:dark cycle. The culture system was composed of 12 glass, 40 L-aquariums connected by a circulating water bath, with a total water volume of around 480 L. Mechanical and biological filtration of the water prevented an increase of the concentration of NH_4^+, NO_2^- and NO_3^- above 0.1, 0.02 and 0.2 mg L^{-1}, respectively, as recommended by Lussier et al. (1988). As the rotifers, the mysids were provided with two types of diet. One group of organisms was fed with 48h-*Artemia* sp. nauplii, enriched previously with lipids by Easy-DHA Selco (INVE, Belgium). Other mysids, in turn, were fed with yeast-grown rotifers, constituting the lipid-poor diet. The daily dose was divided into two administrations and consisted of 100 Artemia $mysid^{-1}$ d^{-1} and 400 rotifers $mysid^{-1}$ d^{-1}, which have been observed to fulfill the mysids demands (Domingues et al., 2001). All these culturing conditions are collected in Table 6.1.

6.2.2 **Experimental design**

Prior to any measurement, *B. plicatilis* and *L. lingvura* were acclimated to the different diets and culturing conditions for one week. To address the effect of

Table 6.1: Summary of the culturing conditions for the rotifer, *Brachionus plicatilis*, and the mysid, *Leptomysis lingvura*. Organisms were acclimated to the different food treatments for one week before experimentation. After the starvation period, both organisms were restored to their prior food levels.

Culturing conditions	*Brachionus plicatilis*	*Leptomysis lingvura*
Temperature (°C)	25	18
Salinity (PSU)	23	35
Day:night cycle (h)	16:8	14:10
Diet *A*: Lipid-rich	*Nannochloropsis* sp.	Enriched *Artemia* sp.
	1.2×10^5 cells rotifer^{-1} d^{-1}	100 artemia mysid^{-1} d^{-1}
Diet *B*: Lipid-poor	Dry yeast	Yeast-grown *B. plicatilis*
	0.8 µg dry yeast rotifer^{-1} d^{-1}	400 rotifers mysid^{-1} d^{-1}

food quality on the respiratory metabolism, organisms were provided with saturating concentrations of each diet and, immediately after feeding, they were assayed. Several replicates of each feeding-treatment were made for statistical strength. Then, rotifers were collected and transferred into new tanks with filtered seawater to study the influence of starvation on the respiratory metabolism. These organisms were food-deprived for 28 h, according to the average starvation survival described by Kirk (1997) in several species of rotifers. Every few hours, seawater exchanges were realized to prevent high bacterial concentrations that could contribute to the rotifers' feeding. Similarly, mysids were moved into new aquariums containing filtered seawater and no food was supplied. In this case, the starvation time was of 60 h according to the observations made by Fernández-Urruzola et al. (2011), who reported an increased mortality in mysids starved over 68 h. During each experiment, both rotifers and mysids from each feeding treatment were sampled at time intervals of 2-12 h, with a higher sampling frequency at the beginning of the experiment. At the end of this period, the food supply was restored and three more measurements were taken (3, 6 and 12 h after the restoration of food) to study the recovery of the organisms. Aside from an influence on the respiratory metabolism, starvation promoted morphological changes in these organisms (see *Appendix* section, Fig. A.1) as well as a decrease in their egg production rates. All the experiments were performed on adult organisms of both *B. plicatilis*

and *L. lingvura*. For that, rotifers were harvested by means of a 100 μm mesh-size net, whereas mysids were hand-picked by a siphon from the experimental aquariums. Before the water-bottle incubations for the physiological measures, the collected organisms were washed twice with filtered seawater to minimize unspecific microbial contribution to the measurements.

6.2.3 **Respiration measurements**

Organisms were transferred by syphoning into gas-tight glass bottles previously filled with filtered and oxygenated seawater. Special care was taken to ensure similar density of organisms on each bottle. All the incubations were performed in darkness at the same temperature of the culturing conditions and lasted between 60 - 90 min. The O_2 consumption rate (R_{O_2}) was determined as the change in the dissolved O_2 concentration during this time. In each experimental run, two control bottles with only filtered seawater were included to correct for any contribution of microbial respiration to the total respiration. The dissolved O_2 concentration was continuously monitored by a 6- channel Strathkelvin 928 Oxygen System ® respirometer that was coupled to a refrigerated recirculator to maintain a stable temperature during the incubation. Previously, the respirometer was calibrated according to the Strathkelvin 928 manual, with O_2-saturated water as the maximum value and Na_2SO_4 treated-water as zero. After each incubation, the organisms were collected, immediately frozen in liquid nitrogen and stored at -80 °C for the subsequent determination of the biochemical parameters.

6.2.4 **Biochemical parameters**

Samples were homogenized by sonication for 45 s with an ultrasonic probe (Cole Parmer) in Milli-Q distilled water. An aliquot of the homogenate was then centrifuged for 8 min at 4000 rpm at 0 °C, and the ETS activity was immediately determined in the supernatant fluid to preclude any loss of activity. Other aliquots were stored at -80 °C for the quantification of the protein, pyridine nucleotides and adenine nucleotides concentrations.

(i) ETS activity. The ETS assay was run according to Owens and King (1975a), with the modifications introduced by Packard et al. (1996). It is based on adding saturating concentrations of the substrates NADH and NADPH (1.7 mM and 0.25 mM, respectively), which are the electron donors for the enzymes

of the ETS. Furthermore, the tetrazolium chloride dye, INT (2-p-iodophenyl-3-p-nitrophenyl monotetrazolium chloride) replaces the O_2 as the electron acceptor and is reduced, producing the INT-formazan. Hence, the absorbance increase of the INT-formazan was continuously monitored at 490 nm for 6 minutes in 1 cm path length-cuvettes at the correspondent culturing temperature for each organisms. The regression line of absorption against time was used to estimate the ETS activity and potential respiration rates (Φ), after Packard and Williams (1981). While the INT accepts two electrons the O_2 accepts four and, consequently, the INT-formazan production rate is stoichiometrically related by a factor of 2 to ETS activity and by a factor of 0.5 to Φ. Blanks were run without the ETS substrates in order to subtract the contribution of the non-enzymatic reduction of the INT (Maldonado et al., 2012).

(ii) Biomass and biovolume calculations. The biomass of the organisms was reported in terms of protein content. It was determined in triplicates by the Lowry method (Lowry et al., 1951) with the modifications described by Rutter (1967). Calibration curves were made from standard solutions of bovine serum albumin (BSA). On the other hand, it was necessary to estimate the intracellular concentration of substrates on a volume basis (i.e., molar units) for the kinetic studies. Accordingly, the biovolume of rotifers was estimated from the protein content by applying a factor of 0.11 μg protein rotifer^{-1} ($\pm$ 0.04, n = 30) and considering the biovolume for adult individuals of 1.36×10^6 μm^3 rotifer^{-1} given in Boraas and Bennett (1988). The biovolume of mysids was calculated from the equation N (mg) = 0.0546 + 0.0137 V (mm^3) provided by Alcaraz et al. (2003), and a protein to N conversion factor of 0.521 (Postel et al., 2000).

(iii) Pyridine nucleotides concentration. The intracellular concentration of pyridine nucleotides was determined according to the method described by Wagner and Scott (1994), although we additionally included the sonication and centrifugation steps described above for the homogenization of the samples. This assay is based on a single-extraction procedure that allows to quantify the oxidized and reduced forms of both NAD and NADP on the same homogenate. One aliquot of the extract was incubated 30 min at 60°C whereas the other remained unheated. The heat destroyed the oxidized forms while had no effect on the reduced forms. Accordingly, the total amount of PNs in the

sample was determined from the unheated extract whereas the reduced fraction was determined from the heated extract. The oxidized forms were calculated as the difference between the two values. Two enzyme cycling buffers were used to quantify the concentrations of the phosphorylated (NADP(H)) and non-phosphorylated (NAD(H)) forms on each extract. They consisted of three serial reactions that ultimately entailed the reduction of the thiazolyl blue dye (MTT) producing the MTT- formazan. The two buffers differed in the enzyme involved in the first reaction: the enzyme in the NAD(H) cycling buffer was alcohol dehydrogenase whereas the enzyme in the NADP(H) cycling buffer was glucose-6-phosphate dehydrogenase. For further information on the sequence of the reactions see the Methods section in Chapter 4 of this thesis. The production of the MTT-formazan was monitored at 570 nm for 3 min, and the slope of the regression line was used to quantify the concentration of nucleotides present in the samples. For that, standard solutions were prepared with known concentrations of pure nucleotides that ranged between 0 and 1 μm and they were assayed as stated above. The regression line of the MTT-formazan production rate versus concentration was, by itself, the standard curve for each nucleotide.

(iv) Adenine nucleotides concentration. Both ADP and ATP were determined by means of a Varian Prostar chromatographic system (Varian Inc., Spain) that consisted of a pump, an autosampler, a column valve module with an internal oven and a diode array detector working at 254 nm (Fig. 6.1). These two molecules were separated on a PRP-1 column (5 μm, 2.1 × 150 mm) (Hamilton, USA) at 50 °C. The mobile phase *A* consisted of 100 mM KH_2PO_4 (pH 7.0), 1mM tetrabutylammonium phosphate and 2.5 % methanol, whereas the mobile phase *B* was prepared with the eluent *A* and 20 % methanol. The elution was performed with a gradient that started with 1 % of mobile phase *B* during the first 3 min and then raised gradually to 15 % in 10 min, to 55 % in 15 min, to 95 % in 16 min and to 99 % in 20 min. At 25 min, the gradient returned to 1 % of mobile phase *B* and stayed for 5 min to equilibrate the column for the next injection. The flow rate was set to 0.3 mL min^{-1} and the injection volume was 10 μL. In order to estimate the concentration of each adenine nucleotide in the samples, standard curves were performed in the range of 0.01-50 μM, which presented correlation coefficients equal or greater than 0.992 in all cases. These standard curves for each compound were constructed

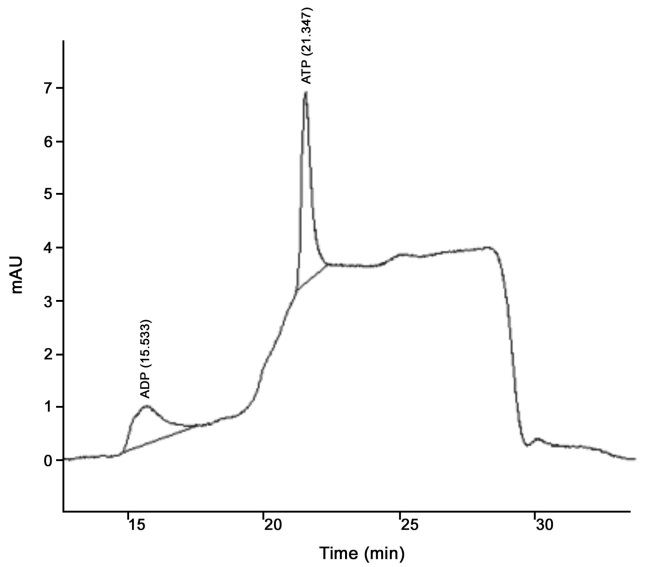

Figure 6.1: Example of the chromatogram obtained for the adenine nucleotides ADP and ATP measurements in the zooplankton samples, using UHPLC coupled to a diode array detector at 254 nm.

from serial dilutions of stock solutions (1.42 mM) that were previously prepared by diluting the appropriate amount of comercial product in the mobile phase. The limits of quantification for the assay were determined as the concentration at which the signal-to-noise ratio was greater than or equal to 10 and they were of 0.002 μM and 0.0005 μM for ADP and ATP, respectively. To evaluate the precision of the measurements, estimated as the relative standard deviation (%RSD), six replicate samples at two concentration levels (0.1 and 10 μM) were analyzed and yielded repeatability values below 9 % in both cases.

6.2.5 **Kinetic constants determination**

In order to obtain the kinetic constants, the ETS was measured as stated above but with six different concentrations of NADH and NADPH, leading to a six-by-six data matrix. The highest concentration of each nucleotide corresponded to the saturating concentration used in the normal assay, i.e., 1.7 mM for NADH and 0.25 mM for NADPH. These concentrations were decreased to

one-third sequentially until the last preparation, where the correspondent nucleotide was not added (0 mM). All these assays were run under temperature controlled conditions. To check the constancy of the kinetic constants during food deprivation, several replicates were performed at the beginning and at the end of the starvation period in the two species.

The data were linearized by the double-reciprocal transformation of Lineweaver-Burk (Lineweaver and Burk, 1934). Primary plots for both NADH (1/*v versus* 1/[NADH]) and NADPH (1/*v versus* 1/[NADPH]) were constructed and served to confirm the sequential reaction mechanisms of the ETS. The slope of each regression line was defined by $(K_{mA} + K_{iaA}K_{mB}/[B])/V$. The ordinate intercept was defined by $(1 + K_{mB}/[B])/V$. In both cases, *A* corresponds to the first binding substrate whereas *B* corresponds to the cosubstrate. The Michaelis constant (K_m) and the dissociation constant (K_{ia}) for each substrate were determined from a secondary plot of the reciprocal concentrations of the cosubstrates against the ordinate intercepts and slopes of the respective lines in the primary plot (Bisswanger, 2008). The considered first binding substrate was changed in order to obtain the K_{ia} values for both NADH and NADPH. Fig. 6.2 shows an example of the primary and secondary plots for the determination of the kinetic constants for the NADH.

6.3 Results

6.3.1 Response of the respiratory metabolism to food quality

The influence of the food quality on the respiratory metabolism of *B. plicatilis* and *L. lingvura* is summarized on Table 6.2. In general, the values of all variables were higher in organisms fed with the lipid-rich treatment (diet *A*) as compared to the lipid-poor treatment (diet *B*) values, although these differences were only significant for certain variables. One of them was R_{O_2}, which was higher both in rotifers and mysids fed with the diet *A*. Φ, in turn, showed significant differences between treatments in *L. lingvura*, but not in *B. plicatilis*. The R_{O_2}/Φ ratio in rotifers feeding on the lipid-rich *Nannochloropsis sp.* (1.14) was higher than the value measured on dry yeast-grown rotifers (1.03), whilst no significant differences were determined in the ratios of mysids feeding on diet *A* and diet *B*. Moreover, R_{O_2}, Φ as well as the R_{O_2}/Φ ratios were always higher in rotifers than in mysids (Table 6.2). Regarding the ETS substrates, NAD and NADP, no influence of the food type was observed on their

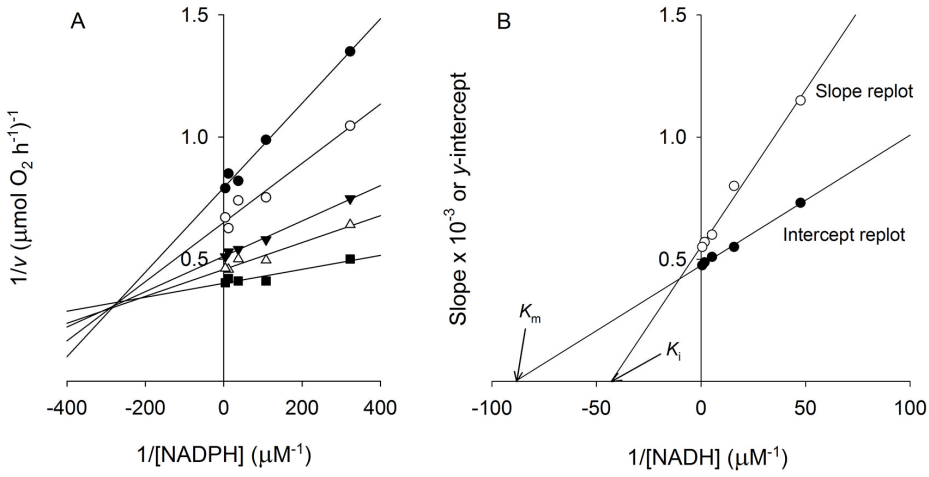

Figure 6.2: Bisubstrate kinetic studies for the determination of the Michaelis constant (K_m) and the dissociation constant (K_{ia}) for the NADH. (A) Double reciprocal diagram (Lineweaver-Burk plot) at various fixed NADH concentrations. (B) Secondary plot constructed from the slopes and *y*-intercepts of the lines in the primary plot versus the reciprocal concentration of NADH.

intracellular concentrations, except for the pool of NADP in rotifers, where the values from the lipid-rich treatment were twice the values from the lipid-poor diet. It is also noteworthy that the concentration of the reduced forms of NAD and NADP were greater than that of the oxidized forms irrespective of the organism and diet. Overall, NADH and NADPH levels were 3 to 8 times higher than the NAD^+ and $NADP^+$ levels. The average NADH concentration for the two food types in mysids was of 24.5 μM and it was significantly higher than the average values determined for rotifers (10.7 μM). The difference between the NADPH values in the two organisms was not that notable, with a range of 4.1 - 7.4 μM in rotifers and an average of 7.1 μM in mysids. Additionally, the concentrations of ADP and ATP were studied in these organisms, resulting in significant differences when the values of the two species were compared but not between treatments. Rotifers showed an averaged ADP concentration of 91.4 μM, while in mysids it was of 17.3 μM. Similarly, the averaged ATP concentration ranged from the 10.3 μM determined in rotifers to the 4.0 μM measured in mysids. During these well-fed conditions, the ratio ADP/ATP was between 8 - 9 in rotifers, while mysids presented a lower value (~ 4).

Table 6.2: Comparison of the oxygen consumption rate (R_{O_2}), potential respiration (Φ) as well as of the intracellular concentration of NAD, NADP, ADP and ATP in rotifers (*B. plicatilis*) and mysids (*L. lingvura*) acclimated to two different types of diet. The R_{O_2}/Φ ratio and the contribution of the reduced (NADH, NADPH) and oxidized (NAD^+, $NADP^+$) forms of NAD and NADP are also shown. Data represent the mean values ± SD, whereas the values in parenthesis indicate the number of replicates. Differences in the mean values between treatments were analyzed by the Student *t*-test; the *p*-values indicate the significance level attained in each comparison. The characteristics of the two treatments for each organism are explained in Table 6.1.

	Diet *A*		Diet *B*		*p*
Brachionus plicatilis	(lipid-rich)		(lipid-poor)		
R_{O_2} (µmol O_2 mg prot^{-1} h^{-1})	2.00 ± 0.42	(20)	1.75 ± 0.17	(20)	*
Φ (µmol O_2 mg prot^{-1} h^{-1})	1.59 ± 0.10	(20)	1.58 ± 0.16	(20)	n.s.
R_{O_2}/Φ	1.14 ± 0.15	(20)	1.03 ± 0.13	(20)	*
Total NAD (µM)	12.48 ± 2.97	(2)	14.00 ± 3.20	(2)	n.s.
NAD^+	1.73 ± 0.34	(2)	3.36 ± 1.57	(2)	n.s.
NADH	10.75 ± 2.95	(15)	10.64 ± 2.79	(15)	n.s.
Total NADP (µM)	8.48 ± 1.12	(2)	4.51 ± 1.48	(2)	*
$NADP^+$	1.12 ± 0.04	(2)	0.46 ± 0.04	(2)	**
NADPH	7.37 ± 1.12	(15)	4.05 ± 1.48	(15)	***
ADP (µM)	93.19 ± 33.41	(5)	89.59 ± 32.00	(5)	n.s.
ATP (µM)	11.24 ± 2.27	(5)	9.37 ± 1.19	(5)	n.s.
Leptomysis lingvura					
R_{O_2} (µmol O_2 mg prot^{-1} h^{-1})	0.90 ± 0.11	(10)	0.74 ± 0.09	(10)	**
Φ (µmol O_2 mg prot^{-1} h^{-1})	0.69 ± 0.21	(10)	0.52 ± 0.11	(10)	*
R_{O_2}/Φ	0.84 ± 0.18	(10)	0.76 ± 0.16	(10)	n.s.
Total NAD (µM)	29.20 ± 7.32	(10)	27.75 ± 4.23	(10)	n.s.
NAD^+	3.63 ± 1.30	(10)	4.29 ± 1.79	(10)	n.s.
NADH	25.57 ± 7.20	(10)	23.46 ± 3.83	(10)	n.s.
Total NADP (µM)	9.45 ± 1.29	(10)	8.40 ± 1.47	(10)	n.s.
$NADP^+$	2.04 ± 0.60	(10)	1.53 ± 0.49	(10)	n.s.
NADPH	7.41 ± 1.14	(10)	6.87 ± 1.39	(10)	n.s.
ADP (µM)	16.85 ± 5.71	(8)	17.70 ± 2.02	(3)	n.s.
ATP (µM)	4.07 ± 1.77	(8)	3.92 ± 1.36	(8)	n.s.

*Significant at a level $p < 0.05$, ** $p < 0.01$, *** $p < 0.001$; n.s.: not significant.

6.3.2 Time courses of respiration and intracellular metabolites during starvation

Aside from addressing the effect of food quality on the respiratory metabolism of rotifers and mysids, we studied the evolution of the same variables on organisms from the two treatments during a food-deprivation and re-feeding experiment (Fig. 6.3). In general, organisms acclimated to the two diets exhibited similar patterns in all the variables during starvation, although the values were normally lower in the lipid-poor treatment. The time course of R_{O_2} declined sharply in the first 2 h, to then continue decreasing at a lower rate towards the end of the starvation period, when they reached the 50 % of their initial values. Φ rates showed a similar fast decrease but, thereafter, they remained relatively constant until the end of starvation. Accordingly, the R_{O_2}/Φ ratio dropped during this period from average values of 1.30 and 0.88 to 0.75 and 0.70, in rotifers and mysids, respectively (Table 6.3). The time courses of the intracellular concentration of NAD, NADP, ADP and ATP resembled the R_{O_2} profiles (Fig. 6.3). As described before for the food quality analysis, the concentration of the reduced forms of NAD and NADP were higher than the levels of the oxidized forms throughout all the experiment. On average, the NADH levels decreased to ~ 70 % of the initial values both in rotifers and mysids, whereas the decline in the NADPH concentration was more pronounced on rotifers (to 30 %) than in mysids (to 50 %). Furthermore, the ratios NAD^+/NADH and $NADP^+$/NADPH, which reflect the redox state of the cells, decreased in the two species during this period, indicating an increased proportion of the reduced forms with starvation. Similarly, the ATP/ADP ratios were higher during well-fed conditions than in starved organisms.

When the food was supplied again (vertical dotted lines in Fig. 6.3), all the variables increased rapidly within the first hours to values equal to or even higher than the initial levels, except Φ, which rose more gradually. This increase was reflected in the R_{O_2}/Φ ratios as well (Table 6.3).

6.3.3 Predicting R_{O_2} from a bisubstrate kinetic model

The bisubstrate kinetic model introduced by Packard et al. (1996) and detailed in Eq. 1 was applied to predict the R_{O_2}. For that, the Michaelis constant (K_m) and the dissociation constant (K_{ia}) for both NADH and NADPH were determined. As shown in Fig. 6.2, double-reciprocal plots were constructed at various concentrations of the cosubstrate, giving a family of straight lines

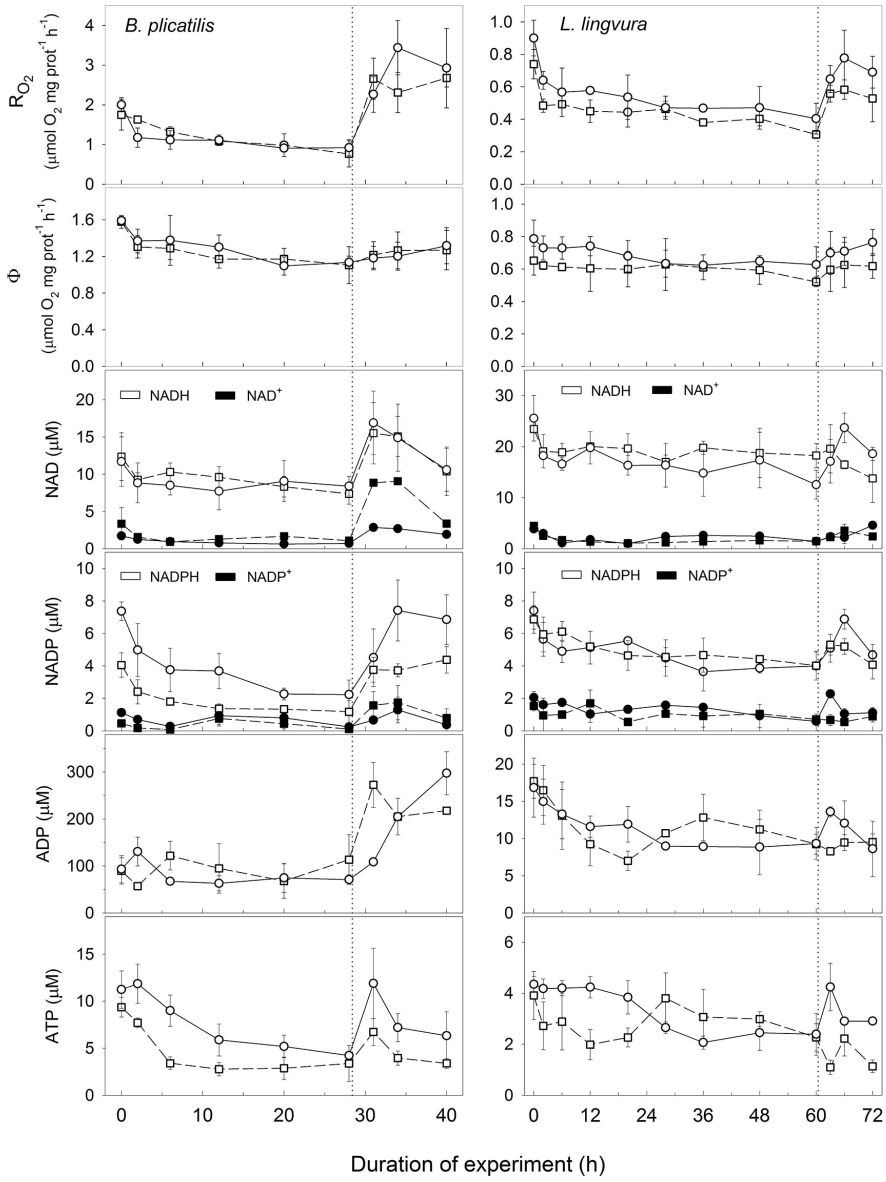

Figure 6.3: Time profiles of the oxygen consumption rates (R_{O_2}), potential respiration (Φ), and the intracellular concentration of NAD, NADP, ADP and ATP for the lipid-rich (dots) and lipid-poor (squares) treatments in *B. plicatilis* (left panels) and *L. lingvura* (right panels). The profiles of the reduced (NADH, NADPH) and oxidized forms (NAD^+, $NADP^+$) of NAD and NADP are given separately. Vertical dashed lines indicate the time when the food was restored. Error bars indicate the 95 % confidence limits.

Table 6.3: Oxygen consumption rate to potential respiration ratios (R_{O_2}/Φ) found in the two species of marine zooplankton fed with a lipid-rich diet (Diet *A*) and a lipid-poor diet (Diet *B*). The starvation experiment lasted 28 h for *B. plicatilis* and 60 h for *L. lingvura*. Afterwards, the food was restored and three more measurements (bold numbers) were made to study the recovery. Mean values ± SD of triplicate samples are given.

Brachionus plicatilis			*Leptomysis lingvura*		
Time (h)	Diet *A*	Diet *B*	Time (h)	Diet *A*	Diet *B*
0	1.26 ± 0.12	1.33 ± 0.25	0	0.95 ± 0.16	0.80 ± 0.15
2	0.86 ± 0.19	1.39 ± 0.15	2	0.88 ± 0.12	0.78 ± 0.07
6	0.81 ± 0.23	1.02 ± 0.14	6	0.78 ± 0.22	0.80 ± 0.01
12	0.85 ± 0.13	0.93 ± 0.11	12	0.78 ± 0.07	0.75 ± 0.21
20	0.83 ± 0.10	0.84 ± 0.26	20	0.79 ± 0.23	0.75 ± 0.20
28	0.81 ± 0.19	0.69 ± 0.32	28	0.74 ± 0.15	0.71 ± 0.20
31	1.91 ± 0.43	2.18 ± 0.50	36	0.75 ± 0.03	0.76 ± 0.08
34	2.86 ± 0.67	1.82 ± 0.49	48	0.73 ± 0.20	0.64 ± 0.13
40	2.22 ± 0.83	2.11 ± 0.40	60	0.64 ± 0.19	0.77 ± 0.06
			63	0.93 ± 0.21	0.94 ± 0.23
			66	1.10 ± 0.28	0.93 ± 0.23
			72	0.90 ± 0.16	0.85 ± 0.25

with different slopes and intercepts that intersected at a common point in the second quadrant of the diagram. Then, these slopes and intercepts were plotted against the reciprocal concentration of the substrate in a secondary plot, in which the K_{ia} and the K_m were determined from the abscissa intercept of each replot. Table 6.4 shows the resultant kinetic constants for *B. plicatilis* and *L. lingvura*. In order to detect any influence of food availability on these constants, several replicates were performed at well-fed and starvation conditions. To a greater or lesser extent, all the kinetic constants increased with starvation, which entailed a reduction of the reaction rates during this period. In rotifers, these differences were only significant for K_{NADPH} (Student *t*-test, $p < 0.05$), whereas in mysids the differences were significant for K_{NADH} (Student *t*-test, $p < 0.05$) as well as for the K_{ia} of both NADH and NADPH (Student *t*-test, $p < 0.001$ and $p < 0.01$, respectively). In general, the K_m values measured in rotifers and mysids were very similar (Table 6.4), indicating a comparable affinity of the ETS enzymes to the NADH and NADPH in both organisms. Contrarily, the K_{ia} values of mysids were generally higher, which indicates a weaker binding in the enzyme-substrate complex in these organisms than in rotifers.

Table 6.4: Kinetic constants of the ETS for *B. plicatilis* and *L. lingvura* measured at well-fed conditions and after a period of starvation. Both the Michaelis constants (K_m) and the dissociation constants (K_{ia}) were estimated from a bisubstrate enzyme controlled reaction, as shown in Fig. 6.1. The K_{ia} are single values and were obtained by alternatively considering NADH and NADPH as the first binding substrate. The maximum velocity of the reaction (V_{max}) was determined at saturating levels of the two substrates (1.7 mM for NADH and 0.25 mM for NADPH). Mean values ± SD and the number of replicates (in parenthesis) are given.

	V_{max}	K_m (µM)		K_{ia} (µM) [a]	
Brachionus plicatilis	(µmol O_2 h^{-1} mg $prot^{-1}$)	NADH	NADPH	NADH	NADPH
Well-fed	1.62 ± 0.06 (4)	12.88 ± 2.68 (4)	0.59 ± 0.20 (4)	144.17 ± 28.60 (4)	1.47 ± 0.46 (4)
Starved	1.26 ± 0.33 (4)	16.30 ± 2.02 (4)	1.39 ± 0.44 (4)	176.33 ± 21.45 (4)	2.08 ± 0.57 (4)
Leptomysis lingvura					
Well-fed	1.05 ± 0.04 (2)	12.80 ± 1.30 (2)	0.52 (1)	51.11 ± 16.80 (2)	1.79 ± 1.10 (2)
Starved	0.71 ± 0.01 (4)	18.38 ± 2.40 (4)	0.93 ± 0.18 (4)	207.21 ± 13.10 (4)	8.53 ± 1.23 (4)

[a] K_{ia} were estimated by alternatively considering the NADH and NADPH as the first binding substrate.

Then, using these kinetic constants and the NADH and NADPH concentrations from Fig. 6.3, the predicted R_{O_2} (V_{O_2}) was determined by applying the Eq. 1. Figs. 6.4*A* and *C* shows the time courses of R_{O_2} and V_{O_2} in rotifers and mysids, respectively, expressed as the percentages of the initial values. This comparison evidenced that R_{O_2} was accurately predicted by the V_{O_2} in both treatments and organisms throughout the entire experiment, although the modeled values yielded lower rates, especially in rotifers. Indeed, the *in vivo* R_{O_2} rates of both organisms presented a much better correlation with the

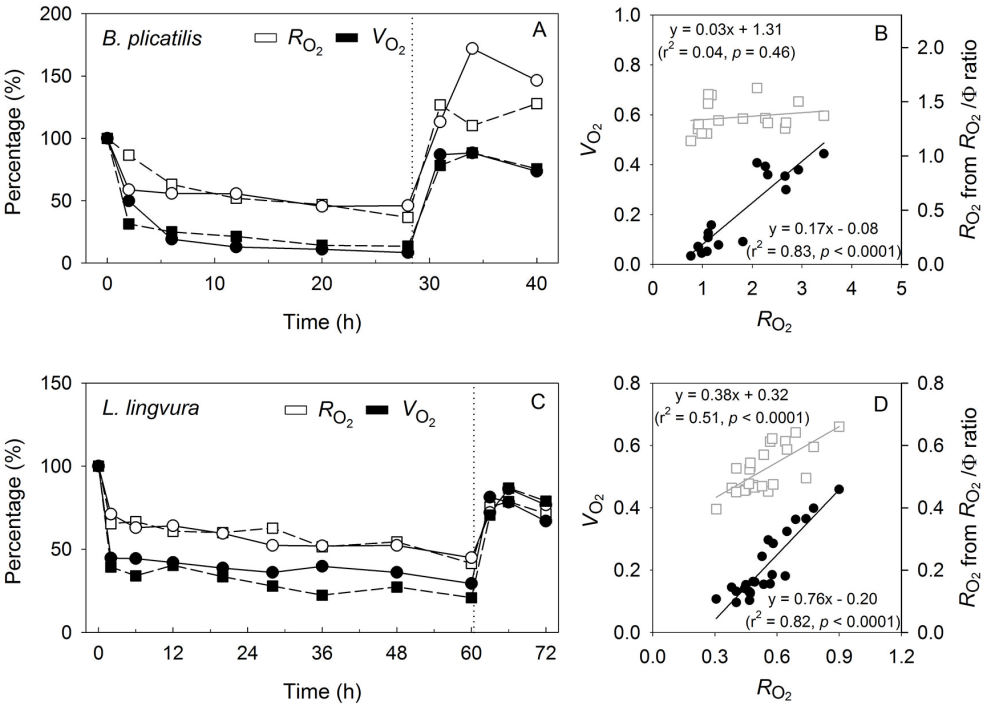

Figure 6.4: Comparison of the measured *in vivo* oxygen consumption rates (R_{O_2}) and the predicted oxygen consumption rates (V_{O_2}) generated from Eq. 1, in both *B. plicatilis* (A and B) and *L. lingvura* (C and D). Panels A and C show the time profiles of the two variables during the experiment, expressed as a percent of the inicial rates. Dots and squares corresponds to the lipid-rich and lipid-poor treatments, respectively. Vertical dashed lines indicate the time when the food was restored. Panels B and D show the regression lines between the R_{O_2} and V_{O_2} (black dots), as well as between the R_{O_2} and the estimated R_{O_2} (grey squares) calculated from the Φ measurements and the R_{O_2}/Φ ratios in Table 6.2.

modeled V_{O_2} values (r^2 = 0.83 and 0.82, for rotifers and mysids, respectively) than with the R_{O_2} estimated from the Φ data on Fig. 6.3 and the fixed R_{O_2}/Φ ratios from Table 6.2 (Figs. 6.4*B* and *D*). Furthermore, the general relationship between the R_{O_2} and the intracellular concentration of ADP reflected a significant correlation between them (r^2 = 0.77, $p < 0.0001$, Fig. 6.5). In order to avoid the variability associated to different biomass, the ADP concentrations were standardized to the Φ rates.

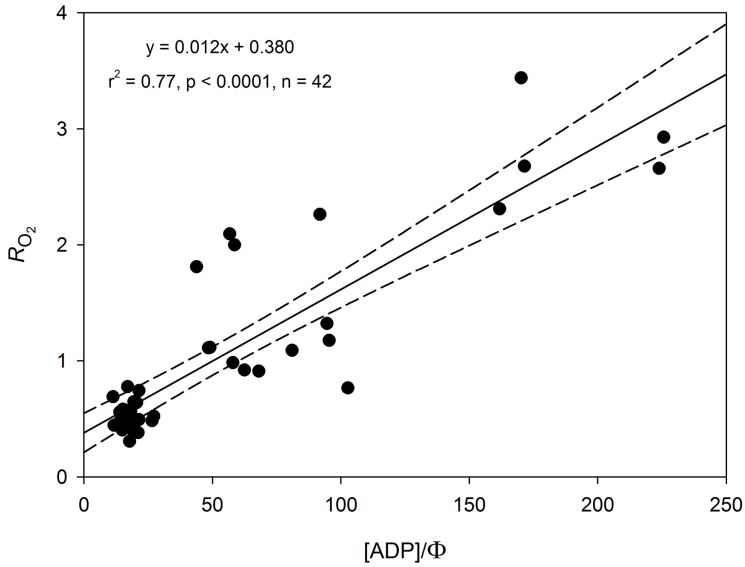

Figure 6.5: Scatter-plot showing the relationship of the measured oxygen consumption rates (R_{O_2}, µmol O_2 h^{-1} mg $prot^{-1}$) with the ratio between the ADP concentration ([ADP], µM) and the potential respiration (Φ, µmol O_2 h^{-1} mg $prot^{-1}$). Dashed lines indicate the 95 % confidence limits. Data for *B. plicatilis* and *L. lingvura* are pooled together.

6.4 Discussion

6.4.1 Response of the respiratory metabolism to food quality

The effect of food quality on the R_{O_2} and Φ as well as on the intracellular concentration of metabolites on rotifers and mysids has been described here (Table 6.2). According to Conover (1966), the composition of food is an important

factor that determines the assimilation by zooplankton and, consequently, it will affect their metabolic rates. In *B. plicatilis*, R_{O_2} was significantly higher in organisms from the lipid-rich diet than from the lipid-poor one, despite they were provided with saturating food conditions in both cases. This is likely related to the distinct catabolic pathways that dominated in each case (Nelson et al., 2008). In organisms acclimated to the more lipidic diet, the β-oxidation pathway would dominate catabolism, whereas in organisms fed with the more proteic diet, the oxidation of amino acids would play a major role. Thus, the complete catabolism of a C16 fatty acid (e.g., palmitic acid) requires the consumption of 23 moles of O_2 and produces 131 moles of ATP. In contrast, the complete oxidation of an equal amount (on a molar basis) of a proteinaceous compound (e.g., glutamic acid) requires 1.5 moles of O_2 and produces only 11 moles of ATP. Accordingly, the production of the same amount of ATP (1 mol), consumes more O_2 when a lipidic compound is oxidized (0.2 moles) than when it is a proteinic compound (0.14 moles). Assuming a similar energetic requirements in the two culture treatments, this could reasonably explain the difference observed between our rates. In agreement with our results (Table 6.2), Ikeda (1977) also reported a higher O_2 requirement for the oxidation of lipids than for the oxidation of proteins. This same rationale can be applied for the R_{O_2} values in *L. lingvura*. Φ values, in turn, did not show such a difference between the organisms adapted to the two diets, although the protein-specific Φ rates in the mysids fed with enriched-*Artemia* sp. were slightly higher.

In general, the intracellular concentration of the metabolites studied here did not show any difference between the food treatments (Table 6.2). The only exception was the NADP level determined in rotifers, which differed significantly between the two diets. This is not surprising considering the role of NADP in biosynthesis and growth processes in the cells. Since yeast-grown rotifers display notably lower growth rates than rotifers fed with live microalgae (Lubzens et al., 1995), higher values of NADP in organisms from the diet A than from diet B were to be expected.

In view of the results, the food quality might be an additional factor that partially contributes to the observed variability of the R_{O_2}/Φ ratios of marine organisms in the field (e.g., *Chapter 4* in this thesis; Hernández-León and Gómez, 1996). Provided that the Φ rates are relatively constant in the short-term, the R_{O_2}/Φ ratios would fluctuate insofar as R_{O_2} changes and, as stated above, it certainly depends on the biochemical composition of the compounds

that are being metabolized. However, the larger variability appears to be related to both taxonomic groups and the nutritional state of the organisms, as will be discussed later.

6.4.2 **Effect of starvation on the respiratory metabolism**

It is well known that food availability influences the metabolic rates of marine zooplankton. The increase in the respiration rates in association with feeding is known as "specific dynamic action" (SDA), and it represents the costs of biosynthesis (Kiørboe et al., 1985). Conversely, respiratory rates in starved organisms are mainly related to basal metabolism. Here, we found that the R_{O_2} during food-saturated conditions was twice the R_{O_2} during starvation in both rotifers and mysids (Fig. 6.3), in clear agreement with previous findings in other zooplankton species (Almeda et al., 2011; Ikeda, 1977; Kiørboe et al., 1985; Mayzaud, 1976). This decrease to a basal metabolic rate is thought to enhance the survival capacity by lowering the energy expenditure (Tsuda, 1994). Furthermore, the response of the R_{O_2} to changing trophic conditions was nearly immediate as evidenced by the rapid decrease within the first 2 - 6 h of food shortage as well as by the fast recovery of the R_{O_2} when the food was restored. In this light, Thor (2003) found that respiration rates of the starved copepod *Acartia tonsa* increased to values even greater to those of non-starved organisms within a few hours after the reintroduction of food. Our respiration rates trended the same way (Fig. 6.3). However, we did not find any difference in the R_{O_2} pattern in organisms acclimated to different food treatments during this time, as could be expected on the basis of the work by Conover (1966). The response of the protein-specific Φ, in contrast, was more attenuated (Fig. 6.3). Aside from the slight decrease in the first 2 h of starvation, it remained fairly constant during the experiment in both rotifers and mysids for the two feeding treatments. The maintenance of substrate-limited enzymes during short-term starvation would constitute an advantageous adaptation of organisms that live in habitats with highly variable food-availability. Accordingly, enzymatic activities have been observed to decrease to a lesser extent than metabolic rates during this period (Bamstedt, 1980; Finlay et al., 1983; Ikeda and Skjoldal, 1980; Packard et al., 1996). Similar studies on starved *L. lingvura* yielded comparable results of metabolic rates and enzymatic activities on their respiratory metabolism (Herrera et al., 2011) as well as on other physiological processes, such as the excretory metabolism (Fernández-Urruzola et al., 2011). Moreover,

Herrera et al. (2011) reported an exponential decrease of the R_{O_2}/Φ ratio with the time of starvation that was also found in our experiment (Table 6.3). The factors affecting the variability of the R_{O_2}/Φ ratio in marine plankton have been studied and discussed before (e.g., *Chapters 4* and *5*, this thesis; Hernández-León and Gómez, 1996). Here we have shown differences between species and in response to food deprivation. However, both organisms displayed a similar rapid increase of the R_{O_2}/Φ ratio when the food was restored.

The intracellular concentration of metabolites resembled the pattern described by the R_{O_2} (Fig. 6.3). They also showed a decrease as organisms starved and increased rapidly in response to the reintroduction of food. On a biomass basis, the average concentration of the total pool of NAD (280 pmol mg prot^{-1}) and NADP (72 pmol mg prot^{-1}) in rotifers was two times lower than that found in our previous work on the marine dinoflagellate *Oxyrrhis marina* (see *Chapter 5*). Conversely, the average values in well-fed mysids (904 pmol NAD mg prot^{-1} and 312 pmol NADP mg prot^{-1}) were slightly higher to those of *O. marina*, but compared well to the levels reported for other eukaryotic organisms (e.g., Agius et al., 2001; Umemura and Kimura, 2005). Although in the present work the reduced forms were always greater than the oxidized forms, the NAD(P)$^+$/NAD(P)H ratios decreased from well-fed to starvation conditions, in accordance with our previous findings (*Chapter 5*). Finally, the intracellular content of the adenine nucleotides ADP and ATP fell during food deprivation, which agrees with that reported by Ikeda and Skjoldal (1980).

6.4.3 Predicted *vs* measured R_{O_2}

A first-principles model for a physiological process should be based on the biochemical principles and properties that control it, such as enzyme activities and substrate concentrations (Packard et al., 2004). In previous applications of this concept, the physiological rate of O_2 consumption was calculated from measurements of the ETS activity, kinetic constants from the literature and modeled time courses of the two main ETS electron donors (Packard et al., 1996; Aguiar-González et al., 2012). Nevertheless, the respiration determined from the bisubstrate kinetic model agreed substantially with the measured rates in both studies. Here, we have obtained a similar degree of success by using measured intracellular NADH and NADPH concentrations as well as empirically determined kinetic constants. Thus in Fig. 6.4, the V_{O_2} tracked the R_{O_2}

during a starvation and re-feeding experiment, under two nutritional regimes, both in rotifers ($r^2 = 0.83$) and mysids ($r^2 = 0.82$). This is the first time that the capability of the model to predict R_{O_2} has been verified by the measurement of all the input parameters. A comparable success was achieved by the application of an analogous model to predict the respiratory CO_2 production from the activity of the isocitrate dehydrogenase, the enzyme involved in the CO_2-side of respiration (Roy and Packard, 2001).

The model introduced by Packard et al. (1996) was based on the hypothesis that substrate-limitation of respiration explained its decrease during starvation. Their results supported the hypothesis in that the *in vitro* ETS activity remained constant during this period and in that the bisubstrate kinetics successfully predicted the R_{O_2} from the ETS activity. Our findings agree with these statements as well (Figs. 6.3 and 6.4). In addition, these authors recognized two assumptions that could challenge the application of this hypothesis. The first one is that the intracellular concentration of NADH and NADPH are dependent on available food sources and that, consequently, their levels decrease as organisms passes into starvation. In support of this, our results have shown that the concentration of both nucleotides dropped during starvation and increased rapidly in response to the food restoration (Fig. 6.3). This finding further suggests that both NADH and NADPH contributes to the R_{O_2}, which agrees with previous observations by Owens and King (1975a) in zooplankton. Furthermore, the fact that $K_m < K_{ia}$ in all cases (Table 6.4) indicated that a previously-bound substrate can improve the binding of a second substrate (Bisswanger, 2008). Accordingly, Eq. 6.1 could not be reduced to a more simple monosubstrate Michaelis-Menten equation. The second assumption was that the kinetic constants remained invariant at the different growth phases or trophic conditions. Contrarily, here we have shown that both constants displayed a certain degree of variability within species and with food availability (Table 6.4). Thus, the K_{NADH} and K_{NADPH} were very similar in rotifers and mysids, although they both showed an influence of food availability. The K_{ia} for NADH and NADPH, in turn, were more variable. A likely explanation for that variability might be the indirect effect that allosteric modulators (e.g. ADP, Ca^{2+}) may have on the enzymes of the ETS, by modifying their affinity for the substrates (Brown, 1992). Nevertheless, these findings do not preclude the use of the bisubstrate kinetic model proposed by Packard et al. (1996), but suggest that it could be improved by incorporating them. Indeed, to our knowledge, this is the first

time that these bisubstrate constants have been addressed on marine plankton and, therefore, there is a complete lack of knowledge about their magnitude in different taxonomical groups or how they vary through an organism's lifetime.

Notwithstanding the good correlation between R_{O_2} and V_{O_2}, the modeled rates yielded lower values than the measured ones, as inferred from the slopes of the regression lines in Figs. 6.4*B* and *D*. This discrepancy was more evident in rotifers than in mysids. One reason that explained this underestimation might be the possible contribution of the succinate to the ETS activity that we do not consider in the model. Thus, succinate donates electrons to the succinate dehydrogenase (complex II) which, together with the NADH dehydrogenase (complex I), supply reducing equivalents to their common electron acceptor in the ETS, a quinone (Cowley and Palmer, 1980). However, it has been noticed that this substrate is of minor importance in the overall reaction (Finlay et al., 1983; Kenner and Ahmed, 1975b; Savenkoff et al., 1995) and that it may even decrease the V_{max} of the reaction by competing with the NADH (Owens and King, 1975a). Accordingly, it is unlikely that succinate would account for the observed difference between R_{O_2} and V_{O_2}. So the most plausible explanation is that the *in vivo* R_{O_2} is controlled by other factors besides the substrate supply. Indeed, since it was first recognized by the work of Chance and Williams (1955), it has been well-established that increased concentration of ADP can promote the ATP synthesis as well as an increase in respiration and substrate utilization. During oxidative phosphorilation in eukaryotic cells, three of the four complexes that comprise the ETS in the inner mitochondrial membrane not only transfer electrons to other carriers but also translocate protons from the matrix to the intermembrane space. This generates a proton gradient that is used by the ATPase to produce ATP from ADP and inorganic phosphate. When the relative concentration of ADP increases, the synthesis of ATP lessens the proton gradient, which stimulate the activity of the ETS complexes. This results in the oxidation of the mitochondrial NADH and NADPH and in the consumption of O_2. Consequently, there is a direct relationship between the ADP concentration and the R_{O_2} (see review by Brown, 1992), that is also evidenced in our results (Fig. 6.5). Nevertheless, the *in vitro* assay of the ETS entails a homogenization of the samples, which disrupt the membranes and the proton gradient. Hence, this assay does not account for the additional effect of the ADP on the total O_2 consumption of intact cells, which would likely be the cause of the difference between the R_{O_2} and V_{O_2}. We suggest that if an

additional term for the activation by the ADP is included in the Eq. 6.1, the R_{O_2} and V_{O_2} values would be more alike. In the same manner, the influence of the ADP on the *in vivo* R_{O_2} may also explain the R_{O_2}/Φ ratios higher than 1 measured here (Table 6.3) and that are usually found in the literature (*Chapter 5*, this thesis; Hernández-León and Gómez, 1996; Herrera et al., 2011; King and Packard, 1975). However, to determine the contribution of the ADP and quantify its kinetic constants it would be necessary to work either on intact cells or isolated mitochondria.

The R_{O_2}/Φ ratios have been commonly used to interpret ETS measurements made in the ocean. However, the application of a universal fixed value requires the understanding of the nutritional state of organisms, due to the well-documented variability of this ratio with changing physiological conditions (*Chapter 5*, this thesis; Hernández-León and Gómez, 1996; Herrera et al., 2011; King and Packard, 1975). Otherwise, it could entail a misleading estimation of R_{O_2}. Thus, our results showed a poor correlation during starvation between the *in vivo* R_{O_2} and the R_{O_2} estimated from ETS measurements and fixed R_{O_2}/Φ ratios (Figs. 6.4*B* and *D*). In contrast, the V_{O_2} was more successful in predicting the R_{O_2} during this period, despite the aforementioned underestimation. Therefore, we suggest that plankton respiration in the field could be assessed more accurately by measuring both the ETS activity and the ETS substrates. Until the contribution of the ADP is quantified and included in the model, the V_{O_2} should also be calibrated against R_{O_2}.

6.5 Conclusions

In this work we have demonstrated the feasibility of a bisubstrate kinetic model to estimate the *in vivo* R_{O_2} from measurements of the ETS activity, kinetic constants and substrate concentrations. Our results have shown that enzyme kinetics can explain stoichiometrically the rates of O_2 consumption in *B. plicatilis* and *L. lingvura*, irrespective of the nutritional composition of the food that is metabolized. Still, future improvements of the model should include the contribution of the ADP in the regulation of the respiratory processes.

Acknowledgements. We are grateful to C. M. Hernández and D. López for kindly providing the cultures of *Nannochloropsis* sp. and *B. plicatilis* from their culturing collection. Thanks are extended to J. J. Santana-Rodríguez for enabling us to perform the HPLC analysis in his

laboratory. This work was founded by the BIOMBA project (CTM2012-32729/MAR) awarded to M. Gomez by the Spanish Ministry of Economy and Competitiveness. N. Osma and I. Fernández-Urruzola received financial support from the Formation and Perfection of the Researcher Personal Program from the Basque Government. T. T. Packard was largely supported by TIAA-CREF and Social Security (USA).

No book can ever be finished. While working on it we learn just enough to find it immature the moment we turn away from it.

Karl R. Popper

CHAPTER 7 CAPÍTULO

Synthesis and Future research

7.1 General discussion

7.1.1 Application of a respiration-based model to biogeochemical cycles

The continental margins, and specially those affected by coastal upwellings, play an important role in the global carbon cycle, as more than 40 % of the carbon sequestration in the ocean occurs in these areas (Muller-Karger et al., 2005). However, the wealth of data on POC fluxes is focused on the open ocean further offshore. This thesis expands the knowledge of short-term changes in the vertical particle fluxes in the Peruvian and Benguela upwelling systems.

The application of a respiration-based approach to quantify vertical carbon fluxes (F_C) was initially proposed by Packard and Christensen (2004). In this thesis, this methodology has allowed the construction of a synoptic cross-shelf section of F_C in the Peruvian upwelling, which would have been nearly imposible to achieve by other methods. Furthermore, from the F_C calculations, the Nutrient Retention Efficiency (NRE) of the system was determined in these waters. This metric was first introduced by (Packard and Gómez, 2013) and has been further developed here. It determines the efficiency by which organic matter is remineralized in the water-column. Consequently, it is inversely related to carbon transfer efficiency (Buesseler et al., 2007b) and, therefore, to the efficiency of the biological pump (*sensu* Volk and Hoffert, 1985) in se-

questering carbon in the deep ocean. In addition to this, the ETS profiles in the Peruvian upwelling proved its utility in estimating the potential heterotrophic energy production associated with plankton metabolism.

Despite its successful application to study carbon fluxes in the Gulf of Maine (Packard and Christensen, 2004) and the Canary Islands (Packard and Gómez, 2013), the F_C method has not been compared with direct measurements of sinking POC until now. This comparison was accomplished on the continental shelf of the Benguela upwelling and is shown in *Chapter 3*. The Eulerian approach applied during the sampling allowed the characterization of the influence of mesoscale structures. Accordingly, both methodologies revealed a major influence of the temporal variability rather than the effect of distance to the core of the coastal upwelling. The comparison between them was mainly influenced by the nature and concentration of the sinking particles. When the fast-sinking particles dominated the water-column, the values from the sediment traps exceeded the F_C values, whereas when the slow-sinking particles dominated the flux, the F_C approach yielded higher values. Thus, these results agreed with that suggested by Alonso-González et al. (2010), who suggested that the apparent mismatch reported between the respiratory carbon requirements of organisms and the POC flux collected by the sediment traps (e.g., Baltar et al., 2009; Burd et al., 2010; Steinberg et al., 2008) might be ultimately dependent of the nature of the sinking particles. In this light, recent research by Giering et al. (2014) has shown a balance between the sources and sinks of carbon in the mesopelagic waters.

One factor that could affect both the F_C values and the sediment trap record is the lateral advection. Although it would not influence the comparison between the two methods, one could argue that the lateral inputs may be relevant in the export of POC in these eastern boundary upwelling ecosystems (Alonso-González et al., 2009) and that it could be a source of error in the estimates of POC flux based on any of these approaches. However, even in upwellings, the vertical dynamics dominate the horizontal ones given the fact that each one operates at a different scale, i.e. from hundred meters to several kilometers, respectively. Thus, the estimated offshore velocity of advected water during the sampling in Benguela was 0.06 m s^{-1}, and the current velocities in the inertial frequency band ranged between 0.02 - 0.06 m s^{-1} (Mohrholz et al., 2014). According to Jaeger et al. (1996), relatively slow currents with velocities below 0.2 m s^{-1} result in little dispersal of the particles, which al-

lows them to reach the seabed close to the point where they left the surface waters, although the final sinking velocity will be mainly determined by their composition (e.g., Iversen and Ploug, 2010).

All in all, the F_C approach has shown itself to be a useful tool in studying carbon fluxes in the ocean when both large temporal and spatial resolution is pursued.

7.1.2 Factors affecting the physiological O_2 consumption and the enzymatic activity of the ETS in marine organisms

In oceanographic research, temperature and body mass have been identified as the most influential factors on the metabolic rates of marine zooplankton (Ikeda, 1985; Ikeda et al., 2001; Ivleva, 1980). However, throughout this thesis it has been shown that both availability and composition of food should also be considered when studying the variability of these rates.

The R_{O_2} values from the different oceanic regions presented in *Chapter 4* reflected the influence of **habitat temperature**. The minimum R_{O_2} rates were found in the cold waters of the Benguela upwelling whereas the highest values corresponded to the warmer waters of the North Atlantic (Fig. 4.3). Indeed, the temperature explained a higher percentage of the variability in the metabolic rates between the different regions studied (Table 4.1), as compared to the influence of the chlorophyll *a*, which was considered a proxy for the food availability. Similar effect of temperature on the Φ rates was observed in our studies and has been described before (Packard et al., 1975). This is not surprising since the R_{O_2} is the direct result of the ETS activity (Nelson et al., 2008). The same relationship that is used to describe the temperature dependence of chemical reactions, i.e. the Arrhenius equation, can be applied to describe the temperature dependence of metabolic rates (Harris et al., 2000) and, consequently, they would vary concurrently with respect to this factor. Hence, the R_{O_2}/Φ ratios do not show any significant influence of temperature (King and Packard, 1975). The variability observed in the ratios from several oceanic regions presented in *Chapter 4* may be ascribed to differences in the taxonomic composition and/or to difference in the food composition that was being metabolized in each area, as will be discussed later.

When the change in the temperature was not significant, as occurred in the temporal study off the Canary Islands (*Chapter 4*), the **food availability** appeared to exert a major influence on both the R_{O_2} and Φ in zooplankton. In

the long-term, organisms will regulate their metabolic rates by promoting or suppressing the synthesis of the complexes from the ETS depending on the energy requirement for the cell maintenance. This would entail either a decrease or an increase of the biomass-specific Φ rates. For instance, well-fed or active organisms will have a higher energy demand so they will present a higher concentration of ETS enzymes per unit of biomass. Therefore, one can compare specific Φ rates in organisms from contrasting areas and attribute the differences to the physiological conditions (e.g., Herrera et al., 2014a). However, in the short-term, the effect of the food limitation is not the same on the R_{O_2} and the Φ. Starvation experiments carried on the marine dinoflagellate *Oxyrrhis marina* (*Chapter 5*) as well as on the rotifer *Brachionus plicatilis* and the mysid *Leptomysis lingvura* (*Chapter 6*) showed a higher impact of food limitation on the R_{O_2} than on the Φ rates. In all the cases, the biomass-specific R_{O_2} decreased to half the initial values after few hours of starvation, which agrees with previous studies in other zooplankton species (Almeda et al., 2011; Ikeda, 1977; Kiørboe et al., 1985; Mayzaud, 1976). In contrast, the biomass-specific Φ rates presented a more sustained decline during the same period. Maintaining relatively high levels of substrate-limited enzymes in the short-term constitutes an advantage for organisms that live in habitats with highly variable food-resources. Once the new energy source appears, they could start immediately making use of it, without the need to wait for a *de novo* synthesis of the enzymatic pool (Finlay et al., 1983; Packard et al., 1996). But if the Φ rates are relatively constant, how does starvation affect the oxygen consumption at the intracellular level? The results from this thesis revealed that the effect may be two-fold. On the one hand, the limitation of carbon sources can initiate a decrease in the intracellular concentration of the pyridine nucleotides (PN), the major substrates of the ETS enzymes. Without a sufficient concentration of these electron donors, the *in vivo* ETS activity would lessen and so would be the O_2 consumption. The results from *Chapters 5* and *6* support this statement. The way PN and R_{O_2} are related is further discussed below. On the other hand, the study of the kinetic constants revealed an increase of the K_m values with starvation (Table 6.4). This means that under food-limitation conditions, the ETS enzymes decrease their affinity for their substrates and, to some extent, this could slow down the *in vivo* ETS activity and decrease the O_2 consumption rates. However, to our knowledge, this is the first time that these bisubstrate kinetic constants have been determined in marine plankton

and, consequently, further research is needed to confirm these measurements. Likely, the effect may be a combination of the two factors. In any case, the distinct effect of short-term starvation on the metabolic rates and the enzymatic activities involves a decrease in the R_{O_2}/Φ ratios, in agreement with previous studies in zooplankton (Hernández-León and Gómez, 1996; Herrera et al., 2011).

Another factor that influenced the R_{O_2} and the Φ was the **food quality**. Again, the major effect was observed on the R_{O_2} rather than on the Φ values. Although the R_{O_2} of organisms acclimated to two feeding-treatments described the same pattern during starvation (Fig. 6.3), the R_{O_2} values at well-fed conditions were higher in organisms from the lipid-rich treatment as compared to the ones from the lipid poor-treatment (Table 6.2). In agreement with this, Ikeda (1977) also reported a higher O_2 requirement for the oxidation of lipids than for the oxidation of proteins. As the Φ rates showed a lower influence of the type of carbon source, the food quality proved to be an additional factor involved in the variability of the R_{O_2}/Φ, as suggested by Hernández-León and Gómez (1996). In relation to this, these authors assumed no variability of K_m for the different species in their study of the variability of the R_{O_2}/Φ ratios. Our results of bisubstrate kinetics on rotifers and mysids support their assumption as they barely varied between them. However, these kinetic parameters should be determined in a larger number of species from different taxonomic groups and with different structural complexities to strengthen our results.

Finally, an overall effect of **body size** on the R_{O_2} and the Φ can be inferred from our results. In agreement with the findings of Ikeda and Mitchell (1982) and in the light of Kleiber's law (Kleiber, 1961), the highest metabolic rates and enzymatic activities were found in the smallest zooplankton, both in the laboratory experiments and in the field samples. For instance, the R_{O_2} of well-fed organisms in *Chapters 6* showed that the rotifer *B. plicatilis* presented higher rates than *L. lingvura*. One could attribute the difference to the distinct culturing temperatures (25 °C *vs* 18 °C). However, if the R_{O_2} of *L. lingvura* is standardized to 25 °C by means of a Q_{10} value of 1.8 (averaged value from Ikeda, 1985), the average rates in *B. plicatilis* will still be higher (1.88 μmol O_2 mg prot^{-1} h^{-1}) than in *L. lingvura* (1.24 μmol O_2 mg prot^{-1} h^{-1}). Similarly, the zooplankton collected in several oceanic regions showed, in all the cases, higher R_{O_2} and Φ rates in the smaller size fractions, regardless of the trophic conditions or the habitat temperature (Table 4.2). The relationship that

respiration maintains with the ETS has been noted to have little dependence on size (Christensen et al., 1980) and, therefore, the significant linear regression between them holds for all organisms from bacteria to large zooplankton, with a size range over 10 orders of magnitude (Christensen et al., 1980; Finlay et al., 1983; King and Packard, 1975). This good correlation between the R_{O_2} and the Φ is further reflected in the oceanic zooplankton studied in this thesis, when all the size fractions are pooled together (Fig. 7.1). The value of the slope, i.e. the R_{O_2}/Φ ratio, agrees with previous values reported in previous studies in planktonic communities (Arístegui and Montero, 1995; del Giorgio, 1992; Hernández-León and Gómez, 1996).

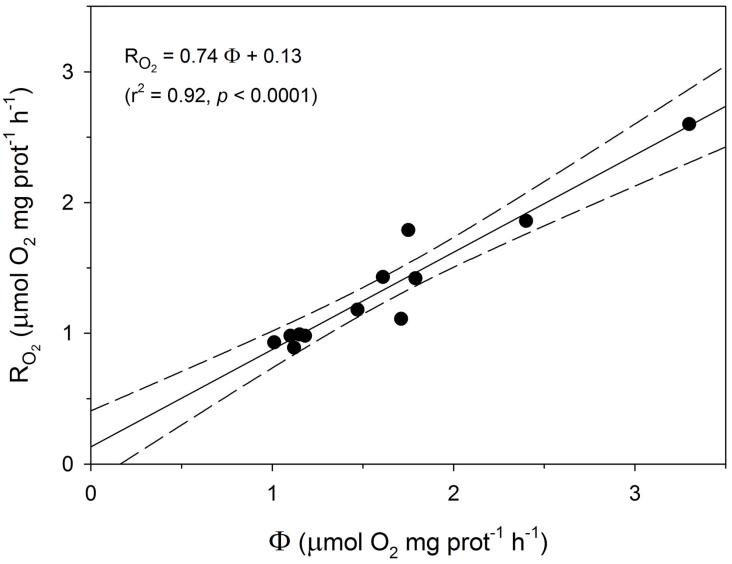

Figure 7.1: Relationship between R_{O_2} and Φ for size-fractionated marine zooplankton. The line of best fit and the 95 % *CI*s are given.

7.1.3 **Role of pyridine nucleotides in the respiratory control**

To our knowledge, this thesis compiles the largest dataset of PN measurements made in marine organisms (Table 7.1). Despite the importance of these electron carriers in almost all the metabolic pathways, little was known about their concentration and behavior in these organisms. This work has shed light on the

effect that factors such as food quality, starvation and taxonomic composition have on the intracellular concentration of both NAD(H) and NADP(H). While no clear influence of the food composition was observed on their values in cultured organisms (Table 6.2), larger zooplankton had higher values than smaller zooplankton. Overall, average levels of NAD(H) and NADP(H) in *O. marina* and *B. plicatilis* were within the range of those reported in several species of aerobic bacteria (e.g., London and Knight, 1966; Setlow and Setlow, 1977; Wimpenny and Firth, 1972). The values in the marine mysid *L. lingvura*, in turn, were closer to those found in other more complex eukaryotes (e.g., Agius et al., 2001; Umemura and Kimura, 2005). Nevertheless, the principal factor affecting the NAD(H) and NADP(H) concentrations was the food availability. In general, the zooplankton from the more productive areas studied in *Chapter 4* (e.g., Benguela upwelling) showed the highest concentrations of PN, supporting the fact that the intracellular levels of NAD(H) and NADP(H) are directly proportional to the nutritional state of the organisms. Provided that the PN are the major electron donors of the ETS enzymes, the correlation between the R_{O_2} and the NAD and NADP concentration was likewise studied in the oceanic zooplankton. However, this relationship was obscured by a distinct impact of environmental factors (i.e., temperature) on the two variables. When the effect of food availability was isolated in laboratory experiments, R_{O_2} was strongly correlated with the NAD and NADP concentration in the three cultured species of marine plankton. Thus, during a period of starvation and a subsequent restoration of food, the pattern described by R_{O_2} tracked that of NAD(H) and NADP(H) (Fig. 6.3).

These results promoted the exploration of an enzyme kinetic model to describe the *in vivo* R_{O_2} on the basis of the ETS activity and the substrate concentrations. The feasibility of a bisubstrate kinetic model, originally introduced by Packard et al. (1996), to predict the *in vivo* R_{O_2} during the exponential growth phase and senescence of marine bacterial cultures has been demonstrated (Aguiar-González et al., 2012). Even though these authors calculated the R_{O_2} without the benefit of intracellular substrate and kinetic constants measurements, they attained a high degree of success in their prediction. In this thesis, the validity of this model has been reinforced by using measured kinetic constants and intracellular concentrations of PN (*Chapter 6*). Thus, the measured R_{O_2} and the estimated R_{O_2} from the model (V_{O_2}) showed a high correlation during starvation in both rotifers and mysids. Still, the linear re-

Table 7.1: Compilation of the average NAD(H) and NADP(H) concentrations determined in the different organisms and zooplankton samples analyzed throughout this thesis. NAD(H) and NADP(H) represent the sum of the reduced and the oxidized forms.

Species	Source	Nutritional condition/ Location	pmol mg prot^{-1} NAD(H)	pmol mg prot^{-1} NADP(H)	Related Chapter
Dinoflagellate					
Oxyrrhis marina	Cultured	well-fed, *Rhodomonas salina*	589	171	*5*
		starved (17 d)	436	50	*5*
Rotifer					
Brachionus plicatilis	Cultured	well-fed, *Nannochloropsis* sp.	160	109	*6*
		well-fed, dry yeast	179	58	*6*
		starved (28 h), *Nannochloropsis* sp.	115	31	*6*
		starved (28 h), dry yeast	108	17	*6*
Mysid					
Leptomysis lingvura	Cultured	well-fed, enriched *Artemia* sp.	905	312	*6*
		well-fed, yeast-grown *B. plicatilis*	834	278	*6*
		starved (60 h), enriched *Artemia* sp.	434	139	*6*
		starved (60 h), yeast-grown *B. plicatilis*	610	146	*6*
Mixed zooplankton					*4*
100 - 500 µm	MALASPINA 2010	North Atlantic	424	140	*4*
		Indian Ocean	300	205	*4*
	CAMVALEX	Coastal waters, Canary Islands	669	173	*4*
	SUCCESSION	Benguela upwelling	–	158	*4*
500 - 1000 µm	MALASPINA 2010	North Atlantic	281	119	*4*
		Indian Ocean	320	186	*4*
	CAMVALEX	Coastal waters, Canary Islands	645	179	*4*
	SUCCESSION	Benguela upwelling	879	306	*4*
> 1000 µm	MALASPINA 2010	North Atlantic	934	194	*4*
		Indian Ocean	455	258	*4*
	CAMVALEX	Coastal waters, Canary Islands	500	180	*4*
	SUCCESSION	Benguela upwelling	896	341	*4*

gression between them also showed that the V_{O_2} underestimated the *in vivo* R_{O_2}, especially in rotifers. On the basis of the seminal work of Chance and Williams (1955) and on the work of many others thereafter, the contribution of the ADP to the control of the overall reaction might explain that discrepancy. The fact that the concentration of ADP in rotifers was almost 8-times higher than in mysids and that this difference agrees with the difference in the underestimation between the two species (Fig. 6.4) further supports this hypothesis. Nevertheless, the role of ADP in the respiratory control should be quantified in future studies and included as an additional term in the kinetic model in order to improve its output.

In contrast to the V_{O_2} results, the current way of estimating respiration in the ocean from Φ measurements and a fixed R_{O_2}/Φ ratio poorly predicted the *in vivo* R_{O_2} during starvation. This is a consequence of the aforementioned effect of the short-term changes of food availability on this ratio. Consequently, considering the goodness of the bisubstrate kinetic model and the factors that can distinctly affect the respiratory metabolism, the findings from this thesis suggest that plankton respiration can be more accurately estimated in the field bye measuring the intracellular concentration of substrates in addition to the ETS activity.

7.2 Conclusions

On the basis of the results reported throughout this thesis, the following conclusions can be drawn:

1. The application of a conceptual model based on plankton respiration profiles has proved to be a useful tool to construct synoptic sections of vertical carbon flux (F_C) in the Peruvian upwelling. These profiles would have been unattainable by other more traditional methodologies, such as sediment traps. Furthermore, the concept "Nutrient retention efficiency (NRE)" has been developed, which determines the capacity of the plankton community in retaining water column nutrients by the remineralization of the sinking POC. It has been demonstrated that the NRE is inversely related with the F_C. Likewise, the measurement of the electron transport system activity (ETS) has proved its utility to estimate the potential heterotrophic energy production rates (HEP) in the ocean associated with plankton metabolism.

2. Vertical particle fluxes in the Benguela upwelling revealed the major influence of the temporal variability rather than the effect of distance to the core of the coastal upwelling, mainly due to the important instabilities that mesoscale structures, like filaments and eddies, caused in this region. The comparison of the C-flux values determined by the F_C approach with the POC flux measured by the sediment traps showed a mismatch between the respiratory carbon demands of water-column organisms and the vertical POC flux. The primary productivity rates, the nature of the sinking particles and their settling velocities ruled the magnitud of the mismatch.

3. Seawater temperature and plankton body size were the major factors in explaining the variability of the O_2 consumption rates (R_{O_2}) and the ETS activities in the zooplankton from several oceanic regions. Conversely, the difference in the productivity regimes was the main factor responsible for the variability in the intracellular concentration of pyridine nucleotides (NAD and NADP). Due to the uneven effect of these environmental factors, the expected relationship between the patterns of the R_{O_2} and the pyridine nucleotides concentration was not found.

4. Starvation had more of an impact on the R_{O_2} and the intracellular concentration of NAD and NADP than on the potential respiration rates (Φ), in the heterotrophic dinoflagellate *Oxyrrhis marina*, the rotifer *Brachionus plicatilis* as well as in the mysid *Leptomysis lingvura*. As a consequence, a decrease of the R_{O_2}/Φ was found during starvation in all these organisms.

   (a) The quantification of the NAD and NADP levels in these organisms represents the first determination ever in marine plankton. It revealed protein-specific values in both *O. marina* and *B. plicatilis* similar to those reported for bacteria, whereas in *L. lingvura*, the values were closer to those determined in other more complex eukaryotes.

   (b) Initially, the strong correlation observed between the R_{O_2} and the concentration of NAD and NADP in the marine dinoflagellate during starvation, suggested a substrate-level regulation of respiration. Later, the study conducted in both rotifers and mysids further demonstrated that this regulation obeys the rules of the bisusbtrate enzyme kinetics.

   (c) The response of the specific Φ to changing food availability was more attenuated in the three species of zooplankton, which confers on this organisms an adaptive advantage to live in environments that are highly patchy in resources.

5. In general, food quality did not affect the intracellular concentration of pyridine and adenine nucleotides in both *B. plicatilis* and *L. lingvura*, but did affect their respiratory metabolism, especially, R_{O_2}. The unequal effect on the Φ and R_{O_2} suggests that the food quality is an additional

factor contributing to the observed variability of the R_{O_2}/Φ ratios in the field.

6. A bisubstrate enzyme kinetic model based on the ETS activity, kinetics constants and substrate concentration successfully predicted R_{O_2}, both in well-fed and starved organisms.

   (a) During starvation, the *in vivo* R_{O_2} showed a stronger correlation with the modeled O_2 consumption rates (V_{O_2}) than with the R_{O_2} estimated from the ETS activity and a fixed R_{O_2}/Φ value. These results suggest that, when the nutritional state of organisms in the field is unknown, it could be assessed more accurately than before by measuring the ETS activity and the ETS substrates.

   (b) The underestimation of the modeled values with respect to the actual rates, jointly with the strong correlation observed between the R_{O_2} and the ADP concentration in the cells, suggest an additional control of the *in vivo* ETS activity from this nucleotide, so its contribution should be considered in future applications of the model.

7.3 Future research

The findings and conclusions obtained in this study have evidenced the need to address the following aspects in the near future:

(i) At the biogeochemical level. The application of a respiration-based model was found to be a useful tool to determine the C flux in the ocean. However, the comparison between the values obtained by this approach and the values measured by a more traditional methodology, i.e. the sediment traps, was largely influenced by the composition of the sinking particles. Therefore, it would be desirable to verify if the patterns described in the *Chapter 3* for the Benguela upwelling hold for other highly productive systems with a different community structure, such as coastal waters or equatorial upwellings. Furthermore, it would be interesting to apply this approach in oligotrophic waters, where the benthic respiration and organic carbon burial is negligible. In these areas, the sediment traps will likely underestimate the vertical C flux due to the contribution of the suspended POC and the effect of the lateral transport. The F_C approach, in turn, would yield a closer estimate of the remineralization

processes that are happening in those waters.

(ii) At the physiological level. The variability of the respiratory O_2 consumption rates and enzymatic activities on different taxonomic groups of the zooplankton has been largely demonstrated, both in previous studies in the literature and throughout this thesis. The influence of the food quality and quantity on the respiratory metabolism as well as the variability associated with the habitat temperature has been likewise addressed. However, little is known about how zooplankton metabolism will be affected by ocean acidification, one of the most important factors associated with global change. Most research on the effect of ocean acidification on marine biota have focused on the primary producers. When it comes to zooplankton, the number of studies decreases dramatically, and there is practically a complete lack of knowledge about its impact on their physiological rates. Due to the role that these organisms play in the remineralization of the organic matter in the ocean, it is of primary importance to understand the impact that an increase in the CO_2 levels and a decrease in the pH of the seawater would have on their respiratory metabolism.

(iii) At the biochemical level. The application of an enzyme kinetic model has shed light on the biochemical processes that control the intracellular O_2 consumption. In this thesis, it has been corroborated that the *in vivo* activity of the ETS enzymes is regulated by the intracellular substrate concentration according to bisubstrate kinetics. Nevertheless, the results showed certain aspects that should be quantified and considered in future applications of this model. First, the study of the kinetics constants revealed an influence of the food availability but did not detect differences between species in their values. Still, these findings are based on merely two species of marine zooplankton under specific nutritional conditions. For the purpose of applying this model on heterogeneous communities in the field, it would be necessary to determine these kinetic parameters in a larger number of species from different taxonomic groups and to further analyze their variability under different trophic conditions. Secondly, our study suggested that the contribution of the ADP to the overall regulation of respiration could explain the differences between the modeled and the measured values. However, in order to address its contribution, it is indispensable to work either with intact cells or isolated mitochon-

dria because otherwise a decoupling between the ETS activity and the ATP production occurs. In this manner, kinetic constants for the ADP should be determined and a new term to account for the activation should be included in the model. On the other hand, these improvements would allow the intramitochondrial concentration of the metabolites involved in respiratory O_2 consumption (i.e., NADH, NADPH, ADP, ATP), to be determined. This, in turn, would greatly improve the output of the model.